Purdue University
Purdue e-Pubs

Open Access Dissertations | Theses and Dissertations

Spring 2015

Design of low-thrust missions to asteroids with analysis of the missed-thrust problem

Frank E. Laipert
Purdue University

Follow this and additional works at: https://docs.lib.purdue.edu/open_access_dissertations

 Part of the Aerospace Engineering Commons

Recommended Citation
Laipert, Frank E., "Design of low-thrust missions to asteroids with analysis of the missed-thrust problem" (2015). *Open Access Dissertations*. 495.
https://docs.lib.purdue.edu/open_access_dissertations/495

This document has been made available through Purdue e-Pubs, a service of the Purdue University Libraries. Please contact epubs@purdue.edu for additional information.

Graduate School Form 30
(Revised 08/14)

PURDUE UNIVERSITY
GRADUATE SCHOOL
Thesis/Dissertation Acceptance

This is to certify that the thesis/dissertation prepared

By Frank E. Laipert

Entitled

Design of Low-Thrust Missions to Asteroids with Analysis of the Missed-Thrust Problem

For the degree of Doctor of Philosophy

Is approved by the final examining committee:

James Longuski

David Minton

Kathleen Howell

William Crossley

To the best of my knowledge and as understood by the student in the Thesis/Dissertation Agreement, Publication Delay, and Certification/Disclaimer (Graduate School Form 32), this thesis/dissertation adheres to the provisions of Purdue University's "Policy on Integrity in Research" and the use of copyrighted material.

James Longuski

Approved by Major Professor(s): _____

_____

Approved by: Wayne Chen 04/24/2015

Head of the Department Graduate Program Date

DESIGN OF LOW-THRUST MISSIONS TO ASTEROIDS WITH ANALYSIS OF THE MISSED-THRUST PROBLEM

A Dissertation

Submitted to the Faculty

of

Purdue University

by

Frank E. Laipert

In Partial Fulfillment of the

Requirements for the Degree

of

Doctor of Philosophy

May 2015

Purdue University

West Lafayette, Indiana

To my parents, Joseph and Linda Laipert. I have been incredibly lucky to receive your unwaivering support throughout my life.

ACKNOWLEDGMENTS

I would first like to thank my advisor, Prof. James Longuski, for all of his guidance throughout my graduate career. I have benefited greatly from his dedication to his students and commitment to education.

I also thank the members of my committee, Prof. Kathleen Howell, Prof. David Minton, and Prof. William Crossley. Each one of them is a superb teacher, and I am honored to have learned from them.

Finally, to my fellow research group members and friends I have made at Purdue and beyond, thank you for being my friend. Each one of you is invaluable to me.

TABLE OF CONTENTS

LIST OF TABLES

LIST OF FIGURES

Figure Page

ABSTRACT

Laipert, Frank E. PhD, Purdue University, May 2015. Design of Low-Thrust Missions to Asteroidswith Analysis of the Missed-Thrust Problem. Major Professor: James M. Longuski.

Small bodies in the Solar System, such as asteroids and dwarf planets, are ideal targets for electric propulsion missions because of the high ΔV required to rendezvous with these targets. We study trajectories to the asteroid belt, including a human mission to Ceres and a sample return mission to (216) Kleopatra, along with trajectories to the Jupiter Trojan asteroids. For the human mission to Ceres, payload masses of 75 Mg are achievable with a 11.7 MW nuclear electric propulsion system and an initial mass in LEO of 289 Mg. For low-thrust sample return missions to the main belt asteroid Kleopatra, Mars and Earth are useful gravity assist bodies, with payload masses of 950–1150 kg possible using a 20 kW solar electric propulsion system. A mission to the Jupiter Trojan asteroids would be well-served by visiting two objects. The pair 1986 TS6 and Hektor stand out as ideal targets to visit for launch dates between 2020 and 2040, with missions possible using the off-the-shelf BPT-4000 Hall thruster and power levels in the 30–40 kW range.

During a low-thrust mission, there is a significant possibility of an event which causes the spacecraft to miss some portion of a thrust arc. These missed thrust events can be overcome for reasonable propellant margins of 5–15%, with higher margins required for higher power levels. Gravity-assist trajectories should feature a coast arc leading up to the flyby. If not, the mission may be lost if a missed-thrust event occurs during a thrust arc prior to the gravity assist.

1. Introduction

Although the idea of electric propulsion has existed for many decades, with the first known reference attributed to rocket pioneer Robert Goddard, it is not until relatively recently that the technology has begun to see substantial application in interplanetary space missions. The missions Deep Space 1 [1], Hayabusa [2], and Dawn [3] have all used the high-ΔV capability of electric propulsion to visit and study small bodies in the Solar System. Notably, Dawn is the first mission to have successfully orbited two separate extraterrestrial objects, the asteroid Vesta and the dwarf planet Ceres.

Several missions are currently in the conceptual or planning stages that may also use electric propulsion. The Mars Sample Return Orbiter [4] and Asteroid Retrieval Mission are two notable examples of missions where electric propulsion may achieve goals that may not be possible with traditional chemical propulsion.

1.1 Electric Propulsion Technology

For the purposes of this work, there are two main components of an electric propulsion system: the thruster and the power source. The thruster takes an input of electric power and converts it to thrust using by ionizing a gas and accelerating it with an electromagnetic field. The propellant is commonly xenon, although other gases are candidate propellants. Currently existing thrusters include NSTAR (used on Dawn) and NEXT (successor to NSTAR), which are gridded ion thrusters, and BPT-4000, which is a Hall effect thruster commonly used on geocentric communication satellites. HiVHAC [5] is another Hall thruster under development by NASA. In practice, the primary difference between gridded ion thrusters and Hall effect thrusters is the specific impulse, with gridded ion thrusters operating at higher specific impulse and lower thrust compared to Hall effect thrusters. Both technologies, however, have

substantially higher specific impulse than chemical propulsion, with a lower limit of around 1500 seconds.

Separate from the thruster is the power source. In general, more power available to the propulsion system results in higher payload masses and overall higher efficiency. The only power source to have ever been used on an electric propulsion mission is solar power. The combination of solar power and an electric thruster is commonly referred to as solar electric propulsion (SEP). SEP has the advantage of using technology that is very mature and flight-proven, however its primary drawback is the rapid drop in power available to the spacecraft as distance from the Sun increases. A mission to Jupiter would see a 27-fold decrease in power as it approaches its target, and a mission to Saturn would see a nearly 100-fold decrease in power.

Another potential power source is a nuclear fission reactor. Combining a nuclear reactor with an electric thruster is commonly referred to as nuclear electric propulsion (NEP), and is not to be confused with nuclear thermal rockets which use heat from the reactor to accelerate propellant. In an NEP spacecraft, the nuclear reactor operates like one on Earth, generating electricity through a thermal cycle. In theory, NEP should be capable of much higher power levels for a given mass than we can expect from SEP. That power would not depend on distance from the Sun, meaning there is no limit to the operating range of an NEP spacecraft. Unfortunately, development of in-space nuclear reactors has been intermittent due to both technological and political obstacles. Nevertheless, NEP remains the most promising propulsion technology for future missions in the long run, especially for very large scale human missions with power levels greater than 1 MW.

1.2 The Trajectory Optimization Problem

Although electric propulsion promises higher payload masses than chemical propulsion, and enables missions that would not be possible with chemical propulsion, the trajectory design process is more complex for spacecraft with electric propulsion. At

the heart of the matter is the fact that the low thrust levels produced by electric propulsion (< 1 N) require the thruster to operate for a long amount of time during the mission, potentially even for the entire length of the trajectory. Thus, we cannot model the impulse from an electric thruster as an instantaneous ΔV, as we can with chemical propulsion. Instead, the trajectory design process is inherently coupled with the spacecraft systems.

The equations of motion for a spacecraft subject to accelerations from gravity and a thruster are

$$\dot{x} = v_x \tag{1.1}$$

$$\dot{y} = v_y \tag{1.2}$$

$$\dot{z} = v_z \tag{1.3}$$

$$\dot{v}_x = -\frac{\mu x}{r^3} + \frac{T u_x}{m} \tag{1.4}$$

$$\dot{v}_y = -\frac{\mu y}{r^3} + \frac{T u_y}{m} \tag{1.5}$$

$$\dot{v}_z = -\frac{\mu z}{r^3} + \frac{T u_z}{m} \tag{1.6}$$

$$\dot{m} = -\frac{T}{g_0 I_{sp}} \tag{1.7}$$

where T is the thrust, $\mathbf{u} = u_x\hat{x} + u_y\hat{y} + u_z\hat{z}$ is the thrust direction, m is the spacecraft mass, I_{sp} is the spacecraft specific impulse, and $g_0 = 9.80665$ m/s^2 is the standard gravitational acceleration on the surface of Earth. The presence of T and I_{sp} in the equations of motion explicitly relate the trajectory to the spacecraft propulsion system. The goal for designing a low thrust trajectory is to find a thrust control law (a function providing thrust magnitude and direction) that satisfies some optimization condition. Typically, this condition is to maximize final mass, minimize time of flight, or some combination of both. Because the answer to the optimization problem is a continuous function, we can consider this an infinite-dimension problem. There is a large body of research dedicated to solving this problem [6–11].

Further complicating matters, T and I_{sp} typically vary during a trajectory for SEP spacecraft, which have a strong dependence between power available and distance from the Sun. The thrust and power are related by

$$T = \frac{2\eta P}{I_{sp} g_0} \tag{1.8}$$

where P is the thruster input power and η is the propulsive efficiency of the thruster ($0 \leq \eta \leq 1$). For an ideal thruster, η and I_{sp} are constants, but in practice they depend on power.

Given these considerations, we present here a study exploring capabilities and mission concepts enabled by electric propulsion. In Chapter 2 we discuss a feasibility study for a human mission to the dwarf planet Ceres. Ceres presents an interesting target for human exploration due to its accessibility and the likely presence of water ice. In Chapter 3, a low-thrust mission concept to the Jupiter Trojan asteroids is explored, with a trajectory search that takes into account the scientific objectives of a mission to the Trojans. In Chapter 4 we present another mission concept study for a sample return mission to the main belt asteroid Kleopatra, which could possibly be the exposed core of an ancient protoplanet. Finally, in Chapter 5, a method to predict the extra propellant and flight time required to complete a low-thrust mission in the event of an unplanned thrust outage is discussed. This analysis is a useful tool in assessing the robustness of a given low-thrust trajectory.

2. A Human Mission to Ceres

Among potential destinations for humans to explore in the Solar System, Ceres stands out as one well-suited to human exploration. However, there has been little research that has addressed the problem of sending a human crew to Ceres. Benton has proposed a nuclear thermal rocket (NTR) vehicle design that could reach Ceres [12], but to our knowledge there has been little else on the matter. Other destinations have been subject to more study. Chief among them is Mars, which has long been considered the natural next step for exploration after the Moon [13–19]. We have also seen proposals to send astronauts to a near-Earth asteroid (NEA) [20] and to a Lagrange point in the Earth-Moon system [21]. While authors have looked at electric propulsion missions to Ceres at least as far back as 1971 [22], they have focused on robotic probes such as Dawn, which reached Ceres in 2015 [3].

We aim to address this gap by presenting a low-thrust mission architecture that assesses the feasibility of a human mission to Ceres. Ceres possesses resources to aid in human exploration. Earth-based observations have demonstrated a high likelihood that significant quantities of water ice are present in the crust of Ceres [23, 24]. When Dawn begins its primary mission at Ceres in 2015, we will greatly expand our knowledge of the dwarf planet.

Reaching Ceres is a challenge because its very low gravity offers little assistance to a vehicle attempting to capture into orbit. Ceres' orbit also has an inclination of about 10.6 deg. At the same time, it lacks any appreciable atmosphere, so landing on Ceres would be similar to landing on the Moon or a large asteroid. On Mars, spacecraft can use the atmosphere to decelerate before landing, saving propellant. However, the atmosphere introduces significant uncertainty during landing, resulting in a target radius on the order of 10 km. On Ceres, thrusters must provide all deceleration, but in principle a more accurate landing should be possible.

We present a high-level mission concept to send human astronauts to Ceres and back. We focus on the low-thrust trajectory design but do not present a detailed design of a transfer vehicle. However, estimates of the masses of the vehicles, the propellant costs, and the total initial mass in low Earth orbit (IMLEO) are provided. In addition, we provide a method to scale the mass results up or down to accommodate a payload mass different from the one assumed here. Our primary goal is to determine whether a human mission to Ceres is feasible given current technology and to identify which technological areas require further development.

2.1 Design Methodology

2.1.1 Mission Architecture Overview

This mission presented here is built around the assumption of a two-vehicle, low-thrust propulsion concept. The first vehicle is the supply transfer vehicle (STV) and its mission is to deliver all supplies necessary to sustain the crew while on Ceres as well as any propellant or equipment required to return to Earth. We assume that its mission must be successfully completed before the astronauts depart.

The second vehicle is the crew transfer vehicle (CTV). We begin our mission analysis assuming the CTV is already assembled in low-Earth orbit. It departs the Earth under the power of its electric propulsion using an elliptical spiral escape, performs an impulsive burn to achieve some departure V_∞, and uses electric propulsion to transfer to Ceres and back again to Earth. We will provide greater detail on each of these mission phases later in the chapter.

2.1.2 Constraints

The need to protect the crew from a lengthy period of deep-space radiation exposure is the main factor driving the trajectory design for the crew mission. While there is great uncertainty in the effects of deep-space radiation on the human body,

most authors indicate that such exposure would likely lead to fatal cases of cancer as well as other non-cancerous diseases [25]. We have constrained the Ceres-bound and Earth-bound legs to be no more than 270 days each, and the total time spent by the crew away from Earth on the Ceres mission to be no more than 2 years. For comparison, the NASA Mars Design Reference Architecture 5.0 (DRA5) specifies a maximum 180-day time of flight each way. While DRA5 has a total of six months less time in deep-space, the crew remains on the Martian surface for over a year, so the total time away from Earth is longer than the 2 year constraint we use here. A preliminary analysis indicated a 270-day constraint provides a good balance between minimizing crew exposure to radiation while still requiring a reasonable IMLEO cost. We will return to the question of how this constraint affects IMLEO later in the chapter.

Cucinotta and Durante [26] estimate that, given flight times similar to what we use here, the increased risk of developing a fatal case of cancer caused by exposure to deep-space radiation is about 4.0% for men and 4.9% for women, although these numbers are highly uncertain. While limiting flight times is one possible way to mitigate the risks faced by the crew, we acknowledge that the risk and uncertainty associated with deep-space radiation remains a major dilemma for human exploration of the Solar System.

Upon arrival at Ceres, the V_∞ is constrained to be zero. This constraint is required because aerobraking is not possible at the atmosphere-free Ceres, and its gravity is so low that an impulsive capture maneuver is prohibitively expensive. When capturing into orbit around an object using chemical propulsion, the capture maneuver is performed at the periapsis of the approach hyperbola, where thrust is most efficient. Smaller objects require greater ΔV to capture compared to larger objects for the same approach V_∞.

2.1.3 Technology Assumptions

To make this mission possible while meeting the constraints, a nuclear electric propulsion (NEP) system is used throughout all stages of the mission. The low gravity and non-existent atmosphere on Ceres means that an impulsively propelled mission would require a significant amount of propellant to capture into orbit around Ceres and land. Unlike Mars, no aerocapture or aerobraking is possible. For these reasons, an electric propulsion system is selected because it allows the spacecraft to reach Ceres on a zero-V_∞ approach and spiral down to a low parking orbit. A nuclear power system is chosen over a solar-electric one because its specific mass is lower and its power output remains constant. For this study, we assume a propulsion system specific mass of $\alpha = 5$ kg/kW. This specific mass is in line with proposed methods of space-based nuclear power generation [27, 28].

In addition to a nuclear power source, the mission requires an electric engine capable of meeting the thrust and specific impulse requirements. The VASIMR engine [29] is one such propulsion concept under development, and the magnetoplasmadynamic thruster (MPD) is another technology that has seen some study [30]. We assume a propulsive efficiency of 70%. As we will see, the architecture presented here–to minimize IMLEO–requires a thruster capable of processing 11.7 MW of input power at a constant specific impulse of 6800 s.

2.1.4 Outbound Trajectory Design

To minimize IMLEO for the mission, we perform a straightforward grid search of the trajectory design space with departure V_∞ and spacecraft power as our design variables. In creating this grid, we search over a range of 6 – 14 MW for power, in increments of 2 MW, and 0 – 3 km/s for V_∞, in increments of 1 km/s. This range yields a total of 20 possible design points. In the grid study, we proceed by first designing the interplanetary trajectory, next computing the ΔV for the Earth-orbit departure, and then designing an elliptical spiral that uses electric propulsion to

escape low-Earth orbit. These steps are described in detail in sections 2.4.1 – 2.4.3, as follows.

Interplanetary Trajectory

At each design point, we use the software package MALTO (Mission Analysis Low-thrust Trajectory Optimization) to design a low-thrust trajectory. MALTO is developed and maintained by the Jet Propulsion Laboratory, and uses a direct method to produce optimal low-thrust trajectories [31]. For this study, we direct MALTO to produce a trajectory from Earth to Ceres that delivers 125 Mg (i.e. metric tons) of mass in 270 days, while minimizing the total departure mass. This 125 Mg includes the propulsion system mass. During the optimization process, the launch date is free, while the specific impulse is chosen from the range of 2000 – 8000 s. At the end of this step, we have the mass of the propellant required for the interplanetary leg and can compute the associated tank mass. We assumed a structural mass factor of 15%.

Earth Orbit Departure

Once we know the mass at the start of the interplanetary leg, we need to compute the mass of the chemical stage which places the transfer vehicle on an escape trajectory with the appropriate departure V_∞. The maneuver occurs at the perigee of a highly elliptical orbit, discussed in the next section. First, the escape ΔV is computed by taking the difference between the hyperbolic perigee velocity and the elliptical perigee velocity:

$$\Delta V = \sqrt{\frac{V_\infty^2}{2} + \frac{2\mu}{r_p}} - \sqrt{\frac{(1+e)\mu}{r_p}} \tag{2.1}$$

To achieve a 3 km/s V_∞ from an orbit with 0.95 eccentricity and 350 km perigee altitude, a ΔV of 543 m/s is required.

Then, the propellant mass is computed using the rocket equation, assuming an LH2/LOX propulsion stage with $I_{sp} = 450$ s:

$$m_0 = m_f \exp\left[\Delta V/(I_{sp} g_0)\right] \tag{2.2}$$

Again, we compute the structural mass assuming a factor of 15%.

Elliptical Spiral

While it is possible to simply spiral away from the Earth with the electric propulsion engine by applying tangential thrust, this method would make it difficult for the crew to rendezvous with the transfer vehicle at the end of the spiral stage. The tangential spiral also makes it difficult to impart a departure V_∞ on the vehicle because the transfer from elliptical to hyperbolic orbit occurs at a point far away from Earth. A direct injection from low Earth orbit (LEO) to interplanetary transfer is also possible with a chemical propulsion stage, but this would be an inefficient use of propellant, especially for a spacecraft already equipped with a highly efficient electric propulsion system.

Instead, we employ an elliptical escape spiral similar to that proposed by Sweetser et al. [32]. Following their method, the spacecraft begins in LEO, and uses its electric propulsion system to spiral away from the Earth (without crew on board) with a steering law that keeps perigee constant while increasing apogee and eccentricity. An example of such a trajectory is shown in Fig. 2.1.

Because MALTO is not capable of computing the propellant required for an elliptical escape spiral, we use MATLAB to integrate the trajectory with the steering law from Sweetser et al., where we derive the steering law in terms of the modi-

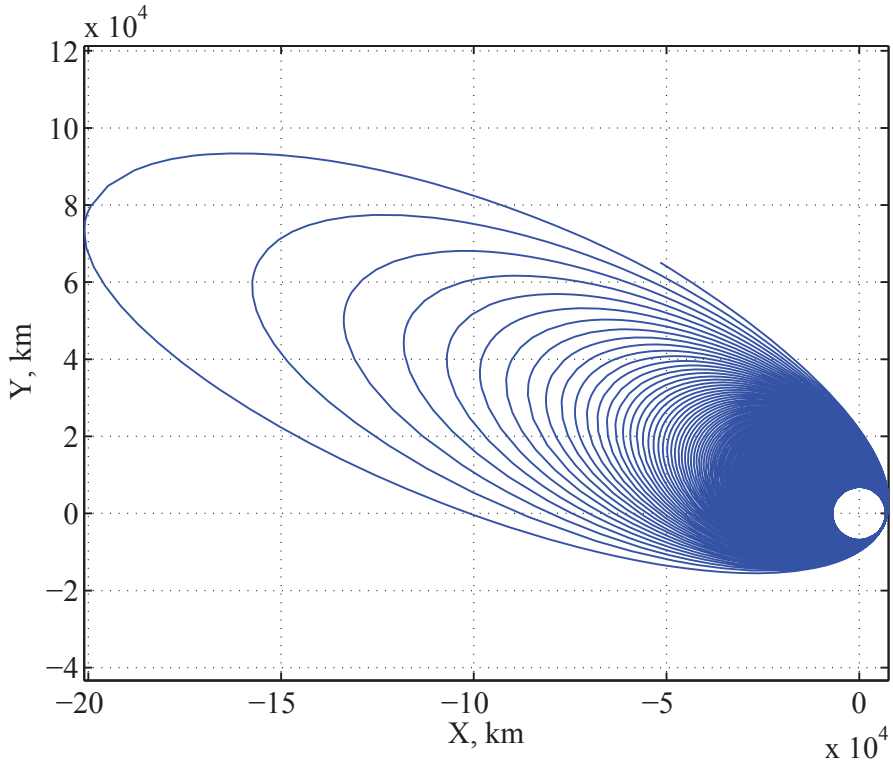

Figure 2.1.. This example shows the elliptical spiral trajectory of the crew transfer vehicle which maintains a constant perigee while using continuous low thrust to raise apogee. To avoid excessive exposure to radiation, the crew boards the crew transfer vehicle only after the orbit eccentricity reaches 0.95.

fied equinoctial elements provided by Walker et al. [33]. The modified equinoctial elements can be obtained by a simple transformation of the classical orbital elements

$$p = a(1 - e^2) \tag{2.3}$$

$$f = e\cos(\omega + \Omega) \tag{2.4}$$

$$g = e\sin(\omega + \Omega) \tag{2.5}$$

$$h = \tan(i/2)\cos\Omega \tag{2.6}$$

$$k = \tan(i/2)\sin\Omega \tag{2.7}$$

$$L = \Omega + \omega + \theta^* \tag{2.8}$$

Gauss' Planetary Equations in terms of the modified equinoctial elements are

$$\dot{p} = \frac{2p}{w}\sqrt{\frac{p}{\mu}}a_\theta \tag{2.9}$$

$$\dot{f} = \sqrt{\frac{p}{\mu}}\left[a_r \sin L + [(w+1)\cos L + f]\,\frac{a_\theta}{w} - (h\sin L - k\cos L)\frac{g a_h}{w}\right] \tag{2.10}$$

$$\dot{g} = \sqrt{\frac{p}{\mu}}\left[-a_r \cos L + [(w+1)\sin L + g]\,\frac{a_\theta}{w} + (h\sin L - k\cos L)\frac{f a_h}{w}\right] \tag{2.11}$$

$$\dot{h} = \sqrt{\frac{p}{\mu}}\frac{s^2 a_h}{2w}\cos L \tag{2.12}$$

$$\dot{k} = \sqrt{\frac{p}{\mu}}\frac{s^2 a_h}{2w}\sin L \tag{2.13}$$

$$\dot{L} = \sqrt{\mu p}\left(\frac{w}{p}\right)^2 + \frac{1}{w}\sqrt{\frac{p}{\mu}}(h\sin L - k\cos L)a_h \tag{2.14}$$

where the a_i are the components of the thrust acceleration in the orbit-fixed frame, s_L and c_L represent $\sin L$ and $\cos L$, respectively,

$$w = 1 + f\cos L + g\sin L \tag{2.15}$$

and

$$s^2 = 1 + h^2 + k^2 \tag{2.16}$$

To derive the steering law, we start by expressing the perigee radius in terms of the modified equinoctial elements:

$$r_p = a(1-e) = \frac{p}{1+\sqrt{f^2+g^2}} \tag{2.17}$$

where a here is the orbit semi-major axis.

Since we are holding perigee constant throughout the trajectory, we differentiate Eq. (2.17) and set the right hand side to zero:

$$\dot{r}_p = (1+\sqrt{f^2+g^2})\dot{p} - pf\dot{f} - pg\dot{g} = 0 \tag{2.18}$$

Next, we substitute Eqs. (2.9), (2.10), and (2.11) into Eq. (2.18) and group together the coefficients of the acceleration components. The a_h terms cancel out leaving us with

$$(-fs_L + gc_L)\, a_r + \left\{ \frac{2(e+e^2)}{w} - \frac{f}{w}[(w+1)c_L + f] - \frac{g}{w}[(w+1)s_L + g] \right\} a_\theta = 0 \tag{2.19}$$

The coefficient of the a_θ term can then be simplified using Eq. (2.15) and noting that $e^2 = f^2 + g^2$

$$(-f\sin L + g\cos L)\, a_r + \frac{1}{w}\left[2e + 2e^2 - (w+1)(f\cos L + g\sin L) - (f^2+g^2)\right] a_\theta = 0 \tag{2.20}$$

$$(-f\sin L + g\cos L)\, a_r + \frac{1}{w}\left[e^2 + 2e - (w^2-1)\right] a_\theta = 0 \tag{2.21}$$

The steering angle, β, is defined here as the angle from the local horizon to the thrust vector, and is given by

$$\tan\beta = \frac{a_r}{a_\theta} = \frac{e^2 + 2e - w^2 + 1}{w(f\sin L - g\cos L)} \tag{2.22}$$

In the form originally given by Sweetser et al. [32], the steering law produced a singularity when the spacecraft reached periapse and apoapse. This singularity required the user to modify the steering law slightly when implementing it numerically. Using the form presented in Eq. (2.22), numerical difficulties did not occur when propagating a trajectory using the elliptical spiral steering law.

While it is not obvious upon examining the control law as presented here, intuitively we can surmise that when the spacecraft is at perigee, thrust should be in the tangential direction, and when the spacecraft is near apogee, thrust cannot be in the tangential direction, or else it will raise perigee. So in general, the thrust direction for true anomalies near 180 degrees will tend towards the radial direction. However, radial thrust does not increase the energy of the orbit and is an inefficient use of propellant if we want the spacecraft to escape. Therefore, we can save propellant by setting a maximum true anomaly, θ_{max}, beyond which the spacecraft will coast. It

will resume thrusting after it passes $2\pi - \theta_{max}$. While this modification to the control law does save propellant, it comes at the expense of increased time in the elliptical spiral stage. For this mission we have found by trial and error that $\theta_{max} = 60$ degrees to strike a good balance between propellant savings and increased time of flight.

We note that there may be a better and more efficient way to increase apogee and eccentricity than the Sweetser method, however the goal of this work is not to find the optimal solution, but a practical one that demonstrates the feasibility of the human mission to Ceres we are proposing here. There may exist a steering law that achieves the same target orbit as the elliptical spiral used here, but at a reduced propellant cost. Additionally, the Moon may be used as a gravity-assist body during the escape phase. These escape strategies should only reduce propellant usage, and hence IMLEO, for the mission. Because this study is intended as a high-level feasibility analysis, we will proceed with the non-optimal escape strategy which, as we will see, is adequate for the mission given our assumptions.

The CTV travels on a spiral trajectory for about 2 years to reach a highly eccentric orbit with $e = 0.95$ and a perigee altitude of 350 km. (Subsequently, the crew is launched in a small capsule to rendezvous with and board the CTV.)

At each point in the grid study, we compute the propellant mass (and tank mass) required to bring the transfer vehicle and chemical departure stage from LEO to the highly elliptical orbit. This computation is done by backwards propagation from an elliptical orbit ($e = 0.95$) with the final mass required for the impulsive escape maneuver to a circular orbit of 350 km altitude. The initial mass (computed at the end of the backward propagation) is a reasonable estimate of the total IMLEO required to complete the mission.

2.1.5 Computing Payload Mass

While each trajectory delivers 125 Mg to Ceres, the payload mass varies because we must deduct the inert mass of the propulsion system from the final mass.

$$m_{pl} = m_f - \alpha P - \mu_p m_p \tag{2.23}$$

The propulsion system inert mass includes the nuclear reactor, the thrusters, and the propellant tanks. So while high-power missions will tend to use less propellant than low-power missions, they will require a larger power system mass. These competing effects generally result in an optimum propulsion power level that balances propellant mass with inert mass.

2.1.6 Scaling the Results

MALTO is able to compute a trajectory that minimizes initial mass given a fixed final mass, but it is not able to do the same given a fixed payload mass. Because of this, the set of trajectories produced by the grid search are unequal in the sense that they do not deliver the same usable payload to Ceres. To account for this fact, we adopt the scaling method presented by Landau et al [34]. This method allows the mission planner to take a trajectory that delivers a particular payload mass, m_{pl}, and scale it up in such a way that the scaled trajectory follows the same course and has the same time of flight, but delivers a new payload mass, m^*_{pl}, to the destination. The first step is to compute the scaling factor, μ_{sc}:

$$\mu_{sc} = m^*_{pl}/m_{pl} \tag{2.24}$$

Then, this factor can be used to scale up other key mission parameters, such as spacecraft power and thrust:

$$P^* = \mu_{sc} P, \quad T^* = \mu_{sc} T \tag{2.25}$$

We are also able to scale up the propellant masses and total IMLEO for the trajectory:

$$m^*_p = \mu_{sc} m_p, \quad m^*_{LEO} = \mu_{sc} m_{LEO} \tag{2.26}$$

For each design point in the grid search, we have scaled the final payload mass to 75 Mg and adjusted the spacecraft power for each design accordingly.

2.1.7 Return Trajectory

To design the return trajectory, we again use MALTO. In a manner similar to designing the outbound trajectory, we fix the mass at Earth arrival to be 125 Mg, constrain the flight time to be no more than 270 days, and direct MALTO to minimize the propellant mass. We assume that the transfer vehicle restocks the propellant it needs for the return leg at Ceres. The return propellant may either be delivered directly in the supply mission, or it may be produced by an in-situ propellant facility delivered on the supply mission. Here we assume it is delivered on the supply mission. Upon return to Earth, the arrival V_∞ is constrained to less than 4.5 km/s, which results in an atmospheric entry velocity of around 12 km/s. For reference, the Apollo entry velocity was about 11 km/s [35]. The ability to use the Earth's atmosphere to capture significantly reduces the propellant required on the return trip compared to the outbound trip.

2.1.8 Supply Mission

Before any mission carrying astronauts departs for Ceres, a mission to bring supplies and resources to Ceres should have been successfully completed. We perform another grid search to estimate the IMLEO of such a cargo mission in a manner much the same as that of the human mission. The supply mission analysis is different from the human mission in that 1) the time of flight is constrained to 2 years, and 2) the grid search is one-dimensional over power.

Departure V_∞ is constrained to be zero. This constraint allows the supply vehicle to depart Earth on a circular spiral, which is possible because the absence of crew removes the need for the elliptical spiral. The power level is varied from 1 – 3 MW in increments of 0.5 MW in search of an optimal solution. Our search range is lower

than that of the human mission because the longer time of flight allows for lower thrust and lower power. Longer TOF constraints are allowed on the supply mission because radiation is not an issue when humans are not present.

2.2 Results

2.2.1 Human Mission

Table 2.1 contains the complete listing of results from the outbound grid search. Of the original twenty design points, four were found to be infeasible given the mission constraints, leaving us with 16 design points. Except for the last column, the results in Table 2.1 are not scaled and all deliver the same final mass of 125 Mg to Ceres. They differ in payload mass because of the different propulsion system masses, but our interest is in delivering a 75 Mg payload. In Table 2.1, m_1 and m_2 refer to the total spacecraft mass after the elliptical spiral and after the impulsive escape burn, respectively. A useful measure of merit to compare the different missions is the ratio of payload mass to IMLEO. We found that the missions which made the most efficient use of the total initial mass were the same ones that required the least initial mass when all the design points were scaled. The final scaled IMLEO is given in the final column as m^*_{leo}. For example, in the first row of Table 2.1, we compute $\mu_{sc} = 75/63 = 1.194$, and then multiply m_{leo} by μ_{sc} to get $m^*_{leo} = 542$ Mg. Similarly, $P^* = 6 \times 1.194 = 7.16$ MW, $m^*_1 = 470$ Mg and $m^*_2 = 406$ Mg (V_∞ is not scaled, so $V_\infty = 3$ km/s).

In Fig. 2.2, we have taken the data from Table 2.1 and scaled the masses so that each design point in the plot delivers 75 Mg of usable payload to Ceres. The minimum solution has a power of 11.2 MW (which was scaled up from 10 MW) and a departure V_∞ from Earth of 3 km/s. Following the trend shown on the plot, a higher departure V_∞ may lower total IMLEO further, but the returns appear to diminish.

A local minimum appears along the power dimension because there is a balance between the increased efficiency at higher power levels and the increased mass of the

Table 2.1.. Results from the grid search before scaling where masses are in Mg (metric tons).

P, MW	V_∞, km/s	m_{leo}	m_1	m_2	m_{pl}	m_{pl}/m_{leo}	Return m_p	m^*_{leo}
6	3	454	394	340	63	0.14	120.0	542
8	1	391	347	330	54	0.14	87.4	541
8	2	320	290	266	64	0.20	72.7	376
8	3	295	271	234	69	0.23	64.8	323
10	0	318	289	279	52	0.16	63.5	459
10	1	273	252	240	58	0.21	54.2	354
10	2	253	235	216	61	0.24	49.7	309
10	3	246	230	199	64	0.26	46.0	289[a]
12	0	253	235	227	50	0.20	45.6	381
12	1	230	216	206	53	0.23	40.4	326
12	2	221	209	192	55	0.25	37.3	302
12	3	221	210	181	57	0.26	35.1	292
14	0	222	210	202	43	0.19	35.5	383
14	1	209	198	189	45	0.22	32.3	345
14	2	203	194	178	47	0.23	30.3	324
14	3	207	198	171	48	0.23	29.3	323

[a] Best performing case, that is, lowest m^*_{leo} for fixed payload mass.

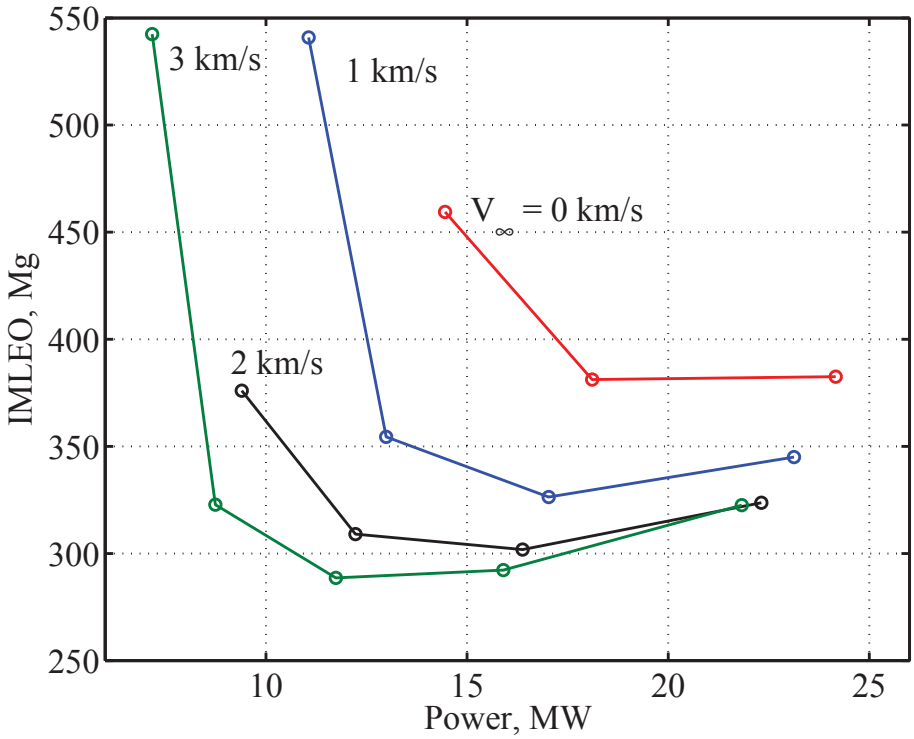

Figure 2.2.. The crew mission study reveals a minimum total IMLEO (after scaling) at a power level of 11.7 MW and departure V_∞ of 3 km/s. The numbers at the left end of each curve indicate the departure V_∞.

power system itself. MALTO is allowed to choose the optimum I_{sp} (within limits) at each design point, and at higher power levels it increases I_{sp} to decrease propellant consumption while keeping acceleration the same for the different trajectories. A similar effect occurs with departure V_∞, where at higher departure velocities, a higher I_{sp} can be used since the total change in orbital energy during the transfer is smaller and less thrust is required.

2.2.2 Scaling Accuracy

Because our result depends on the accuracy of the scaling method we applied, we validate the method by re-running a selection of design points in MALTO using the

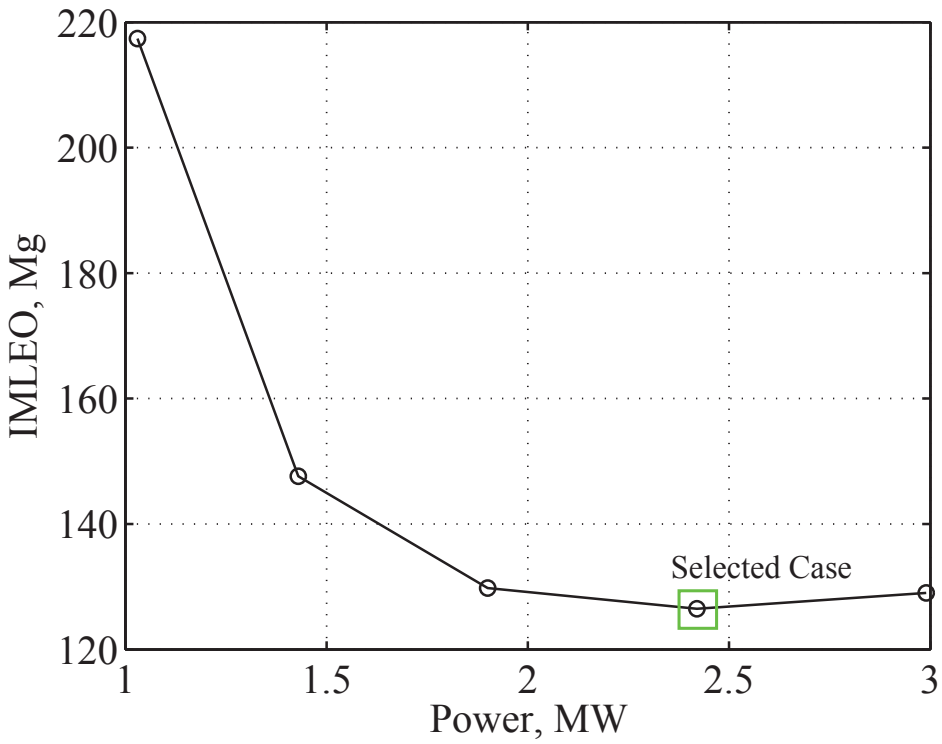

Figure 2.3.. The supply mission study reveals a local minimum IMLEO at about 2.45 MW. These results are scaled so that all the design points deliver an 80 Mg supply payload to Ceres.

scaled final mass as our delivered mass to Ceres (rather than the 125 Mg used in the original search) as well as the scaled power level. We then compute the IMLEO by computing the propellant and structural mass required to depart Earth with the elliptical spiral and chemical escape maneuver, as described in the Design Methodology section. Performing the second analysis with the 10 MW, 3 km/s V_∞ case results in an IMLEO of 289 Mg, while simply scaling the IMLEO from the initial run results in a value of 288 Mg, a difference of only 0.3%. Performing the same check on the second best design point (12 MW, 3 km/s) resulted in the same discrepancy of 0.3%. We conclude that the accuracy of the scaling method is sufficient for the purpose of this study.

2.2.3 Supply Mission

The results of the supply mission analysis, shown in Fig. 2.3, indicate that a minimum IMLEO is obtained using a power source of about 2.45 MW. This mission has an interplanetary flight time of 2 years and a circular spiral to depart Earth and capture into Ceres orbit. The mission brings 80 Mg of supplies and return propellant to Ceres and has an IMLEO of 127 Mg.

The supply mission analysis did not examine the effect of departure V_∞. Since the time constraints and human considerations are far less stringent on the supply mission, a circular spiral is used instead. The circular spiral precludes the use of a chemical escape booster since it cannot leverage a high perigee velocity. The propellant required for the circular spiral stage is computed by MALTO and does not require a separate analysis.

Because it is not evident that a circular escape spiral is more economical than an elliptical escape (as used in the human mission), we perform a simple trade study using an elliptical spiral escape for the supply mission to examine the effect of this escape method on IMLEO. Using the elliptical escape with no coast arc around apogee, we find that the minimum IMLEO occurs again at $P = 2.45$ MW, with an IMLEO of 132 Mg and a flight time of 345 days. This case is both more massive and takes longer than the circular escape method, which has an IMLEO of 127 Mg and escape time of 214 days. We may reduce propellant consumption at the expense of increased flight time by setting a maximum true anomaly past which the spacecraft does not thrust, as described previously. Setting $\theta_{max} = 135^\circ$ results in an IMLEO of 124 Mg—a savings of 3 Mg over the circular spiral. However these savings come at a cost of a 621 day flight time. Lowering θ_{max} to 60° reduces IMLEO to 121 Mg, but the flight time increases to an unacceptable duration of 2318 days.

2.2.4 Design Selection

After performing the grid search, we have identified a near-optimal design point for a human mission to Ceres. As we noted earlier, the selected design has an IMLEO of 289 Mg and a power of 11.7 MW and delivers a 75 Mg payload to Ceres. In Table 2.2 we can see the mass budget for the design after scaling is applied. For the electric propulsion system, the inert mass fraction is 45%. For the overall mission, 47% of the IMLEO is propellant, 27% is inert mass, and 26% is payload. The total IMLEO for the crew mission is 289 Mg, while for the supply mission the total IMLEO is 127 Mg. The combined IMLEO then, with an arbitrary margin of 10%, is 458 Mg. For comparison, the total on-orbit mass of the International Space Station is 450 Mg. We also note that four heavy lift launch vehicles would suffice to enable this mission.

Table 2.2.. Mass table for selected design.

Item	Mass, Mg
Spiral Propellant	18.3
Chemical Escape Propellant	31.3
Transfer Propellant	87.4
Chemical Escape Structure	5.52
Transfer Structure	13.0
Propulsion Inert Mass	58.7
Payload	75.0
Total	289

In Table 2.3 we have the time line for the full mission. The initial supply mission launches in October 2026, the crew mission departs in August 2030, and the crew returns to Earth in May 2032. Since the mission architecture does not involve any gravity-assist bodies, launch opportunities should repeat around the time when Ceres passes the ascending or descending node, or roughly every 2.3 years.

Table 2.3.. Time line of mission events.

Event	Date, m/d/y
STV launches and begins spiral	10/19/2026
Supply mission departs	5/27/2027
Supply Mission Arrives	5/21/2029
Crew Vehicle Begins Spiral	before 7/19/2028[a]
CTV Begins Interplanetary Leg	8/6/2030
CTV Arrives on Ceres	5/3/2031
CTV Departs Ceres	8/23/2031
CTV Returns to Earth	5/19/2032

[a] Spiral phase takes 748 days to complete as designed.

Figure 2.4 depicts the trajectory and events of the crew mission, including the outbound trajectory, the stay on Ceres, and the return trajectory. From a three-dimensional version of the trajectory plot, we learn that the surface operations on Ceres occur when Ceres is near the ecliptic plane and the Sun is between the Earth and Ceres. A simple analysis for our particular mission showed a minimum Sun-Earth-CTV angle of 2.15 degrees, which occurs when the CTV is at Ceres. Depending on the communications architecture used, extra communications infrastructure, such as an Earth-trailing satellite, may be required to ensure an uninterrupted link.

2.2.5 Time-of-Flight Trade Study

As we noted earlier, the question of how to constrain the TOF is not easily answered because of the great uncertainty in how the deep-space radiation environment affects the human body. Ideally, we need a way to directly compute the risk of losing a crew member (as a result of exposure to deep-space radiation on any given mission)

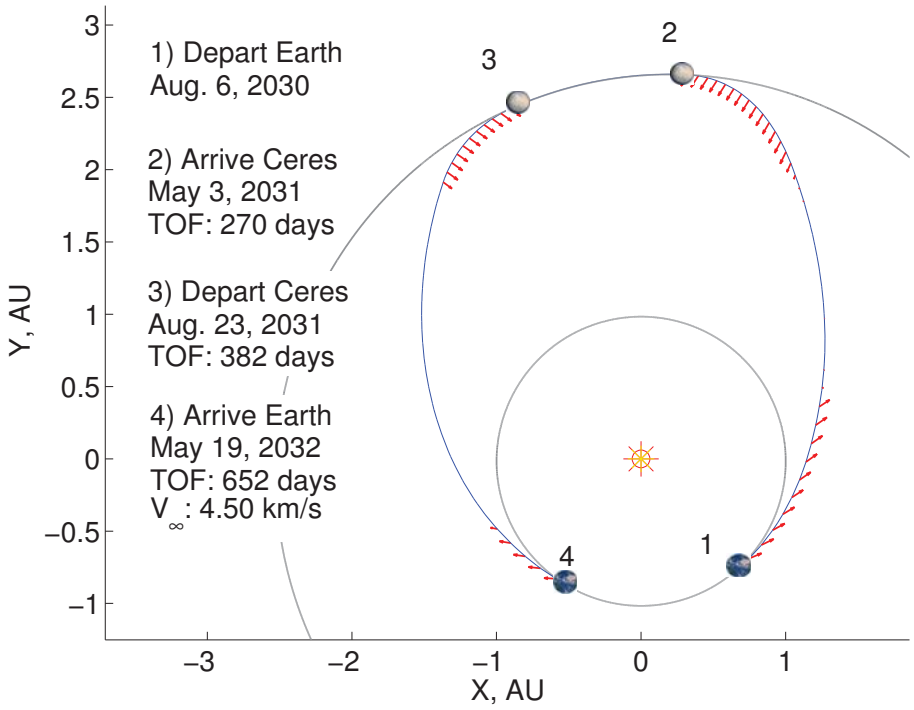

Figure 2.4.. 1) August 6, 2030: Crew departs Earth. 2) May 3, 2031: Crew Arrives at Ceres. 3) August 23, 2031: Crew departs Ceres. 4) May 19, 2032: Crew returns to Earth. Total mission time is 652 days or 1.79 years.

so we could set a TOF constraint directly based on that risk. However until we are able to perform such an analysis, we resort to simply constraining the time of flight to a feasibly low value.

In Fig. 2.5, we present the results of a trade study where we vary the time-of-flight constraint while keeping the payload mass and power constant. MALTO was allowed to adjust the launch and arrival dates, the I_{sp}, and the stay time on Ceres to minimize the initial mass. The I_{sp} was bounded between 2000 and 8000 s, and the stay time on Ceres was set to a lower bound of 90 days. TOF constraints ranged from 240 days

to 360 days in increments of 30 days. For each TOF constraint setting, we calculated the total IMLEO in the same manner as with the initial grid search.

What we see is that the 270-day TOF constraint appears adequate given the assumptions of the trade study. The phasing of the mission is a likely factor preventing significant reductions in IMLEO for longer TOF constraints. MALTO is given freedom to choose the launch dates in the mission, and it has chosen the dates such that the spacecraft arrives and departs Ceres while the dwarf planet is near the ascending node of its orbit. Arriving at Ceres while it is near the ascending node means that most of the plane change required to reach Ceres can be performed at a greater heliocentric distance, where less propellant is needed. Subsequently, when the TOF constraint is loosened, MALTO reduces the time spent on the surface of Ceres so that the arrival still occurs near the ascending node of the orbit, until the lower constraint on stay time (30 days) is reached. When no more time can be taken away from the surface operations and diverted to the transfer, the launch dates must be altered and there is less benefit to an increased TOF.

A more thorough analysis could be achieved by performing an entirely new grid search over power and departure V_∞ for each constraint, in essence adding the TOF constraint as a third design variable. However, in general it is reasonable to assume that a shorter TOF constraint will require more propellant and higher IMLEO, so the question becomes whether the mass savings of a longer TOF can be reassigned to bolster radiation shielding such that overall risk to the astronauts is reduced. We must, of necessity, leave this question open pending a reliable method of quantifying the radiation health risk.

2.3 Discussion

2.3.1 Key Technologies to Develop

The primary technology enabling a human mission to Ceres is a nuclear power system capable of generating 11.7 MW of power with a specific mass of 5 kg/kW. A

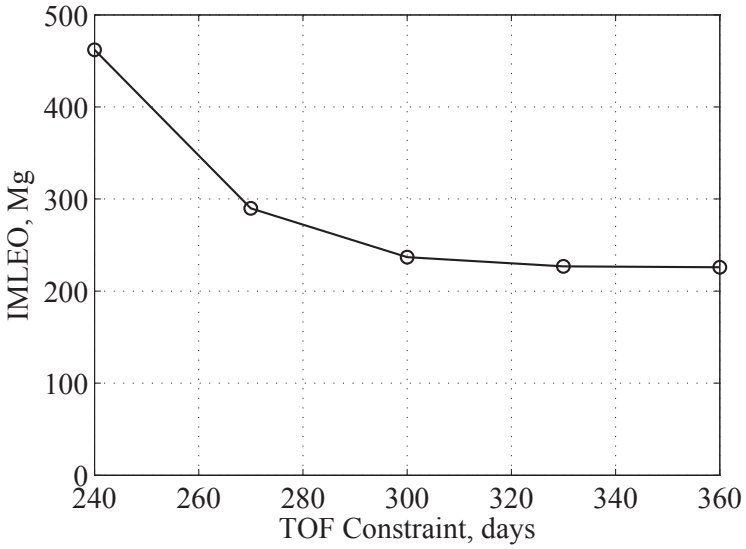

Figure 2.5.. The IMLEO increases dramatically for TOF constraints lower than 240 days. For the case study in this work a TOF of 270 days is assumed.

mission may be feasible with a smaller power system of around 8 – 9 MW, however more propellant and a higher IMLEO would be required. In addition to the power system itself, an electric propulsion technology capable of converting that power into thrust with an efficiency of about 70% is needed.

2.3.2 In-Situ Resource Utilization vs Pre-Delivered Propellant

Given that significant quantities of water ice exist in the regolith of Ceres (i.e. between 3% and 20% of the mass of the regolith), it is possible that a mission to Ceres could use that water to produce propellant for the return mission through electrolysis. The option of in-situ resource utilization would be attractive if the cost of sending the required equipment would be less than that of sending return propellant to Ceres. The in-situ propellant could feed a liquid-oxygen, liquid-hydrogen chemical propulsion system, or it may serve as the propellant for an electric system in the form

of H_2. In the latter case, the electric propulsion system would be limited to high specific impulse because of the very low atomic mass of hydrogen.

2.4 Conclusion

We can draw the following conclusions from this mission design study.

1. A human mission to Ceres could be made feasible with the appropriate investment in propulsion and in-space power technology. Given the assumptions used here, the total IMLEO, with a 10% margin, would be 458 Mg. The mission architecture presented here would deliver a total of 155 Mg of payload to Ceres over two missions. Four heavy-lift launch vehicles would suffice to carry out such a mission.

2. Nuclear electric propulsion technology enables human exploration at Ceres because it has a relatively low specific mass (i.e. about 5 kg/kW) and it avoids a costly impulsive capture maneuver at Ceres. Electric propulsion technologies capable of processing input power up to 11.7 MW (or more) should be further developed to open the possibility of exploring Ceres.

3. Total mission times of less than 2 years (for the crew) are possible with nuclear electric propulsion. In the absence of a proven method of blocking deep-space radiation, limiting mission times is the best way to limit the danger to the crew.

3. Solar Electric Propulsion Trajectories for a Mission to the Jupiter Trojan Asteroids

3.1 Introduction

The Trojan asteroids are objects of great interest to the planetary science community, and have been singled out as a high priority target for a future New Frontiers class space mission in the latest decadal survey [36]. The Trojan asteroids orbit beyond the main asteroid belt near the L4 and L5 Lagrange points of Jupiter. This orbit location means that it is unlikely a spacecraft will perform a flyby of an object in this population while on the way to another target, like the Galileo mission did with the main belt asteroid Ida on its way to Jupiter. Any mission to Jupiter would of necessity bypass the Trojan asteroids, and any mission to the other outer planets would likely perform a gravity assist maneuver at Jupiter, again precluding a Trojan flyby. Because of these considerations, a dedicated mission is likely the only practical way we may closely study a Trojan asteroid.

The objects that comprise the Trojan population are as large as 200 km across. The smallest observed objects are on the order of 1–2 km across, with an even greater unobserved population of smaller objects less than one kilometer across. Studying the Jupiter Trojans and learning where these asteroids came from and how they became locked in orbit with Jupiter could provide key knowledge about the formation history of the Solar System. One model of Solar System formation [37], often called the Nice model (after the city in France), proposes that the orbits of Jupiter and Saturn migrated early in the history of the Solar System, eventually entering a 1:2 mean motion resonance with each other. At this moment the dynamics of the outer Solar System became very unstable and chaotic, causing objects to migrate and scatter. One prediction of this model is that the objects that currently make up the Jupiter

Trojan population migrated inward from the outer regions of the Solar System [38,39]. The alternative to this idea is that the Trojans formed in place along with Jupiter and have remained there since the formation of the Solar System. Because the composition of an object in the Solar System depends how far away from the Sun it formed, these two models predict different compositions for the Jupiter Trojans.

Ground observations in the near-infrared spectrum have shown that the Trojans can be separated into two groups: one with a higher reflectance at longer (redder) wavelengths of light than the other. We refer to these two groups as the "red" group and the "less red" group. This dichotomy in spectral reflectance suggests that these two groups of objects have fundamentally different chemical and mineralogical compositions [40], and may point to two different origins for the different types of Trojans. These observations could be consistent with the Nice model of Solar System evolution, with a mixture of objects in the Jupiter Trojan population that came from different regions of the Solar System.

Ground observations, however powerful, can only tell us so much about the composition of an object, and much more can be learned by sending a spacecraft to study these objects in situ. Much higher resolution spectral data is possible with a spacecraft, giving a spectral map of the surface of an object. A spacecraft can also provide more information about the interior of an object by accurately measuring its density and probing the interior with radio waves. All of this information can be used to paint a more definitive picture of the composition of the Jupiter Trojans, which can in turn provide a more clear understanding of how our Solar System arrived at its current configuration.

For a spacecraft to rendezvous with such small objects (compared to planets), nearly all of the impulse must be provided by the spacecraft propulsion system, with very little assistance from the object's own gravity. For this reason, a rendezvous mission to a Jupiter Trojan may require prohibitively high ΔV for a spacecraft with traditional chemical propulsion, and may instead be better served by an electric propulsion system. Performing the mission with electric propulsion also opens up the

possibility of rendezvous with two or more objects, like the Dawn spacecraft has done at Vesta and Ceres [3].

Prior work has been has been performed studying trajectories to the Trojan asteroids. Stuart et al. [41–44] has studied low-thrust Trajectories to the Trojan asteroids in the circular, restricted three-body problem, presenting an algorithm to search for such trajectories. Diniega et al. consider the spacecraft design in a feasibility study showing a mission to the Trojans can be accomplished within the cost constraints of a New Frontiers class mission [45]. In 2005, Bonfiglio et al. [46] considered the use of radioisotope electric propulsion [an electric propulsion system powered by a radioisotope thermal generator (RTG)] for a mission to the Jupiter Trojans. At that time, electric propulsion systems were still relatively new, especially for interplanetary missions. The past ten years, however, has seen significant development go towards increasing the power available from solar arrays in response to the need for high-power solar electric propulsion (SEP) [47]. Solar arrays capable of generating 30 kW of power (and up) at 1 AU from the Sun are in development, and will enable electric propulsion missions out to the orbit of Jupiter (5.2 AU). At the same time, electric thruster technology has matured, with thrusters such as the BPT-4000 [48] (also designated the XR-5) logging substantial flight time in geocentric missions.

In this study, we search for launch opportunities in the years 2020–2040 for low-thrust missions to the Jupiter Trojan asteroids, with our study grounded in technology that is available today or in the near future (5 years). The search space of Jupiter Trojan asteroids is vast, with thousands of potential objects to visit. To avoid a computationally prohibitive search, we use knowledge of the scientific goals of a mission to the Trojans along with the principles of orbital mechanics to focus on trajectories that are likely to be of high scientific value while also yielding a relatively high payload mass.

3.2 Search Method

There are 6179 known objects classified as a Jupiter Trojan asteroid. Our primary objective is to find trajectories that rendezvous with two Trojans. If we were to simply examine each possible pair of objects, we would need to examine over 38 million pairs, each one requiring many initial guesses of launch and arrival dates to search over a span of time. Fortunately, we may use the basic principles of orbital mechanics combined with information about the scientific objectives of a mission to the Trojans to considerably reduce the search space.

3.2.1 Pruning the Search Space

First, a trajectory between an object in the L5 (trailing) and L4 (leading) camp, while possible, would have a long transfer time and require a large amount of propellant to complete in a reasonable time frame. Since there is no clear scientific advantage to justify such a trajectory, we will not consider such transfers. Additionally, since the L4 camp has almost twice as many objects as the L5 camp, we will restrict our search to trajectories between objects in the L4 camp. This restriction reduces the search space by roughly 50% from over 38 million pairs to just over 16 million.

Second, we limit our search to Trajectories that visit one object each from the red and less red group of Trojans. Some have suggested that one group may comprise of objects that formed in the inner Solar System while the other may comprise of objects that formed towards the outer Solar System, both being captured at Jupiter's Lagrange points along the way. Any mission to the Trojans that illuminates this issue will have broad implications for the story of how our Solar System formed, so a mission that visits one of each spectral type would have a significant scientific advantage over one that does not. We therefore further restrict our search to objects in the L_4 camp for which we have reliable ground observations and to pairs comprised of one of each type of object. In this work, we count objects among the less red group of Trojans

if they are reported in Emery et al. [40] to have 0.85–J color index of less than 0.19, and we count them among the red group otherwise. Reducing the search space on these grounds results in just 440 possible pairs.

While 440 pairs is a far more workable set than the original 38 million, it is still worthwhile to place higher priority on the pairs which are likely to require less propellant to visit. The Trojan asteroids all have relatively similar orbital distances, but they have a range of orbit inclinations and orientations. It requires a significant expenditure of energy (and hence propellant) to change the orientation of the orbit of a spacecraft traveling between two objects, so we will start by examining those pairs which require the least total orbital plane change to visit.

We define the total plane change, α, to be the sum of the inclination of the first body, i_1, and the angle between the orbit angular momentum vectors, β. Figure 3.1 shows a diagram of these angles.

$$\alpha = i_1 + \beta \tag{3.1}$$

A unit vector, $\hat{\mathbf{h}}$ in the direction of angular momentum (normal to the orbit plane) for a given Trojan can be computed from the longitude of the ascending node, Ω, and the inclination, i.

$$\hat{\mathbf{h}} = \cos\Omega \sin i\hat{\mathbf{y}} + \sin\Omega \sin i\hat{\mathbf{y}} + \cos i\hat{\mathbf{z}} \tag{3.2}$$

Then the angle between the orbit normal directions is computed with the dot product.

$$\beta = \cos^{-1}\left(\hat{\mathbf{h}}_1 \cdot \hat{\mathbf{h}}_2\right) \tag{3.3}$$

Finally, pairs of objects in which the sum of the diameters is greater than 200 km are considered. This restriction ensures that we focus on trajectories which visit the larger objects in the Trojan population. In the absence of more information, larger objects will tend to offer more features and return more data than smaller objects.

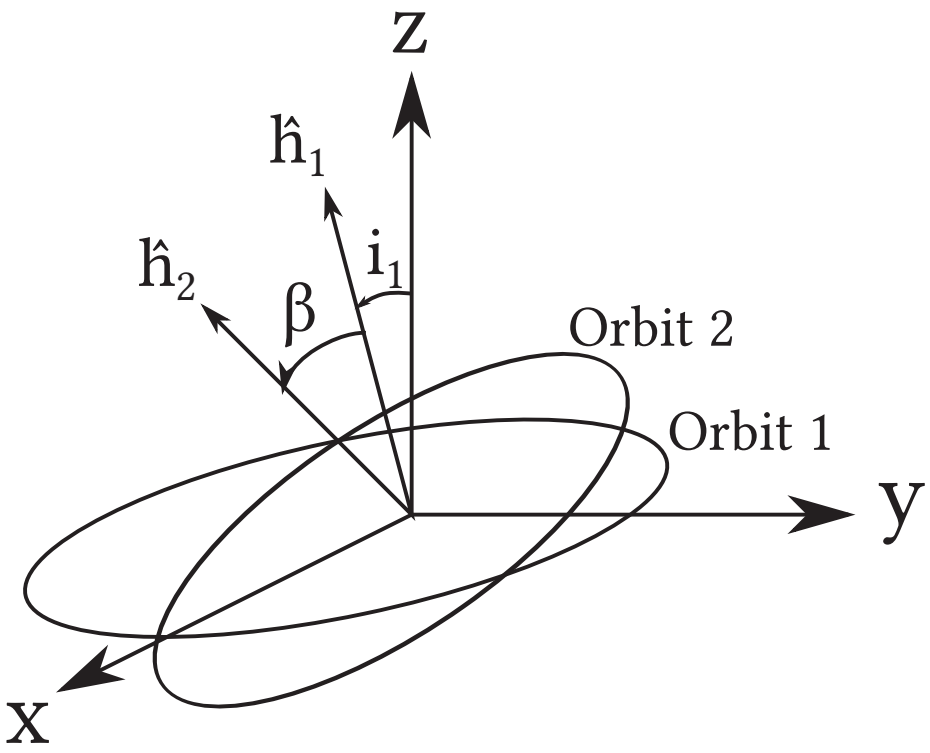

Figure 3.1.. The angle between the orbit normals, β, is the plane change performed by the spacecraft during the transfer between the two asteroids.

In Table 3.1 we have a listing of the pairs of Trojan objects which meet the aforementioned search criteria, listed in order of increasing total plane change. We have also included the plane change between each body. Since the interbody plane change does not depend on the order in which the objects are visited, there will always be an advantage to visiting the body with the lower inclination first. Visiting the bodies in that order will ensure that the total plane change is minimized for that pair.

3.2.2 Trajectory Search

Given a particular pair of Trojans, we must search for low-thrust trajectories during a prescribed time span which launch from Earth and rendezvous with each

Table 3.1.. List of target pairs meeting selection criteria, ranked by increasing total plane change required to visit both bodies.

Pair	$D_1 + D_2$, km	β, deg	$i_1 + \beta$, deg
(4138) Kalchas–(1143) Odysseus	213.6	1.2	3.3
(1143) Odysseus–(5244) Amphilochos	203.6	3.2	6.3
(1143) Odysseus–(659) Nestor	248.8	6.9	10.0
(659) Nestor–(588) Achilles	204.3	7.0	11.5
(1143) Odysseus–(3548) Eurybates	222.4	11.2	14.3
(659) Nestor–(3063) Makhaon	218.8	10.9	15.4
(1143) Odysseus–(5025) 1986 TS6	205.9	13.1	16.2
(1143) Odysseus–(4060) Deipylos	232.5	14.5	17.6
(1143) Odysseus–(23135) 2000 AN146	216.4	15.0	18.1
(659) Nestor–(624) Hektor	310.4	13.8	18.3
(5025) 1986 TS6–(624) Hektor	267.6	7.3	18.3
(588) Achilles–(1437) Diomedes	239.7	10.2	20.5
(1143) Odysseus–(3793) Leonteus	262.3	18.0	21.1
(2456) Palamedes–(1437) Diomedes	212.1	7.4	21.3
(4138) Kalchas–(624) Hektor	275.2	19.7	21.8
(659) Nestor–(911) Agamemnon	251.7	17.4	21.9
(5025) 1986 TS6–(911) Agamemnon	208.8	11.1	22.1
(3063) Makhaon–(1437) Diomedes	254.2	11.2	23.4
(3548) Eurybates–(624) Hektor	284.0	15.9	24.0
(1143) Odysseus–(1437) Diomedes	284.2	21.0	24.1
(3709) Polypoites–(3793) Leonteus	202.4	4.8	24.4
(624) Hektor–(1437) Diomedes	345.8	9.2	27.4
(1437) Diomedes–(911) Agamemnon	287.1	8.1	28.6

object. In this work, "rendezvous" refers specifically to a trajectory which arrives at the target body with zero relative velocity (V_∞). We look for trajectories that maximize final mass subject to a constraint on the time of flight.

$$\text{Minimize} \quad J = -m_f \tag{3.4}$$

subject to the boundary constraints:

$$\mathbf{X}(0) = \mathbf{X}_0 \tag{3.5}$$

$$\mathbf{X}(t_f) = \mathbf{X}_f \tag{3.6}$$

$$t_f \leq \tau_f \tag{3.7}$$

$$\tag{3.8}$$

where m_f is the total final mass of the spacecraft, $\mathbf{X}$ is the spacecraft state vector, t_f is the time of flight from launch to the second object, and τ_f is the maximum allowable time of flight. The objective is to find a launch date, arrival dates at each object, and thrust control history which maximize the final mass (or minimize $-m_f$).

There are numerous methods for solving the trajectory optimization problem, each with their own strengths and weaknesses [6]. Here, a direct method is used which converts the infinite dimensional optimal control problem to a finite parameter optimization problem by approximating the thrust control law as a series of small impulsive ΔV's. The optimization problem is solved with Mission Analysis Low-Thrust Optimization (MALTO) [31], a low-thrust design tool developed at the Jet Propulsion Laboratory (JPL). MALTO finds the thrust profile, launch V_∞ vector, launch dates, and arrival dates which maximize the final mass of the spacecraft using the optimization program SNOPT. However, MALTO alone only finds locally optimal trajectories. To search for a globally optimal solution, we generate a grid of initial guesses for the launch and arrival dates at Earth and the two Trojan targets, and run each initial guess in MALTO. The thrust profile for each guess is initialized at zero.

Our search used initial guesses for the Earth launch date ranging from January 1, 2020 to January 1, 2040, in increments of 200 days. For flight times between bodies,

we used a range of 730–3000 days, in increments of 200 days. Since each initial guess is an independent problem, we run many guesses in parallel to reduce computation time.

3.3 Spacecraft System Assumptions

3.3.1 Spacecraft Propulsion System

Because our goal is to provide a usable estimate for the payload masses we can deliver to the Trojan asteroids, we use propulsion system, power system, and launch vehicle models which closely match technology presently available. For the electric thrusters, we assume the spacecraft has two BPT-4000 Hall effect thrusters [48] which it may operate simultaneously. We use the following polynomials to model the thrust and propellant mass flow rate of the BPT-4000:

$$T(P) = \left(-8.597 + 77.34P - 2.119P^2 - 1.151P^3 + 0.1739P^4\right) \times 10^{-3} \quad \text{N} \tag{3.9}$$

$$\dot{m}(P) = (3.524 + 68.48P - 16.32P^2 + 2.351P^3 - 0.1195P^4) \times 10^{-7} \quad \text{kg/s} \tag{3.10}$$

where P is thruster input power in kilowatts, T is thrust in Newtons, and $\dot{m}$ is the mass flow rate in kilograms per second. Equations 3.9 and 3.10 are usable for power levels between 0.302 and 4.839 kW.

In Fig. 3.2, we have plotted Eq. 3.9, showing a close to linear relationship between thrust and thruster input power.

Figure 3.3 shows that the specific impulse of the BPT-4000 engine depends strongly on the input power, with higher powers yielding a higher specific impulse. In an ideal thruster, specific impulse does not depend on input power. The specific impulse is calculated from Eqs. 3.10 and 3.9 with

$$I_{sp} = \frac{T}{\dot{m} g_0} \tag{3.11}$$

where g_0 is the standard gravitational acceleration at sea level on Earth ($g_0 = 9.80665$ m/s^2).

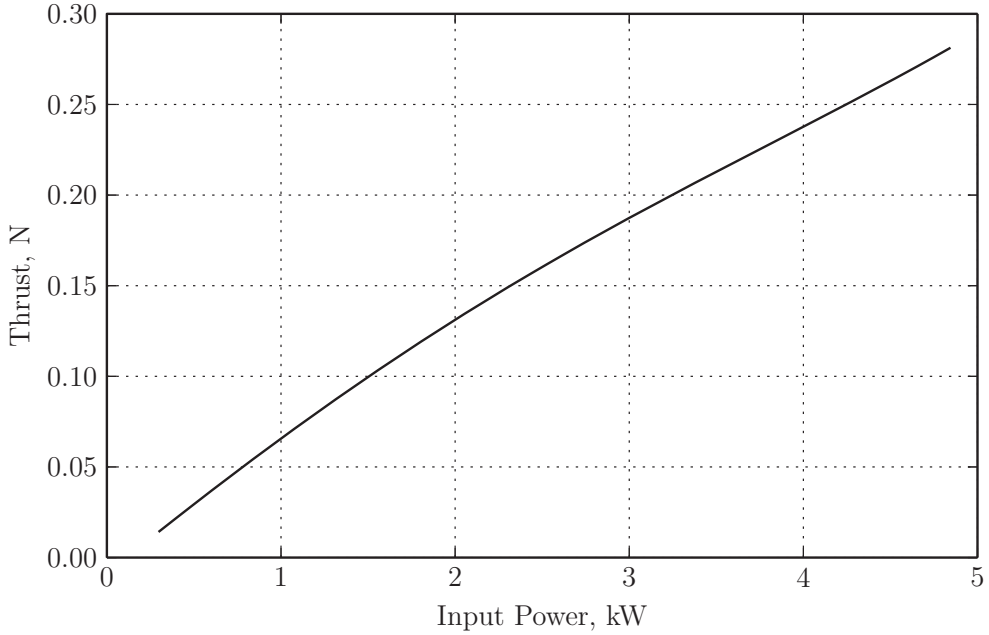

Figure 3.2.. The thrust for the BPT-4000 Hall thruster is a nearly linear function of the input power.

3.3.2 Spacecraft Power System

An important feature of solar electric propulsion is the dependency between power and distance from the Sun. To first order, the power available to the spacecraft follows an inverse square relationship with radial distance. However, this relationship means that very large gains in power are available close to the sun which may not actually be achievable with a real solar array. To account for this, we model the power available from the solar arrays with

$$P(r) = \frac{P_0}{r^2}\left(\frac{1.321 - \frac{0.108}{r} - \frac{0.117}{r^2}}{1 + 0.108r - 0.013r^2}\right) \tag{3.12}$$

The main effect of Eq. 3.12 is to reduce the gains in power realized by traveling to the inner Solar System.

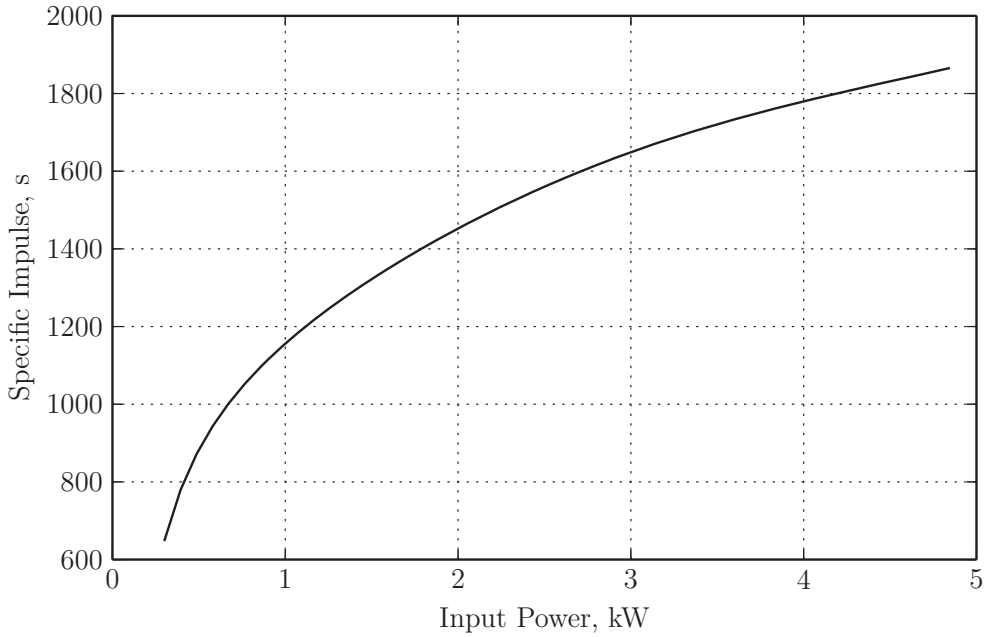

Figure 3.3.. The specific impulse drops significantly at lower power levels, reducing the efficiency of the thruster.

3.3.3 Launch Vehicle

To maximize final mass for a fixed flight time, it is often advantageous to rely on the launch vehicle to provide an initial departure velocity at the expense of a lower initial mass. We model the launch vehicle with a function that provides initial spacecraft mass as a function of launch energy [1] ($C_3 = V_\infty^2$)

$$m_0 = 6105 - 110.5C_3 + 0.6184C_3^2 - 1.926 \times 10^{-5}C_3^3 \tag{3.13}$$

Equation 3.13 gives the relationship between launch energy and initial mass for the Atlas V 551 launch vehicle, and is valid for $0 \leq C_3 \leq 60$ km^2/s^2. This launch vehicle provides the largest launch masses of the Atlas V family.

[1]Data available at: http://elvperf.ksc.nasa.gov/Pages/Query.aspx [Retrieved March 2014].

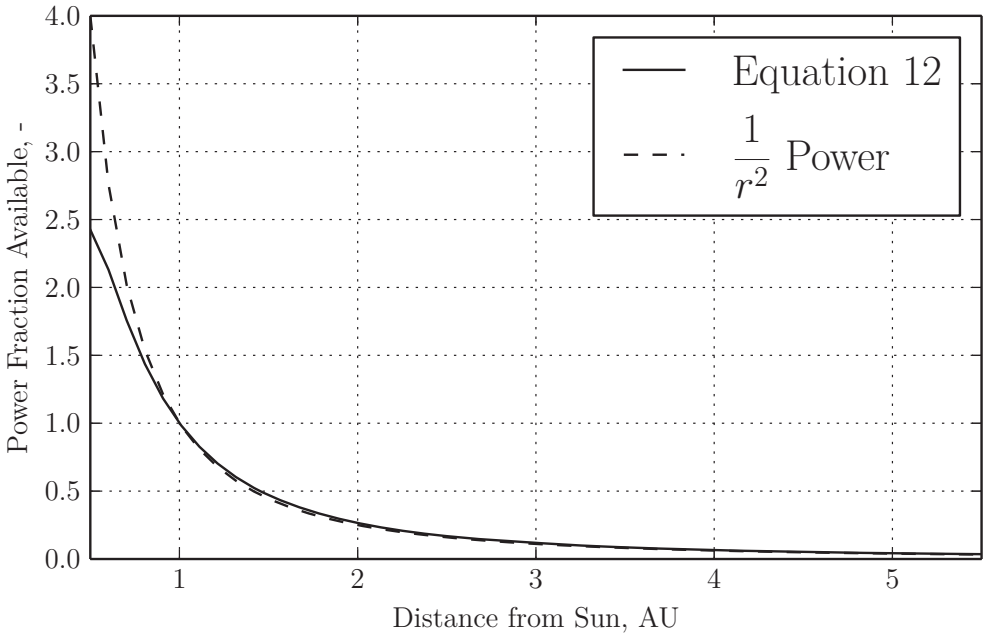

Figure 3.4.. The power available from Eq. 3.12 is shown compared to simple inverse square power.

3.3.4 Trajectory Constraints

For the broad search of trajectories to Trojan pairs, we assume the spacecraft is capable of producing 40 kW of power from its solar array at 1 AU from the Sun. Time of flight from launch at Earth until the end of the nominal mission at the second target is constrained to less than 12 years, assuming 180 day stay times at each of the bodies. Once the broad search is complete and trajectories with the greatest final mass are identified, the cost of tightening those constraints (i.e. lowering the spacecraft power and reducing the TOF constraint) is examined.

In addition to the power and TOF constraints, the propulsion system is modeled with a 90% duty cycle, which means the spacecraft only uses 90% of the thrust available at a given power input. This constraint allows for scheduled downtime during thrust arcs which may be set aside for communication and navigation. The

spacecraft bus is assumed to require 300 W of power to operate, independently of the propulsion system. This assumption effectively reduces the power available to the propulsion system, and is a significant reduction in the region near the Jupiter Trojans, where available power is reduced by a factor of 27.

3.4 Results

In Table 3.2 we have listed the maximum final mass trajectory for each Trojan pair examined, and in Table 3.3 we have a listing of the Trojan pairs which yielded the greatest payload masses for launch dates in each year from 2020 through 2040. We can see that the overall best pair to visit is 1986 TS6–Hektor, with a maximum final mass of 2268 kg for a launch in 2027. In addition, 1986 TS6–Hektor is the pair with the greatest payload mass in the years 2025–2029 and 2035, making it the pair that appears the most often during the search period. Also of note is that in 12 of of the 21 years considered, 1986 TS6 appears as one of the objects in the pair with the highest final mass.

After 1986 TS6–Hektor, the pair with the second best performance is Palamedes–Diomedes, with a maximum final mass of 2168 kg for a launch in 2037. Palamedes–Diomedes also turns out to be the best pair in the years 2036, 2037, and 2038.

In Fig. 3.5 we see a plot of the best results in each year, showing the peaks centered in the years 2027 and 2037. We also see the launch dates with minimum finals masses are 2023, 2033, and 2039. Even though we have searched through a fairly large set of pairs, we see the maximum final mass has a significant dependency on the launch year. Somewhat surprisingly, the pairs with the best performance do not have the lowest total plane change. However, 1986 TS6–Hektor and Palamedes–Diomedes do have relatively low interbody plane changes of 7.3° and 7.4°, respectively.

In Fig. 3.6, we have plotted the maximum final mass found for each target pair vs the total plane change required to rendezvous with each pair. From this plot, we can see the relationship between total plane change and final mass. It appears that

Table 3.2.. The maximum final mass found for each Trojan pair.

Trojan Pair	Max Final Mass, kg	Launch Year
1986 TS6–Hektor	2268	2027
Palamedes–Diomedes	2168	2037
Odysseus–Amphilochos	2164	2030
Odysseus–Nestor	2058	2029
Nestor–Makhaon	2052	2026
1986 TS6–Agamemnon	2049	2027
Odysseus–1986 TS6	1999	2029
Nestor–Achilles	1976	2026
Odysseus–Deipylos	1939	2035
Kalchas–Odysseus	1932	2030
Nestor–Hektor	1923	2028
Polypoites–Leonteus	1824	2037
Odysseus–2000 AN146	1808	2038
Nestor–Agamemnon	1808	2028
Eurybates–Hektor	1715	2022
Achilles–Diomedes	1652	2029
Makhaon–Diomedes	1596	2033
Kalchas–Hektor	1519	2022
Odysseus–Leonteus	1435	2036
Odysseus–Eurybates	1429	2033
Hektor–Diomedes	1316	2022
Odysseus–Diomedes	1198	2031
Diomedes–Agamemnon	965	2028

there is not a strong correlation between the total plane change and final mass for

Table 3.3.. List of trajectories with greatest final mass in each year from 2020–2040.

Year	Trojan Pair	Final Mass, kg	Propellant Mass, kg
2020	Odysseus-Nestor	1957	3265
2021	1986 TS6-Agamemnon	2003	3283
2022	1986 TS6-Agamemnon	1989	3240
2023	1986 TS6-Agamemnon	1872	3226
2024	Nestor-Makhaon	1946	3396
2025	1986 TS6-Hektor	2077	3183
2026	1986 TS6-Hektor	2213	3231
2027	1986 TS6-Hektor	2268	3617
2028	1986 TS6-Hektor	2209	3182
2029	1986 TS6-Hektor	2195	3140
2030	Odysseus-Amphilochos	2164	3188
2031	Odysseus-Nestor	2037	3291
2032	Odysseus-Nestor	1982	3256
2033	1986 TS6-Agamemnon	1845	3377
2034	Odysseus-Deipylos	1939	3393
2035	1986 TS6-Hektor	1944	3239
2036	Palamedes-Diomedes	2071	3261
2037	Palamedes-Diomedes	2168	3685
2038	Palamedes-Diomedes	2148	3148
2039	Odysseus-1986 TS6	1540	2952
2040	Odysseus-1986 TS6	1847	3178

plane change values below 20°. Beyond 20°, we can see final mass values begin to trend downward.

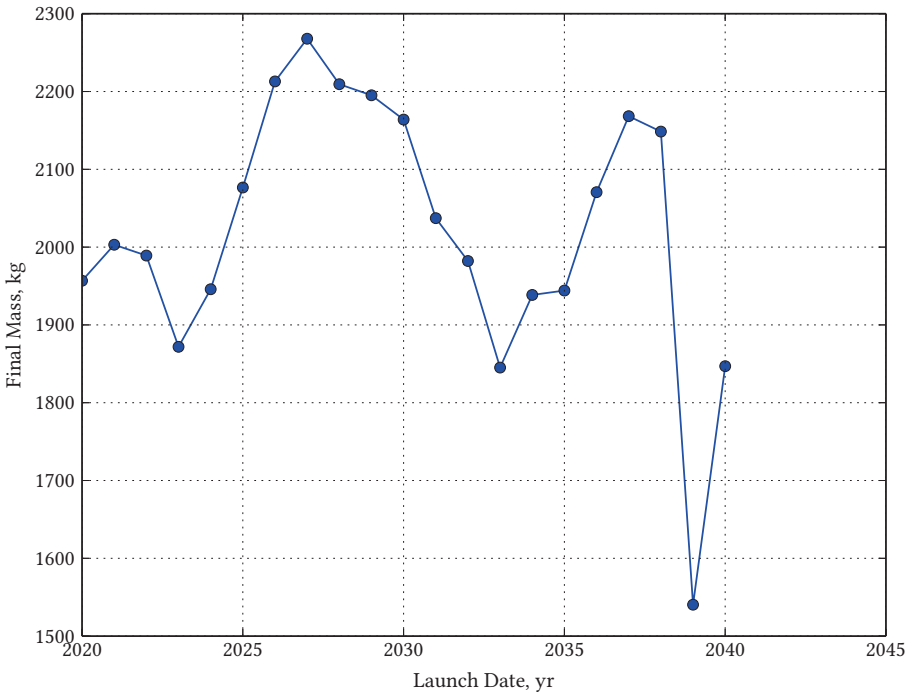

Figure 3.5.. The ideal launch dates for a mission to a pair of Trojan asteroids is 2026–2030, with the second best launch window occurring 2037–2038.

In Fig. 3.7, we have instead plotted the maximum final mass found for each target pair vs the plane change required to travel between the two bodies. This plot ignores the inclination change required to reach the first body. In this plot, we can see that interbody plane change is more important than total plane change, with a downward trend beginning at about 10°. Changing the orientation of the orbit when transferring between the Trojan asteroids requires more propellant than changing the orientation before reaching the first target because the transfer between bodies likely occurs in a more circularized orbit than in the trajectory to the first object. The circularized orbit may have higher velocities in general compared to the outbound trajectory and hence would require more impulse to reorient.

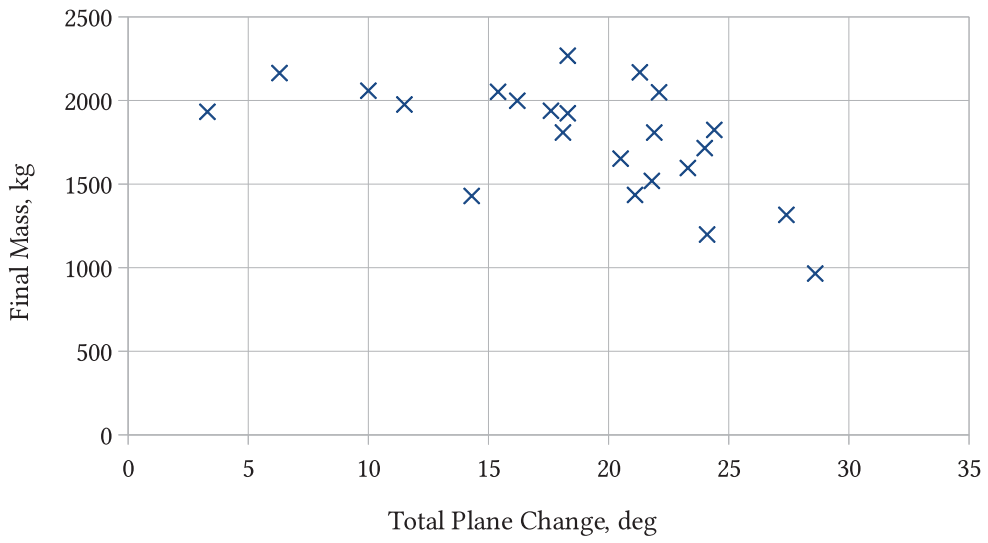

Figure 3.6.. The best result for each pair is plotted vs the total plane change required to rendezvous with each pair.

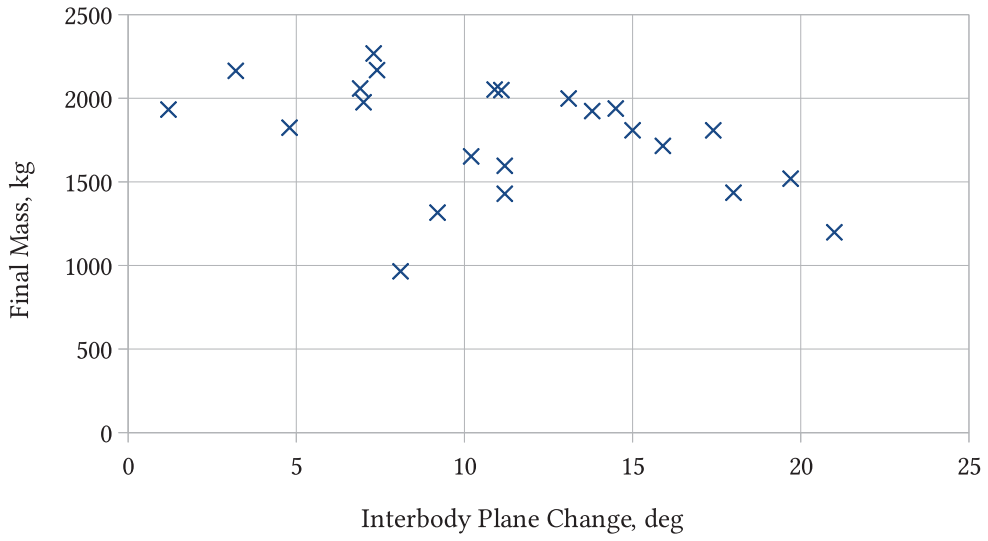

Figure 3.7.. The best result for each pair is plotted vs the interbody plane change required to rendezvous with each pair.

3.4.1 Highest Final Mass Results

From the broad search of trajectories to Trojan target pairs, we have identified two that yield results with the highest final masses. The trajectory with the highest overall final mass visits the objects 1986 TS6 and Hektor, in that order. 1986 TS6 is among the less red group of Trojans, and may be the primary member of a collisional family [49]. Hektor is the largest of the Trojan asteroids, and is the only known Trojan asteroid with a natural satellite [50]. In Table 3.4 we have a listing of the key characteristics of the trajectory.

Table 3.4.. Maximum Final Mass Trajectory to 1986 TS6 and Hektor

Parameter	Value
Power (1 AU)	40 kW
Initial Mass	5885 kg
Final Mass	2268 kg
Propellant Mass	3617 kg
Launch C_3	2.02 km^2/s^2
Cumulative ΔV	18.1 km/s
Launch Date	Feb. 10, 2027
1986 TS6 Arrival	Aug. 3, 2035
Hektor Arrival	Aug. 11, 2038

In Fig. 3.8 we have a plot of the trajectory to 1986 TS6 and Hektor. The spacecraft performs 2 complete revolutions around the Sun before its rendezvous with 1986 TS6, indicating it is more efficient to use the electric propulsion system for the initial impulse rather than launching on a higher C_3 departure with a lower initial mass. The transfer time from Earth to 1986 TS6 is 8 years 6 months, with a 180 day stay at 1986 TS6. The transfer from 1986 TS6 to Hektor is 3 years. Including a 180 day

mission at Hektor, 12 years total will elapse between Earth launch and the end of the mission.

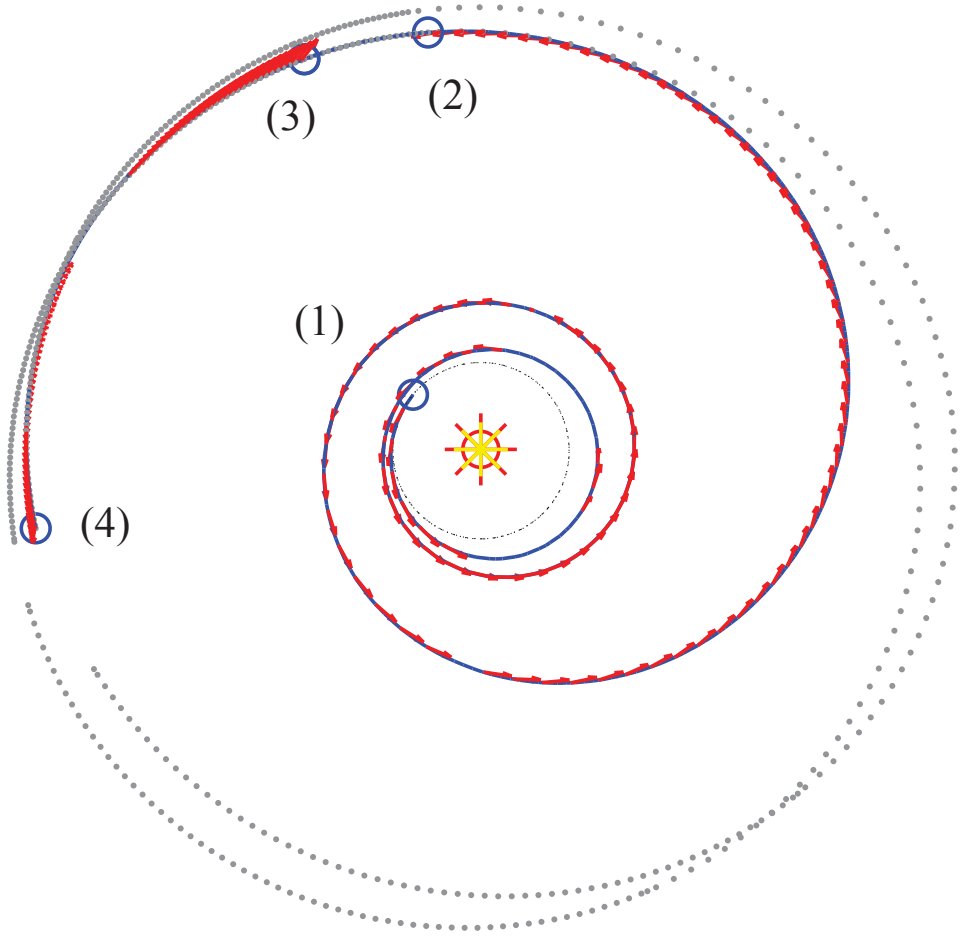

Figure 3.8.. The trajectory to 1986 TS6 and Hektor launches from Earth at (1), arrives at 1986 TS6 at (2), departs 1986 TS6 at (3), and arrives at Hektor at (4).

After the opportunities to launch to 1986 TS6-Hektor, which occur in the late 2020's, the next best opportunity is a mission to Palamedes and Diomedes, with a nominal launch in March 2037. Table 3.5 lists the characteristics of the trajectory to Palamedes and Diomedes.

Table 3.5.. Maximum Final Mass Trajectory to Palamedes and Diomedes

Parameter	Value
Power (1 AU)	40 kW
Initial Mass	5853 kg
Final Mass	2168 kg
Propellant Mass	3685 kg
Launch C_3	2.31 km^2/s^2
Cumulative ΔV	18.8 km/s
Launch Date	Mar. 19, 2037
Palamedes Arrival	Sep. 12, 2045
Diomedes Arrival	Sep. 17, 2048

In Fig. 3.9 we have plotted the trajectory from Earth launch to the rendevous with Palamedes and then Diomedes. Like the trajectory to 1986 TS6 and Hektor, the Palamedes-Diomedes trajectory launches on a low-C_3 trajectory and spends time spiraling around the Sun before its rendezvous with Palamedes.

For the broad search of trajectories over many target pairs, we considered only one spacecraft power level (40 kW) and one time of flight (12 years) which yielded two pairs of targets that resulted in the greatest final mass. Now we may consider each of those two nominal trajectories and perform a trade study over power and time of flight to examine the effects of these constraints on the payload. In general, shorter time of flight and lower power levels will result in lower final mass, however the associated cost savings may ultimately be the best choice for the mission.

To fairly compare two missions at different power levels, we use the net mass, m_{net}, to compensate for the higher propulsion system mass associated with a higher power level.

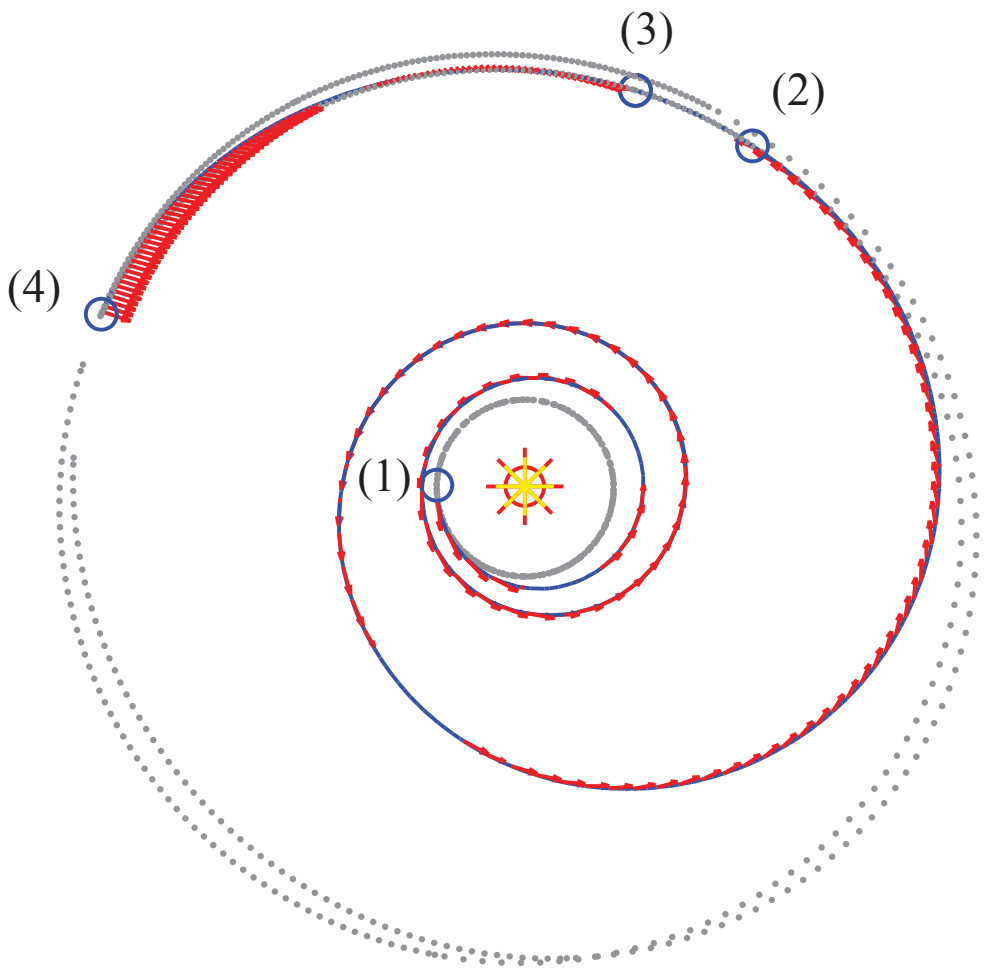

Figure 3.9.. The trajectory to Palamedes and Diomedes launches from Earth at (1), arrives at Palamedes at (2), departs Palamedes at (3), and arrives at Diomedes at (4).

$$m_{net} = m_f - \alpha P_0 - \mu_{tank} m_{prop} \tag{3.14}$$

where α is the propulsion system specific mass in kg/kW, μ_{tank} is the propellant tank mass fraction, and m_{prop} is the propellant mass. Here, we consider the propulsion system to comprise of the solar panels, thrusters, and power processing unit. Thus, m_{net} is the mass of all other spacecraft components that would be sized independently

of the propulsion system. For this analysis, $\alpha = 15$ kg/kW is used as a representative value, and is consistent with other sources in the literature [34]. A value of $\mu_{tank} = 0.05$ is used, based on the xenon propellant tank developed for the Dawn mission.

In Figs. 3.10 and 3.11 we have plotted contours of constant m_{net} for varying spacecraft P_0 and time of flight. For the trajectory to 1986 TS6 and Hektor, we can see that flight times can be reduced to 11.3 years without a severe reduction in net mass. However, feasible solutions do not appear available at shorter flight times. P_0 can be reduced to 30 kW at an expense of about 150 kg of net mass.

For the trajectory to Palamedes and Diomedes, shown in Fig. 3.11, we can see that 4 families of trajectories exist with flight times down to 10 years. These different families represent trajectories with different numbers of heliocentric revolutions. While flight times of 10 years come with reduced net mass, significant cost savings may be attained by reducing the mission time by 2 years from the baseline 12 year mission.

3.4.2 Triple Trojan Trajectory

While the wide search for Trojan asteroid targets considered only trajectories which visit two objects, we may also consider whether it is possible (and how much propellant it costs) to launch a mission to three Trojans. The broad search uncovered 1986 TS6 and Hektor as the most mass optimal pair in the launch period considered. Once the spacecraft is at Hektor, the object Agamemnon is in an orbit inclined only 4° relative to Hektor's orbit. This inclination change is the smallest of the other objects in the search population. Using the trajectory to 1986 TS6 and Hektor shown in Fig. 3.8 as an initial guess, we find a trajectory that continues on to Agamemnon. The trajectory is shown in Fig. 3.12, with accompanying data in Table 3.6. This trajectory was designed with the same 40 kW propulsion system used in the broad search, however the time constraint was increased to 15 years to accommodate the extra rendezvous.

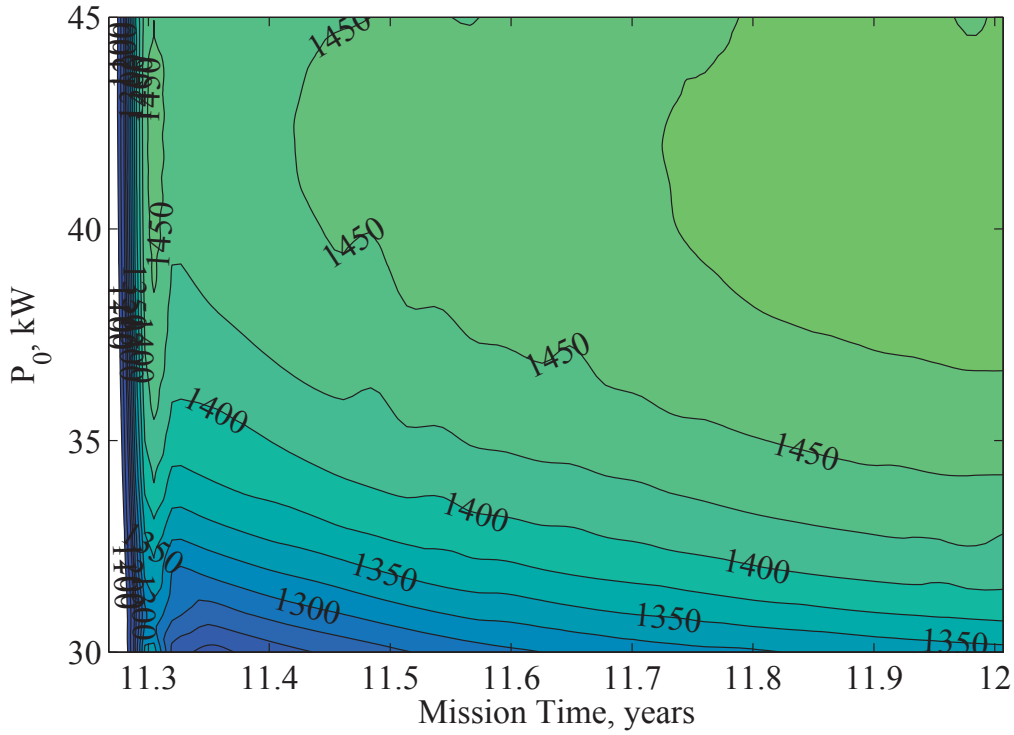

Figure 3.10.. Contours of constant net mass for varying TOF and P_0 for the trajectory to 1986 TS6 and Hektor.

The trajectory to 1986 TS6, Hektor, and Agamemnon arrives at the last object with a final mass of 1480 kg—788 kg (and 35%) less than the trajectory without Agamemnon.

3.5 Discussion

3.5.1 Effect of Jupiter's Gravity

Considering that the gravitational influence of Jupiter is responsible for the orbits of the Trojan asteroids, it would be prudent to check if Jupiter's pull would effect the trajectory to the extent that the optimal cases could not be used without significant modification. In Fig. 3.13, we have plotted the distance between the spacecraft and

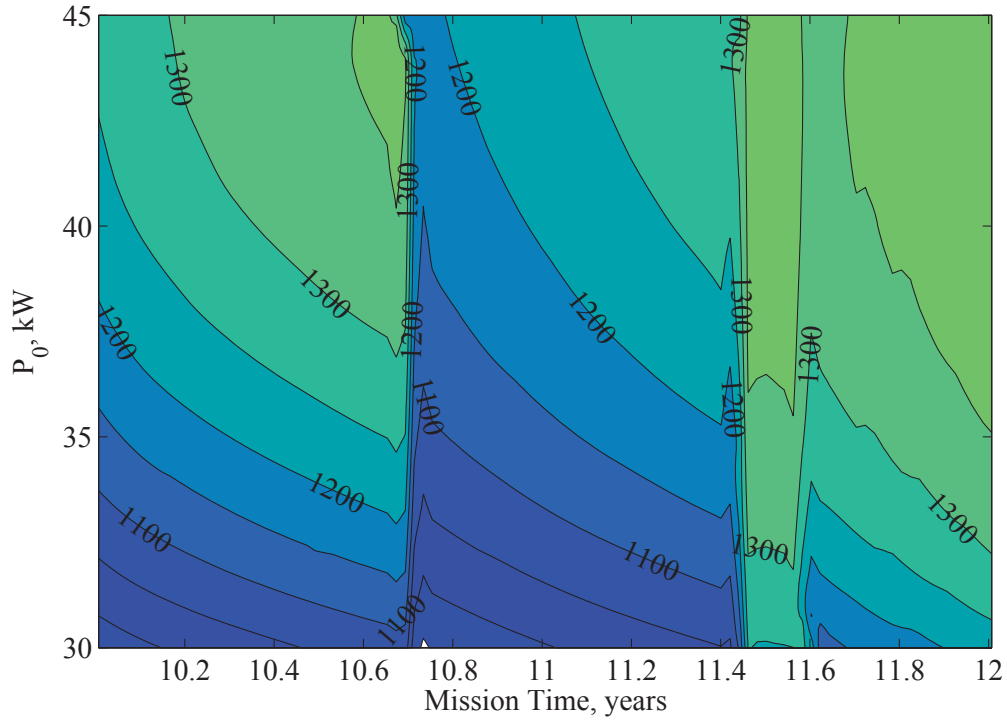

Figure 3.11.. Contours of constant net mass for varying TOF and P_0 for the trajectory to Palamedes and Diomedes.

Jupiter during the trajectory to 1986 TS6 and Hektor. The closest approach to Jupiter is 438.4 million km 1500 days into the mission. At that distance, Jupiter exerts an acceleration of 6.59×10^{-7} m/s^2. Meanwhile, at that point in the mission the thruster is capable of creating a 2.43×10^{-5} m/s^2 acceleration. The acceleration from Jupiter, at its greatest, is then 2.7% of the acceleration from the spacecraft propulsion system. We recall that the trajectory was designed with a 90% duty cycle, meaning that there is 10% more thrust available to the spacecraft with the given propulsion system. Even if the perturbation from Jupiter was aligned opposite to the optimal thrust acceleration direction at its maximum level of 2.7% of the thrust acceleration, the margin carried in the duty cycle is more than enough to make up for the disturbance.

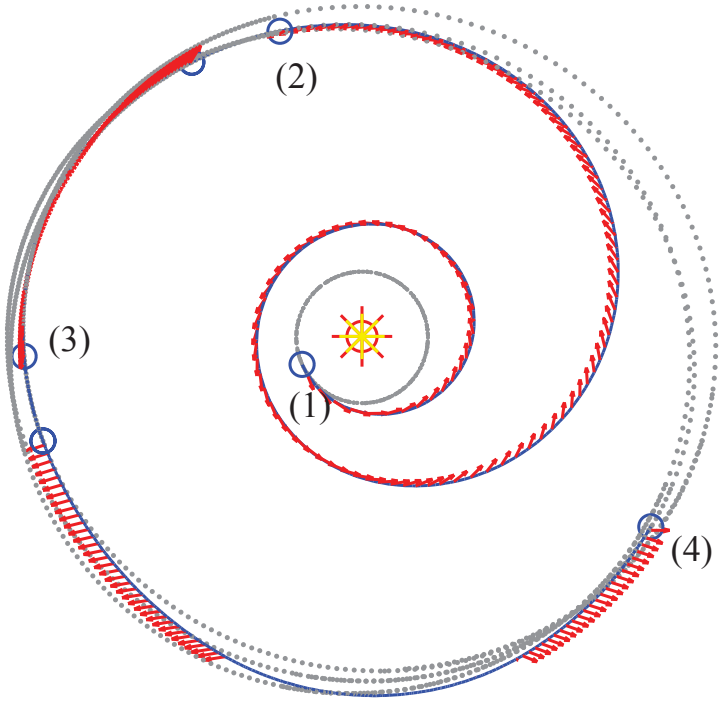

Figure 3.12.. A trajectory that (1) launches from Earth and rendezvous with (2) 1986 TS6, (3) Hektor, and (4) Agamemnon.

Table 3.6.. Trajectory to 1986 TS6, Hektor, and Agamemnon

Parameter	Value
Power (1 AU)	40 kW
Initial Mass	5041 kg
Final Mass	1480 kg
Propellant Mass	3561 kg
Launch C_3	10.2 km^2/s^2
Cumulative ΔV	21.4 km/s
Launch Date	Apr. 15, 2029
1986 TS6 Arrival	Oct. 23, 2035
Hektor Arrival	May 21, 2038
Agamemnon Arrival	Oct. 11, 2043

3.5.2 Using Jupiter as a Gravity Assist Body

In general, Jupiter is considered an attractive body use for a gravity assist because of its very large mass, so one might consider performing a gravity assist at Jupiter on the way to a Trojan asteroid rendezvous. This is especially true because Jupiter is able to impart an inclination change of over 20° to a spacecraft, which is useful to reach the Trojan population.

However, a search for trajectories to the Trojan asteroids performed with the same parameters as the search discussed previously resulted in trajectories having significantly lower final masses. Most launch years had best final masses of less than 1600 kg, with only one year having a final mass of 1800 kg. The worst case among the trajectories not using a gravity assist still had more than 1800 kg of final mass. It appears that, given the constraints of the mission, using Jupiter for a gravity assist is not helpful. This is likely because after performing the gravity assist maneuver, the

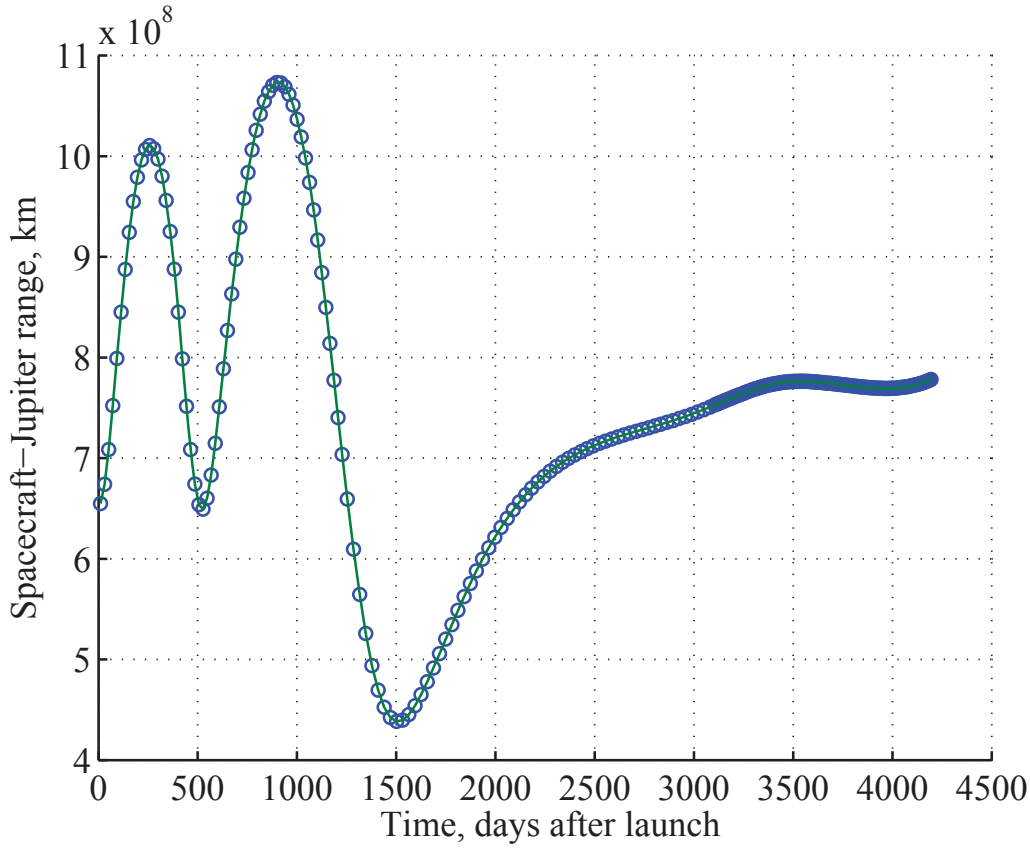

Figure 3.13.. The distance from the spacecraft to Jupiter for the trajectory to 1986 TS6 and Hektor.

spacecraft must spend propellant catching up to the L_4 Trojan population, which is phased 60° ahead of Jupiter.

3.6 Conclusion

We have performed an extensive search for trajectories which visit the L_4 camp of Trojan asteroids and rendezvous with objects of different compositional types. All of the trajectories were found assuming a spacecraft equipped with mature low-thrust propulsion technology and are within the capabilities of the Atlas V family of launch vehicles. We have found that, for launch dates between 2020 and 2040, two pairs

of objects stand out as having opportunities with the highest payload masses: 1986 TS6 and Hektor for launch dates between 2025 and 2029, and Palamedes-Diomedes for launch dates between 2036 and 2038. These trajectories result in final masses of up to 2268 kg in the case of 1986 TS6-Hektor and up to 2168 kg in the case of Palamedes-Diomedes.

4. Sample Return Trajectories to the Asteroid (216) Kleopatra

4.1 Introduction

The asteroid (216) Kleopatra, shown in Figure 4.1, is a large, dog-bone shaped, M-type asteroid located in the main asteroid belt with two natural satellites in orbit around it. An asteroid is classified as an M-type because it has a flat, relatively featureless spectrum, making it difficult for scientists to determine what materials the object is composed of. A composition similar to iron meteorites is consistent with a flat spectrum, but other materials may yield similar observations. In addition to the flat M-type spectrum, Kleopatra lacks a hydration feature that the stony-iron W-type asteroids (e.g. Lutetia) have, indicating water is mostly absent from the asteroid, and it has one of the highest radar albedos of any object in the asteroid belt. A high radar albedo (meaning the object reflects a high portion of radar waves) is also consistent with an iron composition. Ockert-Bell et al. [51] report that the spectral data for Kleopatra make it the best match for the parent body of the Hoba meteorite, a giant iron meteorite in Namibia.

If indeed Kleopatra is an iron asteroid, it would likely be the exposed core of an ancient protoplanet, with its outer layers stripped away in a large collision with another body. Such an object could provide great insight into the history of our Solar System and the interiors of the planets. However, other lines of evidence present further questions that prevent us from conclusively stating that Kleopatra is an iron asteroid. Descamps et al. [52] have recently measured Kleopatra's bulk density to be 3.6 ± 0.4 g/cm^3. This measurement is made by observing the orbits of Kleopatra's moons (yielding the mass of the system) and by obtaining a shape model using the Arecibo telescope (yielding the volume). Such a density is much lower than that of a

solid metal asteroid (7–8 g/cm^3). If Kleopatra is made of metal, why does it have a relatively low density?

A possible explanation for the low density of Kleopatra is that it was formed in a giant impact which produced the asteroid's moons as well as its unusual dog bone shape. This impact would have left the central body broken up and very porous, causing the bulk density to drop. Descamps et al. use an approximation of the tidal evolution of the moons' orbits to estimate that Kleopatra formed between 10–100 million years ago, a short time relative to the age of the Solar System. However, generally giant impacts of this sort in the asteroid belt leave behind a group of objects in orbits similar to that of the parent body. These groups are called collisional families. Several such families are known, however there does not appear to be one for Kleopatra. If a giant impact formed Kleopatra, why do we not see a collisional family? Much of our knowledge of tidal dynamics comes from objects which are largely comprised of silicates, such as the planets. It is possible the tidal evolution timescales are longer for an iron object if energy is dissipated more slowly than for a stony object.

While much has been learned by observing Kleopatra from the ground, there is still much that is not known about this object. We propose that the best way to answer these questions is by sending a spacecraft to study Kleopatra up close and return a sample to Earth for further analysis.

To date, two missions have successfully returned samples from small bodies in the Solar System: Stardust returned dust from the coma of the comet Wild 2 in 2006 [53] and Hayabusa returned a sample from the asteroid Itokawa in 2010 [54]. Further asteroid sample return missions are in the planning stages, with the OSIRIS-REx mission planning to launch in 2016 to the near-Earth asteroid Bennu [55] and MarcoPolo-R being developed by ESA [56]. Meteoritic samples of Vesta exist that can be traced back to their parent body based on spectral observations, but this connection has not yet been made for any M-type asteroid. Interestingly, returning a sample from Kleopatra may allow scientists to connect meteor samples to the asteroid,

expanding the mass of known sample material. For example, if a sample returned from Kleopatra can be matched to the Hoba meteorite (a metallic meteorite discovered in Namibia in 1920), in effect the returned sample of around 1 kg would lead to over 90 metric tons of material on Earth known to come from Kleopatra.

Table 4.1.. Orbital Parameters and Physical Properties of Kleopatra

Property	Value	Units
a	2.80	AU
e	0.25	-
i	13.1	deg
Ω	215.5	deg
ω	180.2	deg
Period	4.67	yr
Mass	4.64×10^{18}	kg
Dimensions	$217 \times 94 \times 81$	km

The objective of this study is to find low-thrust trajectories that transport a sample return spacecraft from Earth, to Kleopatra, and back to Earth. Kleopatra orbits with a relatively high eccentricity ($e = 0.25$) and high inclination ($i = 13.1°$), presenting challenges to the trajectory design. A listing of Kleopatra's orbital elements and physical characteristics is shown in Table 4.1. Low-thrust propulsion is ideally suited for missions to the asteroid belt because the low gravity of the target bodies means a high ΔV is generally required for rendezvous.

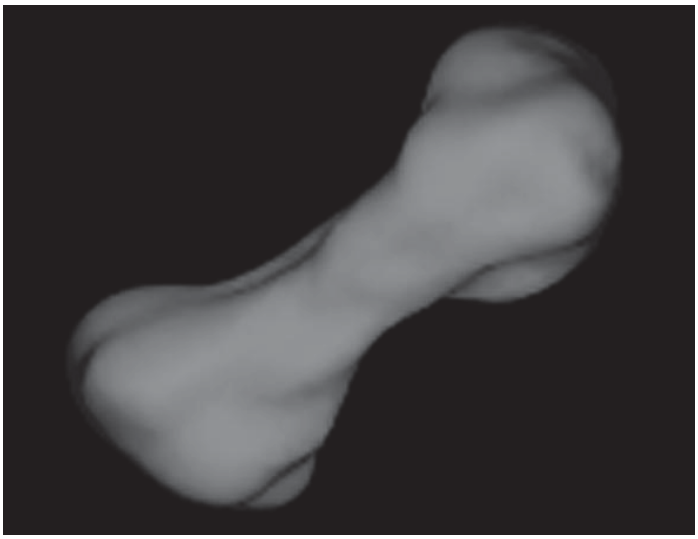

Figure 4.1.. This radar model of (216) Kleopatra was created with observations from the Aricebo telescope.

4.2 Method

4.2.1 Trajectory Search

The software package MALTO (Mission Analysis Low-thrust Trajectory Optimization) is used to compute the low-thrust trajectories while maximizing final mass. MALTO is developed and maintained by the Jet Propulsion Laboratory, and uses a direct method to produce optimal low-thrust trajectories [31].

MALTO requires initial guesses of the launch date from Earth and the arrival dates at any bodies the spacecraft will encounter during the mission. While MALTO can vary these dates, in practice it does not stray far from the initial guesses. To search over a wide range of launch dates, additional software was developed that generates a large set of initial guesses to run in MALTO. This software acts as a wrapper for MALTO, and is named PAM (**P**AM **A**utomates **M**ALTO). The user specifies a range of dates, an increment to step through for the launch date, a minimum and maximum flight time between bodies, and a time of flight increment. PAM

then automatically runs MALTO for each guess case, saving cases that converge on a solution and discarding those that do not. PAM is capable of running many instances of MALTO simultaneously on a multi-core machine. For this study it was limited to 32 parallel instances because of constraints on computing resources.

In the search for sample return trajectories to Kleopatra, launch date guesses between 2020 and 2040 were examined, in increments of 100 days. Flight times ranging from 300 to 1100 days, in increments of 200 days, were used to generate initial guesses of arrival dates at each of the bodies. For a sample return mission with one gravity assist on the way to Kleopatra and a direct return to Earth, these search parameters resulted in 9250 candidate solutions. Because these candidates are only initial guesses, MALTO is free to vary the dates while searching for an optimal trajectory. So, for example, even though a minimum flight time of 300 days was used to generate the initial guesses, actual flight times between bodies of less than 300 days may appear in the cases that converge on a solution.

4.2.2 Launch and Arrival Constraints

The spacecraft is limited to a total inital mass of 2500 kg, including propellant, and is assumed to depart Earth with a maximum V_∞ of 1 km/s (in the numerical results to follow, MALTO always places the V_∞ on the upper bound). The launch declinition is constrained to ± 29 degrees. These constraints allow for a launch from Kennedy Space Center aboard an Atlas V 401 or a Falcon 9. The performance data for these two launch vehicles, obtained from the NASA Launch Services Program Web Site[1], is shown in Figure 4.2.

Arrival at Kleopatra is constrained to a rendezvous with zero V_∞, allowing the spacecraft to capture into orbit around the asteroid using its electric propulsion system. Departure from Kleopatra is also constrained to zero V_∞. MALTO is allowed

[1]http://elvperf.ksc.nasa.gov/elvMap/staticPages/launch_vehicle_info1.html

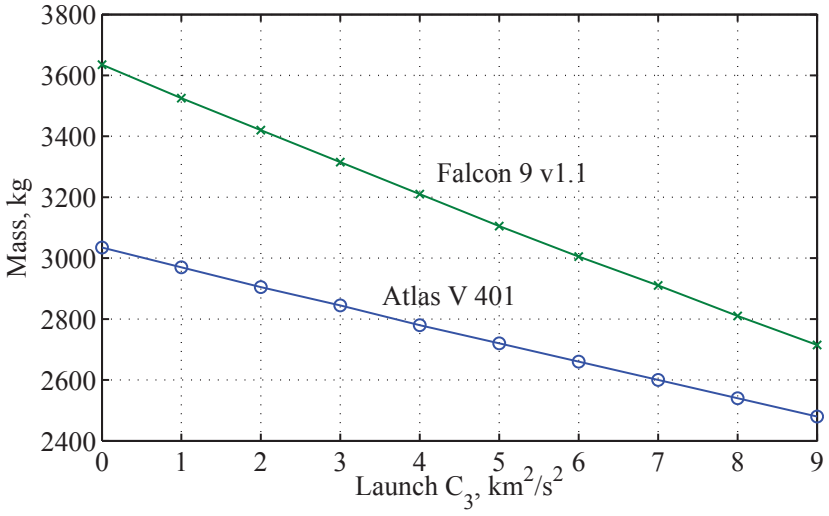

Figure 4.2.. Launch Vehicle Performance Curves for the Atlas V 401 and the Falcon 9 v1.1.

to vary the stay time between 120 and 270 days, but in the results to follow, nearly all trajectories had stay times on the lower bound of 120 days.

4.2.3 Propulsion Assumptions

The spacecraft propulsion system is assumed to have an I_{sp} of 4000 s and a propulsive efficiency of 70%. The specific impulse and efficiency are assumed to be independent of input power. The solar array is assumed to generate 20 kW of electrical power at 1 AU from the Sun, and the thruster is able to use all of the power available. The propulsion system assumed here approximately corresponds to the capabilities of the NEXT ion propulsion system in development by NASA [57], and represents a modest advancement over that used by the Dawn mission [3], which provided 10 kW of electrical power at 1 AU.

The propulsion system is assumed to have a specific mass, α, of 15 kg/kW, while a structural factor of $\mu_s = 0.15$ is assumed for the propellant tanks. To calculate the

spacecraft net mass, the propulsion system mass and tank mass are subtracted from the final mass at return to Earth (after the propellant has been spent):

$$m_{net} = m_f - \alpha P - \mu_s m_p \tag{4.1}$$

The net mass, as defined in Landau et al., [34] can be thought of as the dry mass without the propulsion system and main propellant tank, however it includes any maneuvering and stationkeeping propellant and thrusters. Any propellant margin is also included in the net mass.

4.3 Results

Using PAM to run MALTO as described, six types of low-thrust gravity-assist trajectories were searched for: Earth-Kleoptra-Earth, Mars-Kleopatra-Earth, and Venus-Kleopatra-Earth, Venus-Earth-Kleopatra-Earth, Earth-Mars-Kleopatra-Earth, and Mars-Earth-Kleopatra-Earth. Direct missions with no gravity assists were also examined. No solutions were found using only a Venus gravity assist that met the mission constraints, however Earth and Mars both yielded a range of viable trajectories.

4.3.1 Trajectory Search

Figure 4.3 displays the net mass results from the trajectory search plotted agains launch date. Launch opportunities that deliver a net mass of greater than 1000 kg are available at regular intervals between 2020 and 2040. The opportunities that deliver the most mass tend to occur at intervals that correspond with the 4.7 year period of Kleopatra's orbit. Trajectories that maximize net mass tend to have the spacecraft in Kleopatra's orbit while the asteroid is near perihelion.

Trajectories using a single gravity assist from Earth or Mars typically have a net mass advantage of around 100 kg compared to direct trajectories to Kleopatra or those using two gravity assists.

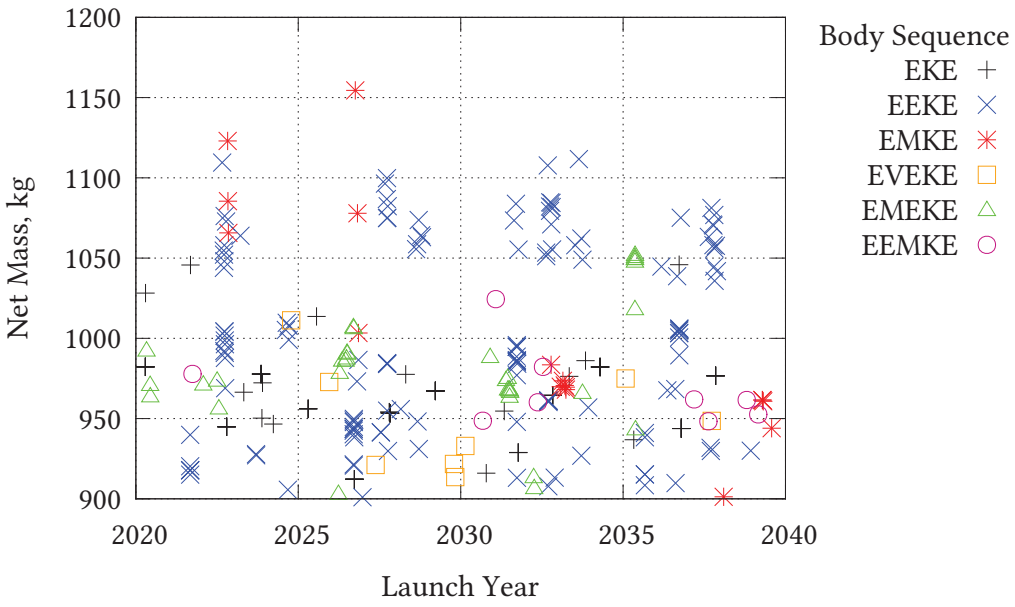

Figure 4.3.. Net masses of greater than 1000 kg are feasible at regular intervals primarily using Earth as a gravity assist body.

Figure 4.4 demonstrates that total mission durations (from launch to Earth return) of 6.5–7.5 years are available with a regularity that roughly matches Kleopatra's orbital period. This trend is similar to that shown in Figure 4.3. While direct trajectories do not deliver as much net mass, the absence of a gravity assist maneuver generally allows for a shorter overall mission time.

In Figure 4.5, we have plotted the trajectory results with mass on the vertical axis and TOF on the horizontal axis, showing the pareto-optimal front to the upper left of the plot. We can see the group of results using an Earth flyby offer higher net mass but longer TOF compared to the group of results using Mars as a gravity assist body.

Table 4.2 contains a few examples of trajectories found in the search which featured a desirable combination of high net mass and reasonable mission durations. The first column, labeled "Path" lists the sequence of bodies visited by the spacecraft after launch. An opportunity launching in October 2026 using a Mars gravity assist

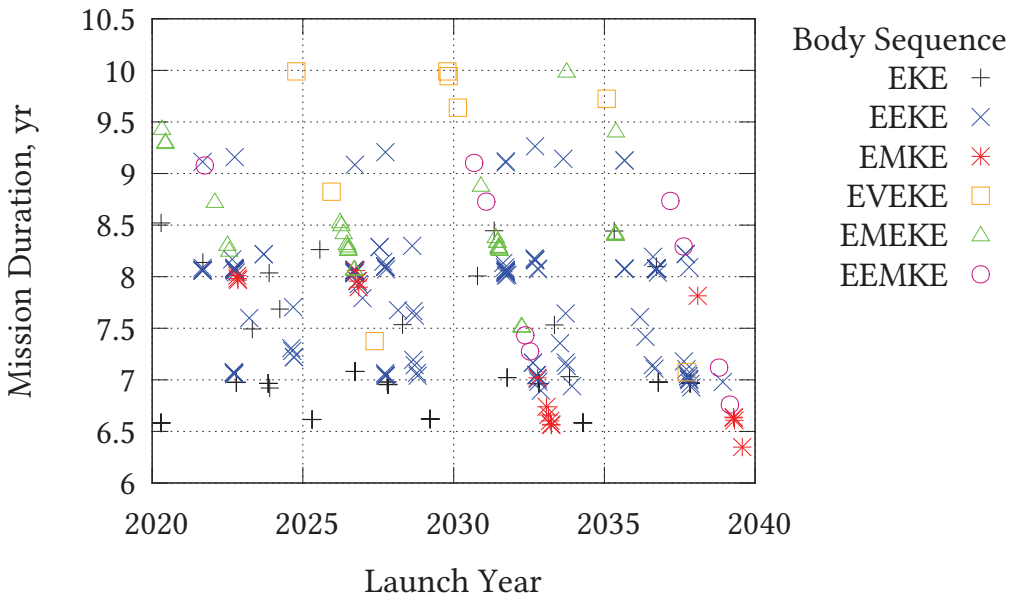

Figure 4.4.. Trajectories with total mission durations of 6.5 – 7.5 years are possible at regular opportunities using Earth and Mars gravity assists. All trajectories in this plot deliver a net mass of at least 900 kg.

provides the maximum net mass of all the trajectories found, however it occurs rather soon to reasonably be considered for a sample return mission.

4.3.2 Trajectory Examples

Figures 4.6 and 4.7 are examples of trajectories found during the search. The descending node of Kleopatra's orbit roughly coincides with perihelion in the first quadrant of the trajectory plots. The best performing trajectories found in the search tended to be those where the surface operations occur near perihelion. This type of trajectory is exemplified in Figure 4.7.

The trajectory in Figure 4.6 features an Earth gravity assist 390 days after launch, which is close to a 1:1 resonance with Earth. After the Earth flyby, the V_∞ is boosted to 6.62 km/s from the initial 1 km/s. Such trajectories are typical of the best per-

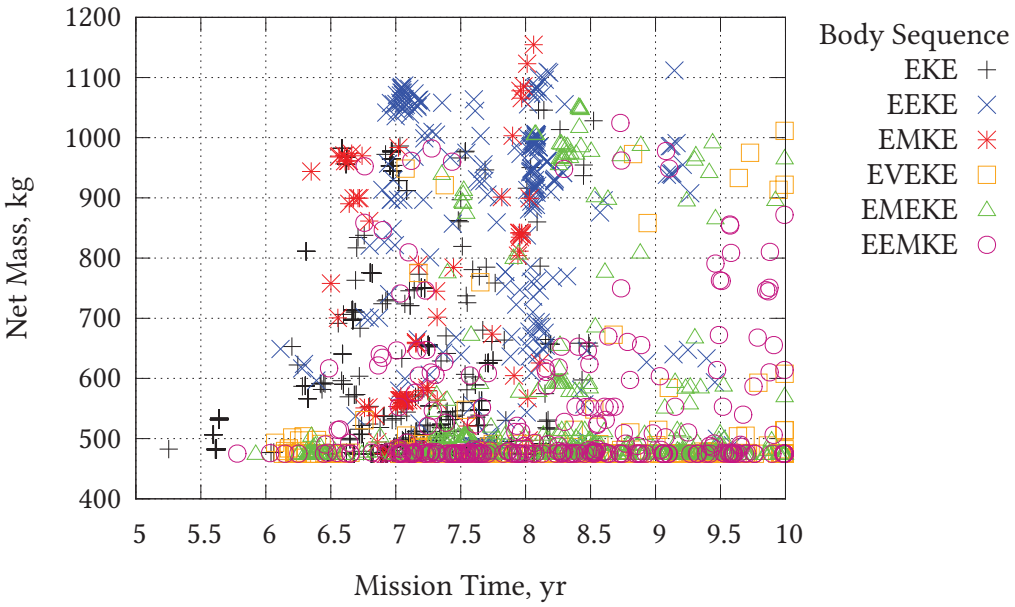

Figure 4.5.. Mass is plotted vs TOF, showing the pareto-optimal front among the trajectory results.

forming cases using an Earth gravity assist, and work similarly to the V_∞ leveraging technique discussed by Sims et al. [58].

Figures 4.8 and 4.9 show trajectories using two gravity assists before reaching Kleopatra. While these trajectories provide acceptable performance in terms of final mass, they tend to require more time in transit, and do not present a clear advantage over the single-gravity-assist options.

4.4 Conclusion

The constraints for these missions are that the initial mass is 2500 kg, the departure V_∞ is less than or equal to 1 km/s, and the mission duration is less than 10 years. Using a selection of one or two gravity assists with Venus, Earth, and Mars, sample return missions are found to be feasible with a 20 kW SEP system. Launch opportunities satisfying the constraints are regularly available between 2020 and 2040 and

Table 4.2.. Summary of Best Launch Opportunities[a]

Path	Launch Date (m/d/y)	Net Mass (kg)	Mission Time (y)
EMKE	10/28/2022	1104	8.0
EMKE	10/3/2026	1155	8.1
EEKE	9/23/2027	1086	7.1
EEMKE	7/14/2032	982	7.3
EEKE	10/2/2032	1085	7.0
EMKE	3/15/2033	970	6.6
EMEKE	5/15/2035	1052	8.4
EEKE	10/22/2037	1077	8.1
EMKE	4/17/2039	961	6.6

[a] All launches are constrained to a launch V_∞ of 1 km/s or less.

deliver a spacecraft net mass of at least 1000 kg. Earth and Mars stand out as useful gravity-assist bodies while Venus does not appear to help in getting to Kleopatra. Adding gravity-assist bodies does not increase net mass given the mission constraints used here.

The results imply that a sample return mission to Kleopatra is quite feasible, at least as far as the interplanetary trajectory is concerned. Kleopatra is fascinating not only because of its dog-bone shape and two moons, but also because of the unanswered questions regarding its internal make-up and composition. The mission described here could potentially return the first sample of an M-type asteroid and provide further insight into the origins of the asteroid belt and the Solar System.

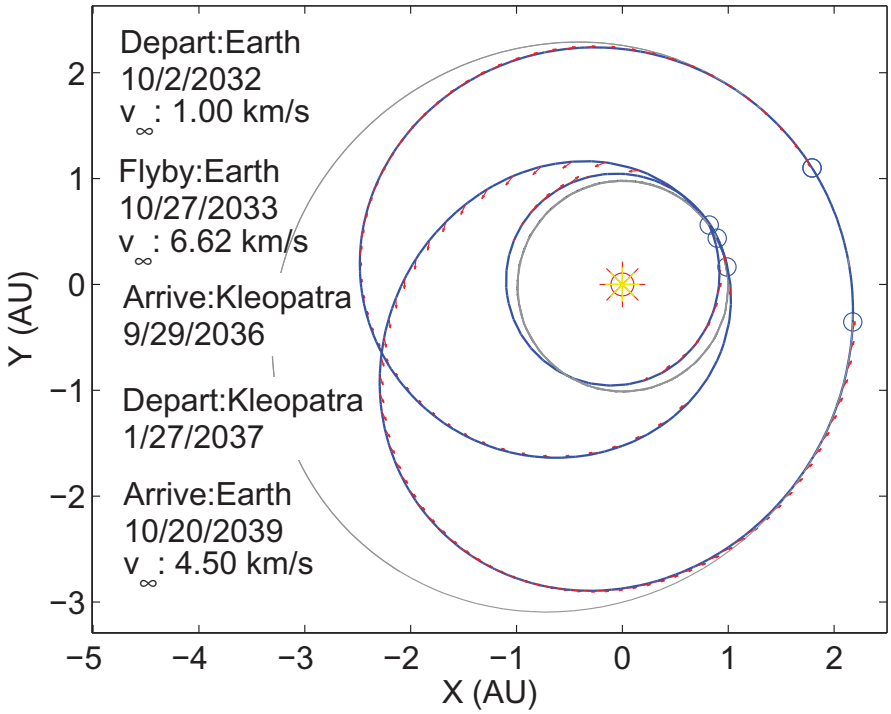

Figure 4.6.. This Earth gravity assist trajectory uses a nearly 1-year resonant orbit to return to Earth and perform the gravity assist.

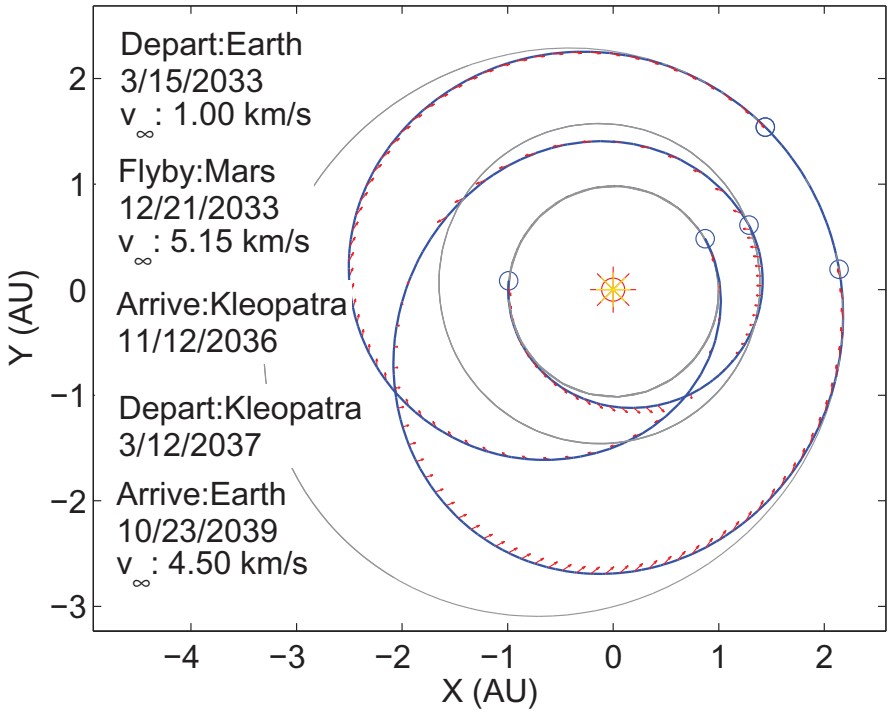

Figure 4.7.. Mars can be a useful gravity assist body for trajectories to the asteroid belt.

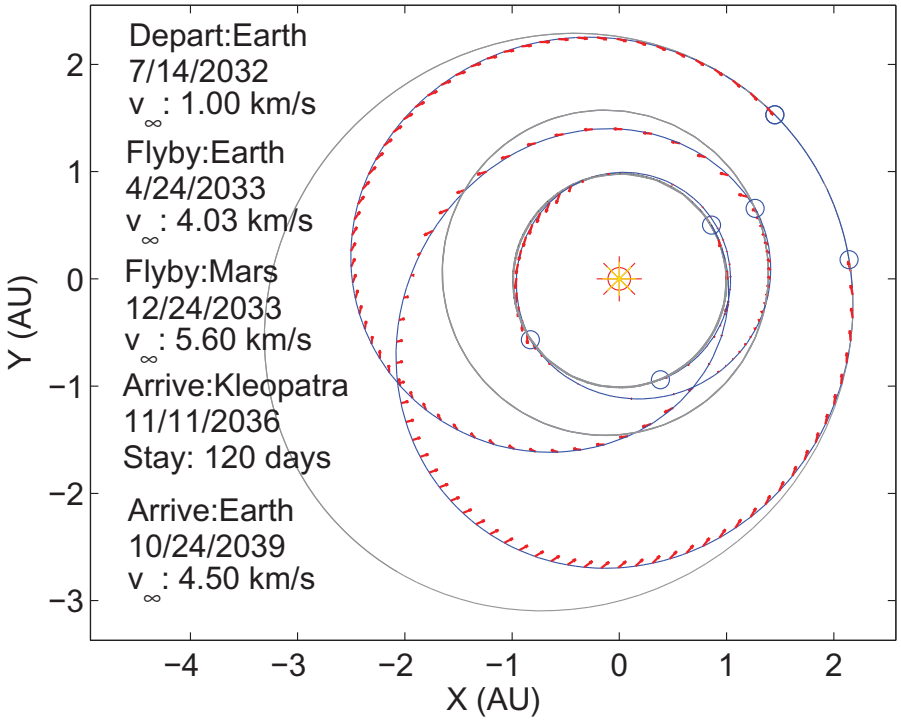

Figure 4.8.. Trajectory with an Earth-Mars gravity assist sequence.

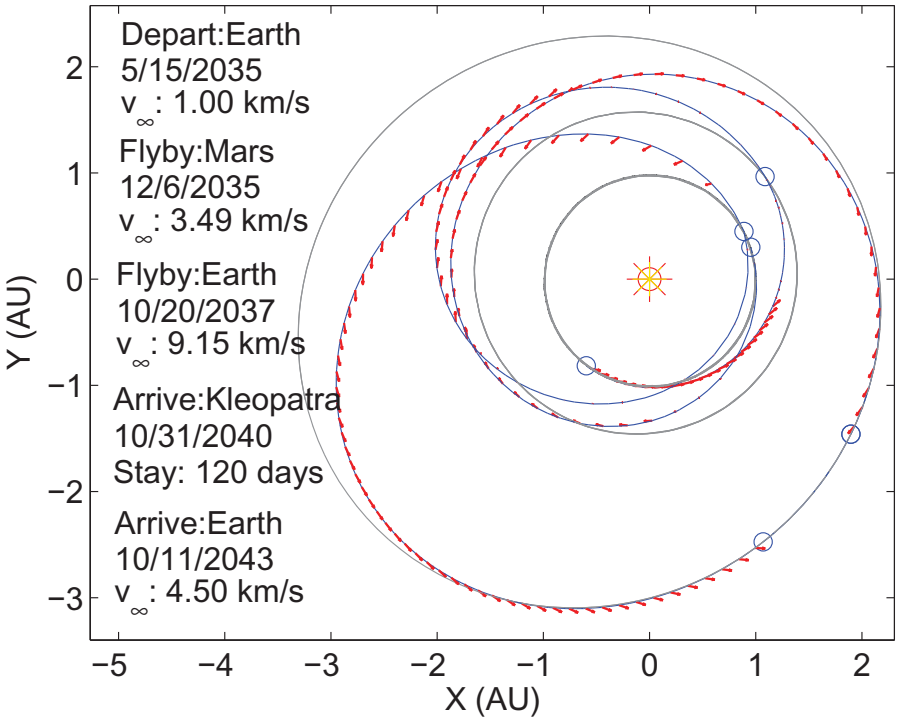

Figure 4.9.. Trajectory with a Mars-Earth gravity assist sequence.

5. Automated Missed-Thrust Propellant Margin Analysis for Low-Thrust Trajectories

5.1 Introduction

On September 11, 2014, a high energy particle collided with an electrical component of the Dawn spacecraft, causing it to enter safe mode [59]. During this time, the spacecraft thruster was supposed to be operating, however it shut down as a result of the safe mode. This loss of thrust caused the spacecraft to drift from its nominal trajectory. If allowed to continue, the situation could eventually result in a severe degradation or even failure of the mission. Fortunately, Dawn's operators at the Jet Propulsion Laboratory (JPL) were able to resolve the issue and the spacecraft resumed thrusting four days later, avoiding any serious consequences. However, this incident demonstrates that the potential for a missed thrust is something that must be considered during the design and planning of a low-thrust mission.

A significant body of research covers the design and optimization of low-thrust trajectories [6–8, 11, 60–64], focusing mainly on maximizing final payload mass. Indeed, electric propulsion offers significant gains in payload mass over chemical propulsion for a wide range of missions. However, the low thrust levels of electric propulsion systems mean they must operate for a large portion of the mission. In the event of a fault on the spacecraft, the system may be forced to shut down while mission operators attempt to fix the problem. When the problem is resolved, the spacecraft should ideally be able to resume thrusting and complete its primary mission. This event is depicted in Fig. 5.1. This missed-thrust problem applies to both electric propulsion and solar sail missions [65].

As described by Rayman et al. [66], accounting for the missed-thrust problem while planning a mission can be a laborious process. To determine how well a given

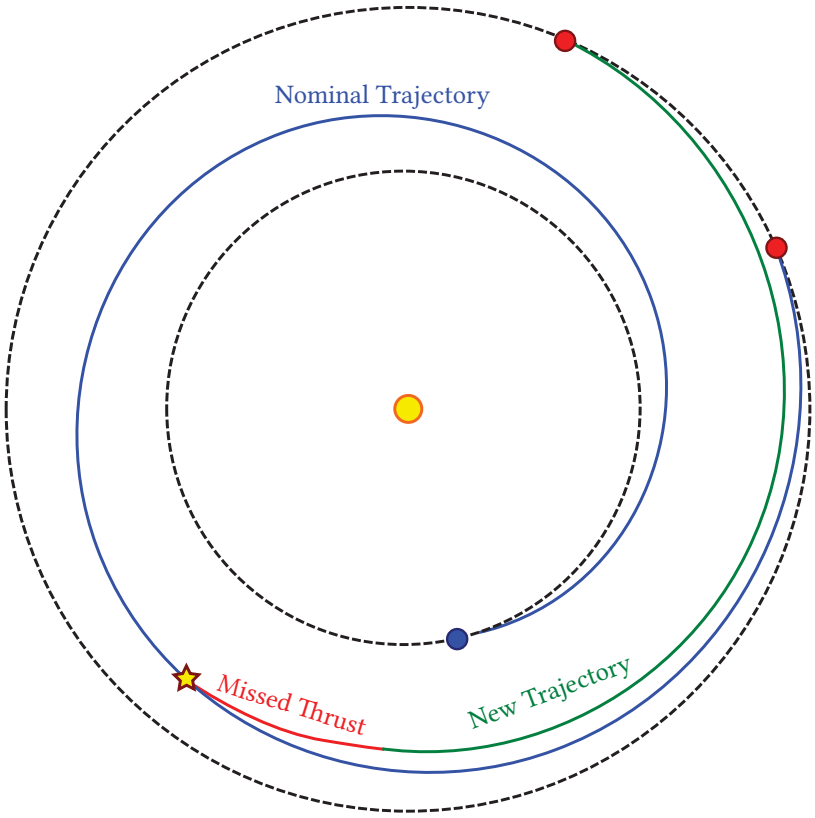

Figure 5.1.. A missed-thrust event causes the spacecraft to drift from the nominal trajectory. When thrust resumes, the spacecraft must follow a new trajectory to the target.

trajectory holds up to a missed-thrust event, mission designers simulate an unplanned coast period at every point along the trajectory and check to see if a new trajectory can be computed which achieves the goals of the mission. To ensure a mission can recover from a missed thrust, spacecraft carry a certain amount of reserve propellant equal to the amount needed if a shut-down occurs at the worst point in the trajectory. However, this reserve propellant ultimately comes at the expense of payload mass (and science return), and in some cases a mission may not be considered feasible after considering the effects of missed thrust.

Oh et al. [67] describe a procedure for incorporating a missed-thrust analysis into the trajectory selection process, as used in the Dawn mission. In the method they

describe, the spacecraft follows a trajectory with a rolling forced coast period ahead of the spacecraft. If nothing causes the spacecraft to miss thrusting, the trajectory is re-optimized with the forced coast pushed back. In the nominal case, the forced coast is never actually reached, but the nominal trajectory will always be close to a forced coast trajectory, providing robustness in the event of a missed thrust.

Alizadeh and Villac [68] present a method of measuring a position and velocity margin in the three-body problem, with potential applications to the missed-thrust problem by guiding the placement of coast arcs in a low-thrust trajectory.

Despite the aforementioned studies, the missed-thrust problem is still dealt with in an approximate manner, especially during the preliminary stages of mission design. A rough estimate of propellant margin may be given to account for missed thrust, however this may not be based on analysis specific to the trajectory planned for the mission. This study presents a method for quantifying the effect of missed thrust and estimating how much propellant margin should be carried to provide a mission with the capability to recover in the event of a missed thrust. Associated with that propellant margin, we also quantify the extra time a spacecraft must spend to reach its destination. The method presented here is intended for use with interplanetary trajectories, although it may also be adapted for geocentric missions.

This analysis is applied to three example cases. The first is a direct rendezvous trajectory from Earth to Mars, in which three power levels are examined. The second is a rendezvous with the Main Belt asteroid Psyche with a Mars gravity assist along the way. This example shows the effect of a gravity assist on the sensitivity to missed thrust. Third, a solar sail mission to the near-Earth asteroid 1991 VG is studied. The solar sail mission does not miss thrust, but rather is directed to thrust radially in the event of a safe mode.

5.2 The Missed-Thrust Problem

Formulating a metric with which to quantify the effect of a missed thrust on a mission is an important first step in approaching the problem. One approach, used by Olympio and Yam [69], is to measure a mission margin as the maximum length of time at a given point in the trajectory a spacecraft may coast and still reach the target destination. This margin varies during the mission. While computing this margin will tell mission planners if a constraint on minimum allowable missed-thrust time is violated at some point in the mission, it does not directly provide information about what it will cost (in terms of propellant and time) for a mission to recover from the missed thrust.

Here, two quantities are used to measure the effect of missed thrust on a trajectory: propellant margin, M, and lateness, L. The propellant margin is the extra propellant required to recover from a missed thrust of a given duration occurring at a given time in the trajectory, and is measured as a percentage of the propellant used in the nominal trajectory.

$$M = \frac{m_f^* - \tilde{m}_f}{m_{prop}^*} \tag{5.1}$$

where m_f^* is the total final mass in the nominal case, $\tilde{m}_f$ is the total final mass in the case with a missed thrust, and m_{prop}^* is the propellant mass used in the nominal case.

Lateness is how late the spacecraft will be in arriving at its destination as a result of a missed thrust, and is measured here in days.

$$L = \tilde{T}_f - T_f^* \tag{5.2}$$

where T_f^* is the time of flight in the nominal case and $\tilde{T}_f$ is the time of flight in the missed thrust case. Both the propellant margin and lateness are functions of the date at which the missed thrust begins, T_{mt}, the duration of the thrust outage, t_{mt}, and the relative importance mission planners place on propellant vs time of flight, η.

Generally, after recovering from a missed thrust, the mission may either spend more propellant and try to arrive as close to the planned arrival date as possible, or it

may choose to save propellant by delaying the arrival at the target body. The relative importance is given as a weighting factor between time and mass in the optimization objective function used in calculating the low thrust trajectory.

$$J = -m_f + \eta T_f \tag{5.3}$$

where m_f is the final mass and T_f is the time of flight. The case where η is zero corresponds to pure mass optimization (i.e. maximize final mass); large η corresponds to time optimization (i.e. minimize time). In practice, the importance of time relative to mass will depend on the goals of the mission. For example, it may be important to the science goals of a mission to view an object during an equinox if that object's rotation axis has a significant tilt relative to the Sun. In such a case, η should be given a high value. For other missions, the date of arrival may not be as important, and η can be given a low value close to zero.

In this work, the objective is to measure M and L for a given nominal trajectory. The nominal trajectory (without any missed thrust) is designed by solving the pure mass optimization problem:

$$\text{Minimize} \quad J = -m_f \tag{5.4}$$

subject to the boundary constraints:

$$\mathbf{X}(0) = \mathbf{X}_0 \tag{5.5}$$

$$\mathbf{X}(t_f) = \mathbf{X}_f \tag{5.6}$$

$$t_f \leq \tau_f \tag{5.7}$$

where $\mathbf{X}$ is the spacecraft state vector and τ_f is the constraint on time-of-flight. The nominal trajectory serves as a baseline from which the effect of missed thrust is computed. A given nominal trajectory has an associated propulsion system (power, thrust, and specific impulse), and departure energy. To examine the effect of these propulsion system variables on the sensitivity of a trajectory to missed thrust, a new nominal trajectory must be computed before performing the missed-thrust analysis.

Intuitively, it can be surmised that certain features of a complex low-thrust trajectory will cause spans of the trajectory to be more sensitive to missed thrust. While each trajectory will have a different nominal switching strategy between coast arcs and thrust arcs, all rendezvous trajectories must end with a thrust arc on approach to the target body. Missed thrust is likely to be more damaging during this thrust arc because the relative velocity between the spacecraft and the target body is low. This low relative velocity between the spacecraft and the target body means that any deviations from the nominal trajectory will take longer to recover from. There may also be much less power available to the spacecraft if it is a solar-powered mission to Mars, the asteroid belt, or an outer planet.

In addition, gravity assists are likely to cause high sensitivity to missed thrust in the period ahead of the flyby. Unless constrained to coast before the gravity assist, the trajectory optimizer may find a solution in which the gravity assist occurs in the middle of a thrust arc. A missed thrust before the gravity assist may cause the spacecraft to miss the flyby entirely, with severe consequences for the mission. The effect of missed thrust on a gravity-assist trajectory will be examined as an example case for the analysis method discussed here.

5.3 Method

We approach the missed-thrust problem first by writing a software program that can accept an existing optimized low-thrust trajectory (as the nominal trajectory), simulate a missed-thrust event of a user-specified duration and epoch, and attempt to re-optimize the portion of the nominal trajectory following the missed-thrust event. This method requires an existing trajectory optimization program for which a script can be written that automatically generates the missed-thrust cases and runs them in the optimizer. We use the Mission Analysis Low-Thrust Optimization (MALTO) program [31] as our trajectory optimizer, but our method may be used with other programs, such as the Evolutionary Mission Trajectory Generator (EMTG) [70]. MALTO

solves the trajectory optimization problem by modeling the thrust profile as a series of many small impulsive ΔV's and models gravity assists as instantaneous rotations of the velocity vector.

The software program that generates the missed-thrust cases is recursively named PAM Automates MALTO (PAM), and is written in Python. PAM reads the output from MALTO and generates new inputs for the missed-thrust analysis. The inputs generated by PAM for this analysis are entirely determined from the nominal trajectory and are run in parallel to reduce the computation time.

5.3.1 Missed-Thrust Algorithm

The algorithm for performing the missed-thrust analysis is summarized as follows:

1. Obtain the spacecraft state vector and mass at a specified epoch (T_{mt}) from the output of a nominal trajectory run.

2. Propagate the state vector ballistically for a specified coast time, t_{mt}. In the case of a solar sail mission which may not turn off thrust, a specified thrust program for safe mode is assumed. Radial thrust is used in the example presented here, but another thrust program may be specified.

3. Create several new optimization cases starting from the new state vector at the end of the coast and carrying through the rest of the trajectory. In these cases, Eq. 5.3 is used for the objective function. Any time-of-flight or mass constraints present in the nominal trajectory are removed for the missed-thrust cases.

4. Iterate over t_{mt} and T_{mt}, and examine the difference between the final mass and arrival epoch in each missed-thrust case and the final mass and arrival epoch of the nominal case. The increase in final mass in the missed-thrust case is the extra propellant the spacecraft would need to spend to reach its target, and the delay in arrival epoch is how late the spacecraft will be on arrival.

For each missed-thrust simulation, performing a range of optimizations between mass-optimal and time-optimal provides mission designers with bounds on what is achievable in the event of a missed thrust of that duration and at that epoch. For our analysis, η is varied between 0.05 and 10.0. We do not run cases with pure mass optimization ($\eta = 0$) because such cases often jump to solutions with much greater TOF (sometimes doubling or tripling the nominal TOF) where sensitivity to missed thrust is greatest. While such long-TOF solutions may be of interest in the event of a missed thrust, we exclude them to more clearly show the relationship between propellant margin and lateness for trajectories close to the nominal trajectory. For the upper limit on η, we have found through trial and error that a value of $\eta = 10.0$ closely matches the time-optimal case.

Often, missions may be planned by maximizing final mass subject to a constraint on time-of-flight, but in the event of a missed thrust, mission planners may be interested in lifting the time constraint in the interest of saving the mission. However, lifting the time-of-flight constraint may cause the optimizer to use much more time to reach the target to save propellant, resulting in a solution with an unrealistic flight time.

By performing many unconstrained optimizations (between mass optimal and time optimal), mission planners should be able to see the trade between time of flight and propellant mass in the event of a missed thrust of a given duration and at a given point in the mission. This information can be used to plan how much margin propellant to carry and to estimate how late the spacecraft will arrive at its destination using that margin in the event of a missed thrust.

5.3.2 Alternative Formulation

There is an alternative method to perform the analysis described here where the constraint on TOF is varied instead of the objective function weighting. In the alternative formulation, the trajectory after the missed-thrust event is designed to simply

maximize final mass subject to a constraint on TOF which is varied from the nominal TOF to some maximum value chosen by the user. The solutions with the TOF constraint equal to the nominal TOF roughly correspond to solutions with higher values for η in the previous formulation, while solutions with very loose constraints on TOF correspond to those with very low values for η. This method would have the advantage of only examining flight times which are of interest to the mission designers, and avoiding solutions which do not add insight into the problem.

5.3.3 Example Cases

We perform our analysis on three example cases: one a direct transfer to Mars using electric propulsion, the second a low-thrust gravity-assist trajectory to the Asteroid Belt, and the third a solar sail mission to a near-Earth asteroid. At Mars, electric propulsion may enable future sample return and human missions [16, 71]. In the solar sail mission thrust is not "missed" in the same sense as the electric propulsion mission. Instead, in the event of a problem causing the spacecraft to enter safe mode, we assume the spacecraft points its solar panels and sails at the Sun, resulting in a radial thrust from the sail.

5.4 Results

5.4.1 Transfer to Mars

Propulsion System Model

For the transfer to Mars, the spacecraft launches from Earth aboard a Falcon 9 v1.1[1] rocket and has two XR-5 Hall thrusters. (The XR-5 was previously designated

[1]Data available at: http://elvperf.ksc.nasa.gov/Pages/Query.aspx [Retrieved March 2014].

the BPT-4000.) The thruster is modeled with two polynomials [48] giving thrust and mass flow rate as functions of input power, P:

$$T(P) = \left(-8.597 + 77.34P - 2.119P^2 - 1.151P^3 + 0.1739P^4\right) \times 10^{-3} \quad \text{N} \tag{5.8}$$

$$\dot{m}(P) = (3.524 + 68.48P - 16.32P^2 + 2.351P^3 - 0.1195P^4) \times 10^{-7} \quad \text{kg/s} \tag{5.9}$$

where power is in kW and is limited to between 0.302 and 4.839 kW. At the maximum power level, 281 mN of thrust is produced. The thruster has a specific impulse ranging between 650 seconds to 1850 seconds over its operating range, with higher specific impulse at higher input power. A 95% duty cycle was applied to the thruster performance to account for planned outages used for communication and other spacecraft operations. Power available to the propulsion system is a function of the distance between the spacecraft and the Sun:

$$P(r) = \frac{P_0}{r^2}\left(\frac{1.321 - \frac{0.108}{r} - \frac{0.117}{r^2}}{1 + 0.108r - 0.013r^2}\right) \tag{5.10}$$

where r is in AU and P_0 is the power available at 1 AU from the Sun. Equation 5.10 is intended to model the behavior of triple junction gallium arsenide solar panels. The term in parentheses has the main effect of reducing the gain in power for distances closer to the Sun. For the example missions in this work, which are restricted to the region between Earth and the main asteroid belt, the parenthetical term in Eq. 5.10 is close to unity.

Sensitivity to Missed Thrust Throughout the Mission

The nominal trajectory has a transfer time of 440 days with a 30-day built-in "check-out" period following launch where thrust is off. We examine power levels of 10 kW, 15 kW, and 20 kW, which each deliver 2294 kg, 2584 kg, and 2643 kg of total mass to Mars, respectively. Information about the transfers are summarized in Table 5.1. Trajectory plots for the 10 kW and 20 kW nominal cases are shown in Figs. 5.2 and 5.3. One notable difference between the 10 and 20 kW trajectories is the presence of an optimal coast arc in the 20 kW trajectory, while the thruster is

operating for the entirety of the 10 kW trajectory. Initially, it was thought the coast arc in the 20 kW trajectory could provide added buffer to make up for a missed thrust in the initial thrust arc. Although not pictured here, the 15 kW trajectory also has a thrust-coast-thrust control structure.

The nominal trajectories also feature a spiral down to low Mars orbit between phases 3 and 4, however this phase does not affect the missed-thrust analysis, and the final mass reported is the mass at the date of arrival at Mars, before the spiral. The arrival date before the spiral is also used as the reference date when computing the lateness in the missed-thrust cases.

Table 5.1.. Summary of nominal test cases for trajectories to Mars

Power, kW	10	15	20
Final Mass, kg	2294	2584	2643
Propellant Mass, kg	532	655	657
Launch C_3, km^2/s^2	7.83	3.71	3.12
Cumulative ΔV, km/s	3.56	3.84	3.97
Launch Date (1), m/d/y	9/23/2024	8/31/2024	8/24/2024
End check-out (2), m/d/y	10/23/2024	9/30/2024	9/23/2024
Arrival Date (3), m/d/y	12/7/2025	11/14/2025	11/7/2025
End Spiral (4), m/d/y	10/5/2026	6/12/2026	4/22/2026

In Figs. 5.4–5.9, we can see the effect of missed thrust on the Mars transfer. The analysis is only performed between the end of the "check-out" phase and the start of the spiral down to low Mars orbit. The spacecraft is not thrusting during the check-out phase, and missed thrust during the spiral down to low Mars orbit is outside the scope of this study. Each figure corresponds to a particular power level and missed-thrust duration. Here we present results for 10-day missed thrusts and 20-day missed thrusts. While a finer-grained analysis (i.e. more missed-thrust durations) would be desirable when planning a mission, preforming the analysis for 10 and 20

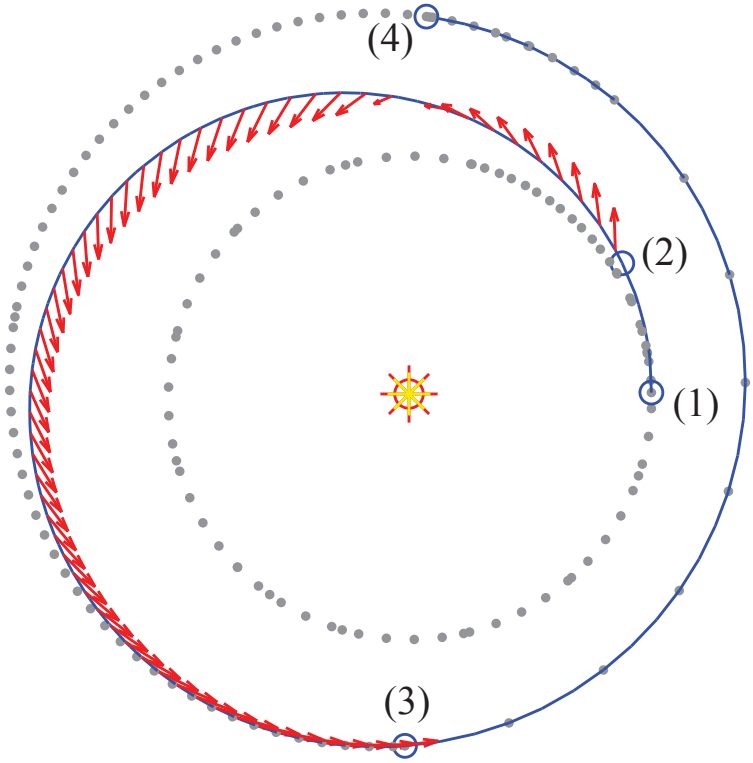

Figure 5.2.. The nominal trajectory for the 10 kW spacecraft is one continuous thrust arc without any coast periods. (1) Depart Earth (2) End "check-out" coast (3) Rendezvous with Mars (4) End spiral to low-Mars orbit. Red arrows indicate thrust direction. Dates of events given in Table 5.1.

days is sufficient to demonstrate the analysis method and identify times when the trajectory is more sensitive to missed thrust. Plots for 5-day, 15-day, 25-day, and 30-day missed thrusts are shown in Appendix A. Each colored circle in the plot represents a trajectory starting from the end of a missed thrust and continuing through the rest of the mission (in this case ending with a rendezvous at Mars). Circles closer to the bottom of the plot are the result of optimizations with an objective function weighted towards more mass optimal. These trajectories use less mass to recover from the missed thrust at the expense of a greater delay. Conversely, circles near the top represent more time-optimal trajectories which use more propellant to complete

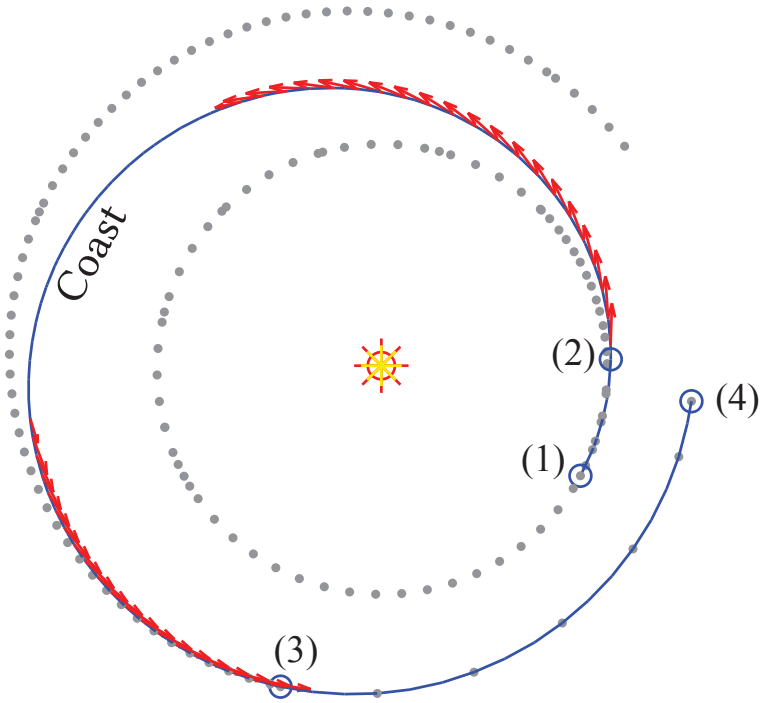

Figure 5.3.. The nominal trajectory for the 20 kW spacecraft features a coast arc between two thrust arcs. (1) Depart Earth, (2) End "check-out" coast, (3) Rendezvous with Mars, (4) End spiral to low-Mars orbit. Red arrows indicate thrust direction. Dates of events given in Table 5.1

the mission. The colors of each circle correspond to the delay in arrival compared to the nominal trajectory. Shaded portions of the plot denote the presence of an optimal coast arc in the nominal trajectory.

These plots are intended for use as a tool during the preliminary mission design phase to aid in the selection of a propellant margin and to determine whether a particular trajectory is especially vulnerable to a missed-thrust event. The plots can be interpreted as follows:

1. Pick a missed-thrust duration a mission should be able to recover from. Then pick a power level to consider. For example, we will look at a 20-day missed thrust for a 10 kW spacecraft.

2. Pick a propellant margin to carry aboard the spacecraft. For our example we will use 5%.

3. Trace a horizontal line at the chosen propellant margin across the plot. The colors the line passes through provide an estimate of how late the spacecraft will arrive in the event of a missed thrust at each point along the trajectory. In our example, a 5% propellant margin will allow a 10 kW spacecraft to recover from a 20-day missed thrust with not more than a 100–150 day delay in arrival. If a line of constant propellant margin passes below the solid black line (representing a mass-optimal trajectory), then that propellant margin may not be sufficient to recover from a missed thrust at that point in the trajectory.

4. Repeat for different power levels to compare performance in the event of a missed thrust.

Upon examining the plots of Figs. 5.4–5.9, we see a general trend of increased robustness to missed thrust for lower power levels. This result may seem counter-intuitive because higher power is associated with more capability, and higher power (and hence higher thrust) trajectories often have optimal coast arcs during which missed thrust may be "made up". However, by increasing the power level and decreasing the duration of thrusting, each moment of thrust is more important compared to a lower power trajectory, and missing thrust requires more propellant and time to make up.

In our example for a 20-day missed thrust and a 10 kW spacecraft, a 5% propellant margin is sufficient to account for a missed thrust anywhere in the trajectory. However, for a 20 kW spacecraft, a 5% propellant margin is not enough for the spacecraft to recover and reach its target if a 20-day missed thrust occurs early in the mission. In Fig. 5.9, we can see that a horizontal line drawn at 5% margin passes below where the solid black line spikes up, indicating that margin is not sufficient for the spacecraft to reach its target at that point. A propellant margin of approximately 15% is required for the 20 kW spacecraft to recover from a 20-day missed thrust anywhere in the

trajectory. In essence, increasing the power level is analogous to pushing towards the extreme case of an impulsive trajectory, in which a missed thrust (i.e. a missed burn) cannot be recovered from. On the other hand, the coast arc present in the higher power trajectories provides a time during the mission which is completely robust to a missed thrust.

In Figs. 5.4–5.9 certain cases take on negative values for M, especially in the left sides of Figs. 5.4 and 5.5. A negative value for the propellant margin occurs when the final mass in the missed-thrust case is greater than the final mass in the nominal case. While it may seem unusual for a trajectory to perform better with missed thrust, this result can occur when the nominal trajectory was designed with a time constraint. In the missed-thrust case the time constraint is lifted and a weighted optimization problem is solved. Solutions with negative propellant margin arrive at the target later than the nominal case. Similarly, some solutions take on negative values for L, indicating they arrive early at the target. These are solutions with higher values for η. If η is high enough, the optimizer will spend more propellant to minimize TOF, overriding the effect of missed thrust. These solutions do not impact the main results of the analysis, and can be ignored.

Despite the fact that the higher power trajectories require a higher propellant margin to account for missed thrust, they still achieve higher overall performance in terms of final mass. To compare the final mass of trajectories with different power levels, we must subtract the missed-thrust propellant margin and propulsion system masses, resulting in a usable final mass. These subtractions come out of the total final mass, holding the initial launch mass constant. Subtracting a 15% propellant margin from the final mass of the 20 kW nominal case results in a new final mass of 2544 kg, while subtracting a 5% propellant margin from the final mass of the 10 kW trajectories yields a new final mass of 2267 kg. Taking it a step further, if we assume a 15 kg/kW specific mass [34, 72] for the propulsion system (including the solar arrays, thruster assemblies, and power processing unit), we can subtract the propulsion system mass from the final mass of the spacecraft, leaving 2244 kg for

the 20 kW trajectory and 2117 kg for the 10 kW trajectory. This analysis, while only an approximation, indicates that for this particular mission a 20 kW spacecraft outperforms a 10 kW spacecraft even when accounting for the difference in propulsion system mass and the effects of missed thrust. However, the dependency between propellant margin and power level leaves open the possibility that for a different mission, designing around a lower power system may actually increase performance.

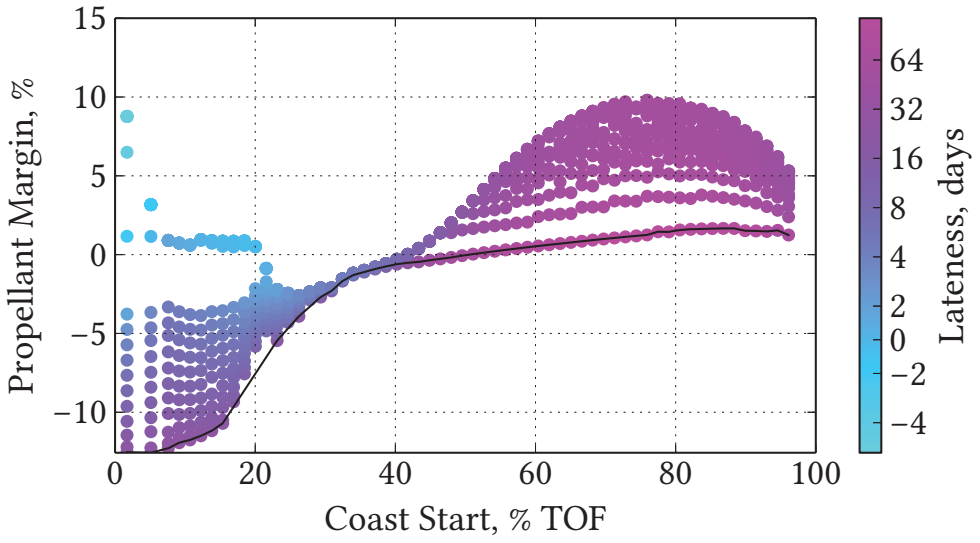

Figure 5.4.. Lateness vs Propellant margin for the 10 kW case with a 10-day missed thrust.

Propellant Margin vs Time Margin

The results shown previously allow mission planners to see the how the sensitivity to missed thrust changes along a trajectory. However, it may be useful to condense the information and show only the worst-case lateness a mission could face as a result of a missed thrust as a function of the propellant margin carried on the mission. These plots are shown in Figs. 5.10 and 5.11, where it is shown that carrying more propellant margin than the minimum required for a given missed-thrust duration can

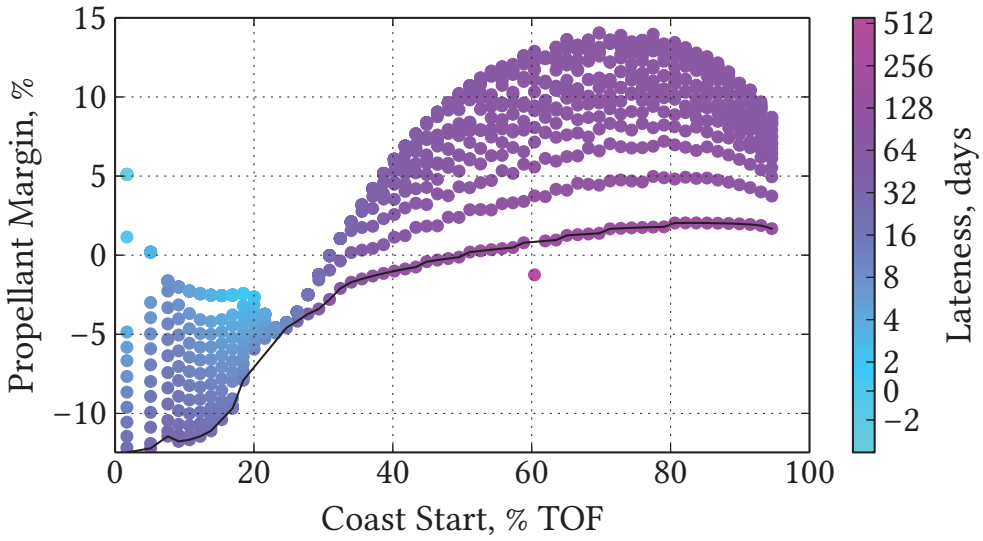

Figure 5.5.. Lateness and propellant margin for the 10 kW case with a 20-day missed thrust.

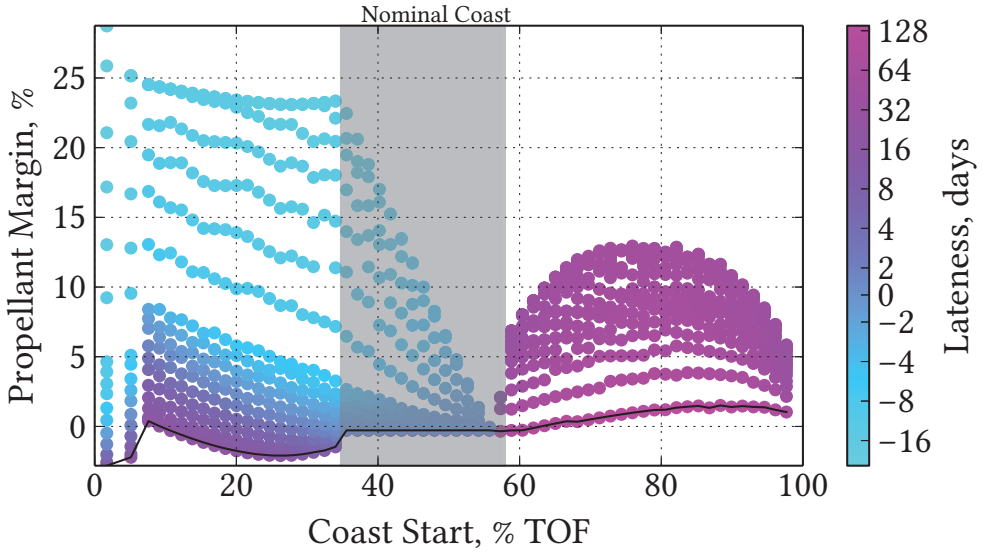

Figure 5.6.. Lateness and propellant margin for the 15 kW case with a 10-day missed thrust.

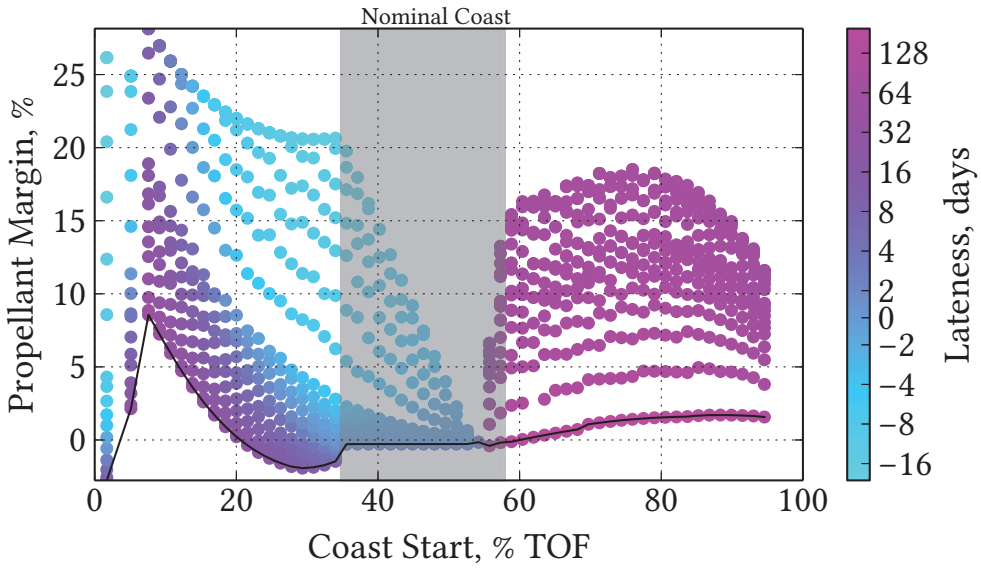

Figure 5.7.. Lateness and propellant margin for the 15 kW case with a 20-day missed thrust.

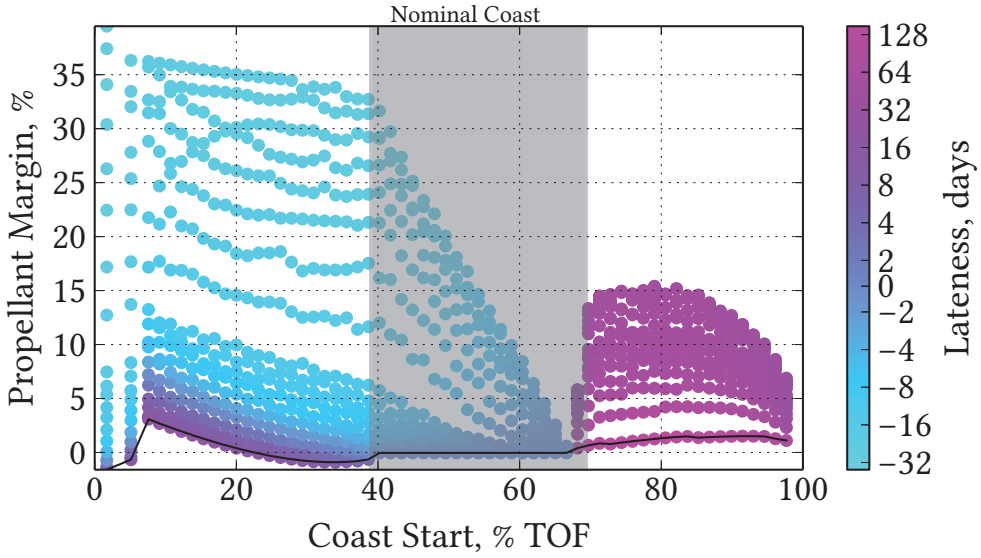

Figure 5.8.. Lateness and propellant margin for the 20 kW case with a 10-day missed thrust.

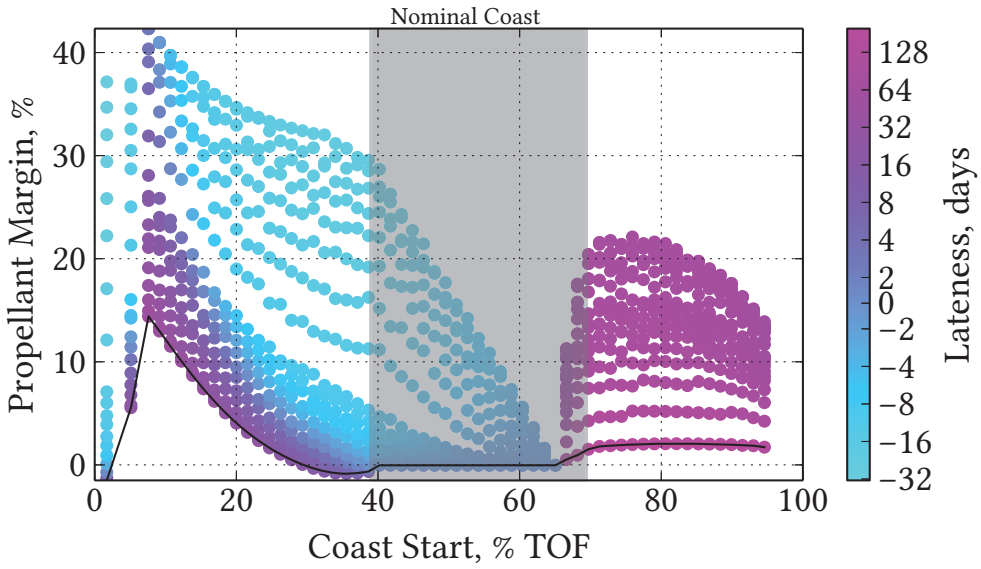

Figure 5.9.. Lateness and propellant margin for the 20 kW case with a 20-day missed thrust.

reduce potential delays in arrival. The amount of margin propellant carried can then be determined based on the relative importance of arriving on time for a particular mission. Additionally, mission planners can see the propellant margin after which carrying additional margin is no longer of use for missed thrust.

5.4.2 Gravity-Assist Trajectory to the Asteroid Belt

The gravity-assist example is a trajectory departing Earth for a rendezvous with the asteroid Psyche via a Mars gravity assist. Psyche is a large asteroid in the main asteroid belt with a diameter of 253 km, and is of interest to the planetary science community as possibly being an exposed iron core of an ancient protoplanet. Psyche's orbital characteristics are listed in Table 5.2 [2].

[2]Orbit data available at: http://ssd.jpl.nasa.gov/sbdb.cgi [Retrieved November 2014]

Table 5.2.. Orbital information for asteroid (16) Psyche

Parameter	Value
a	2.92 AU
e	0.14
i	3.10 deg
Ω	150.3 deg
ω	227.1 deg
Time of Periapsis	JD 2457128.99
Time of Periapsis	Apr. 16, 2015
Period	1825 d

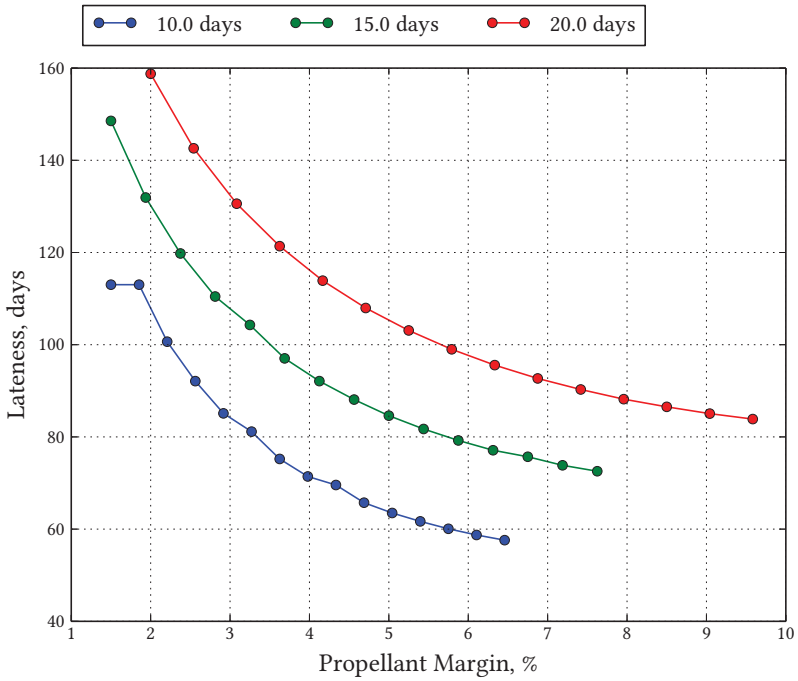

Figure 5.10.. The maximum lateness is plotted as a function of the propellant margin carried for the 10 kW nominal trajectory.

Nominal Trajectory to Psyche

The example mission to Psyche follows a nominal trajectory that launches from Earth aboard a SpaceX Falcon 9 launch vehicle and takes 4 years to rendezvous with Psyche with a Mars gravity assist along the way. The trajectory is optimized for maximum final mass subject to a 4-year time-of-flight constraint. More information about the trajectory to Psyche is listed in Table 5.3. The propulsion system is the same as that for the Mars rendezvous case, and consists of two BPT-4000 Hall effect thrusters. The propulsion and power system model is given by Eqs. 5.8, 5.9, and 5.10.

A plot of the nominal trajectory to Psyche is shown in Fig. 5.12. The gravity assist with Mars occurs during a thrust arc, and it is expected that a missed thrust during the thrust arc leading up to the gravity assist will result in severe consequences to the mission.

Table 5.3.. Nominal Trajectory to Psyche

Parameter	Value
Power (1 AU)	20 kW
Final Mass	1539 kg
Propellant Mass	1844 kg
Launch C_3	2.34 km^2/s^2
Cumulative ΔV	13.5 km/s
Launch Date	Jan. 12, 2025
Mars Flyby Date	Nov. 9, 2026
Psyche Arrival Date	Jan. 11, 2029

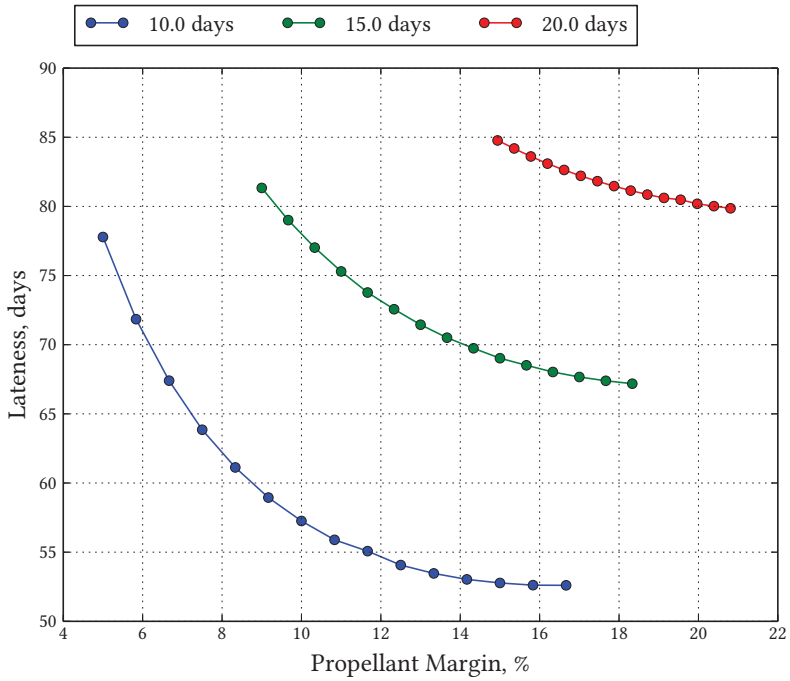

Figure 5.11.. The maximum lateness is plotted as a function of the propellant margin carried for the 20 kW nominal trajectory.

The results from the missed-thrust analysis of the gravity-assist trajectory to Psyche are shown in Figs. 5.13–5.16. The plots are structured the same as in Figs. 5.4–5.9. In addition, the epoch of the Mars gravity assist is marked with a blue vertical line. The most significant result to note is the gap in the data centered in the second half of 2026, which indicates the optimizer did not converge on a solution following a missed thrust during that time. From Fig. 5.13, we can see that even a 1-day missed thrust is problematic within 30 days before the gravity assist, and may result in the loss of a mission. Prior to this period, a spike in the propellant margin required to recover from the missed thrust is present. In addition, prior to the rendezvous with Psyche, the effect of a missed thrust is shown to delay arrival at the target. This result agrees with the analysis of the Mars rendezvous example.

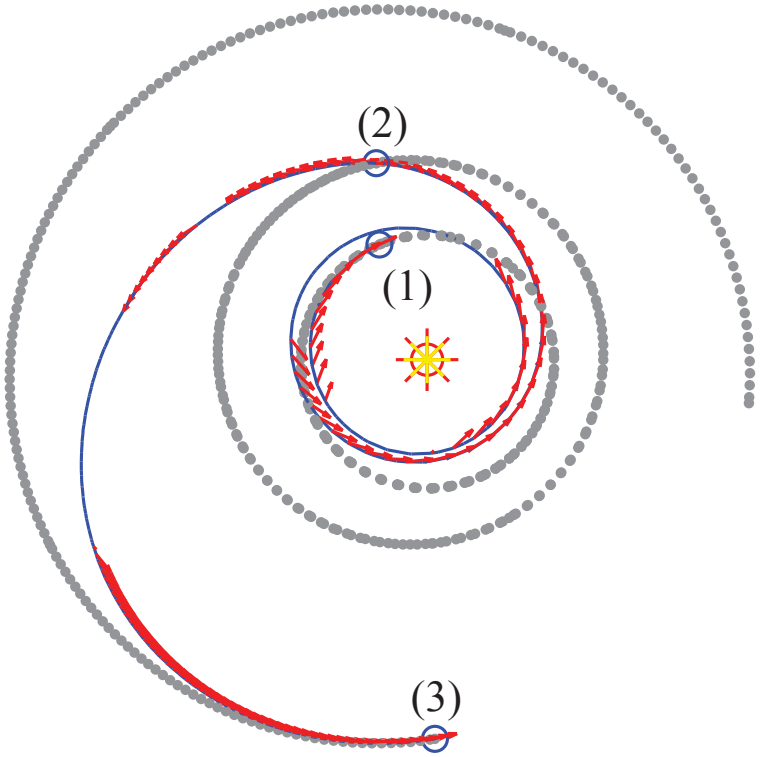

Figure 5.12.. The nominal trajectory to Psyche features a gravity assist with Mars during a thrust arc. (1) Depart Earth, (2) Mars gravity assist, (3) Rendezvous with Psyche.

Redesign: Force a Coast Before the Gravity Assist

We have shown that a trajectory in which a gravity assist occurs during a thrust arc is inherently not robust to missed thrust, so we now attempt to resolve the problem by modifying the nominal trajectory such that the gravity assist occurs during a coast arc. Constraining the spacecraft to coast before the gravity assist may provide a buffer period where missed thrust can be made up. This idea is tested by performing a missed-thrust analysis on a version of the nominal trajectory to Psyche which is constrained to coast for 30 days leading up to the Mars gravity assist. Enforcing this coast constraint results in a final mass just 18 kg less than the final mass of the nominal trajectory without the coast.

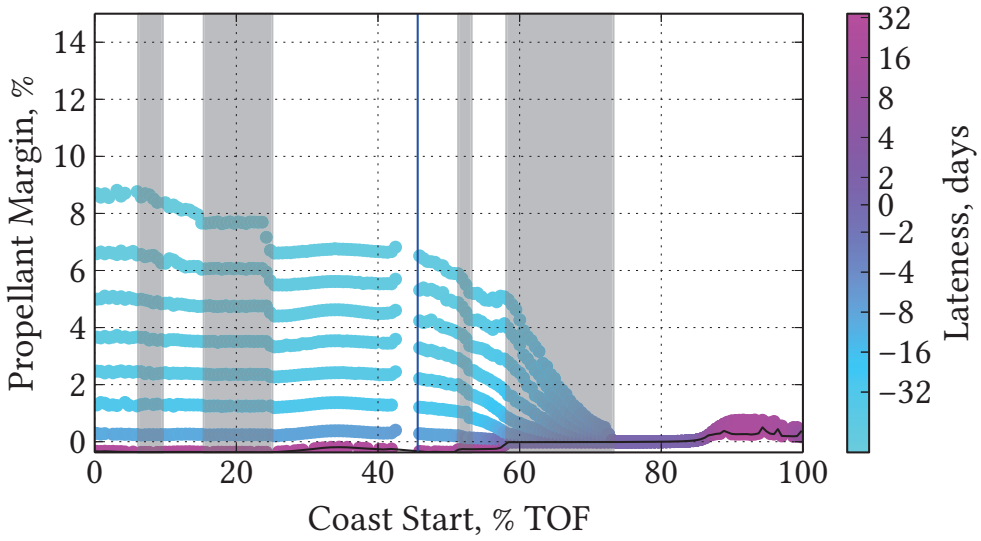

Figure 5.13.. Lateness and propellant margin for a 1-day missed thrust during a gravity-assist trajectory to Psyche.

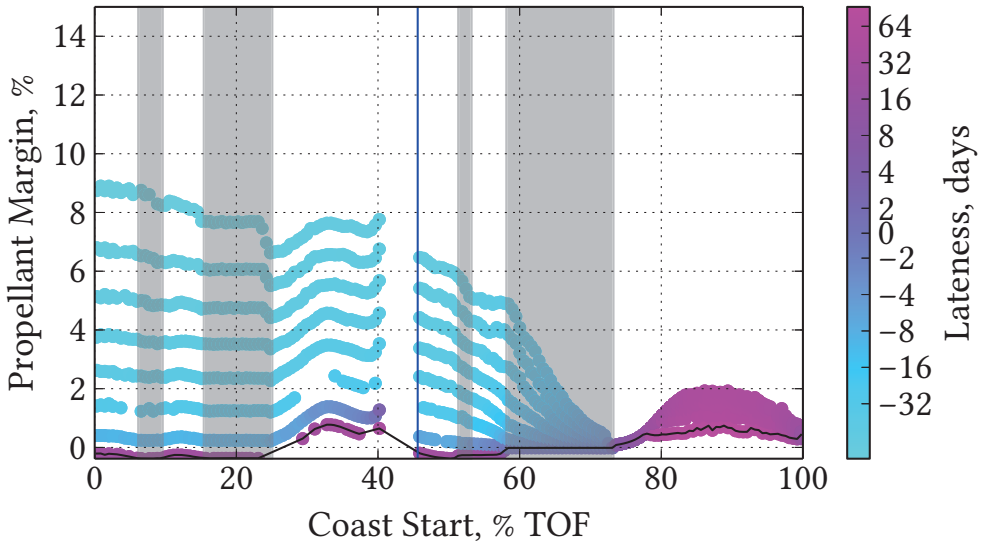

Figure 5.14.. Lateness and propellant margin for a 5-day missed thrust during a gravity-assist trajectory to Psyche.

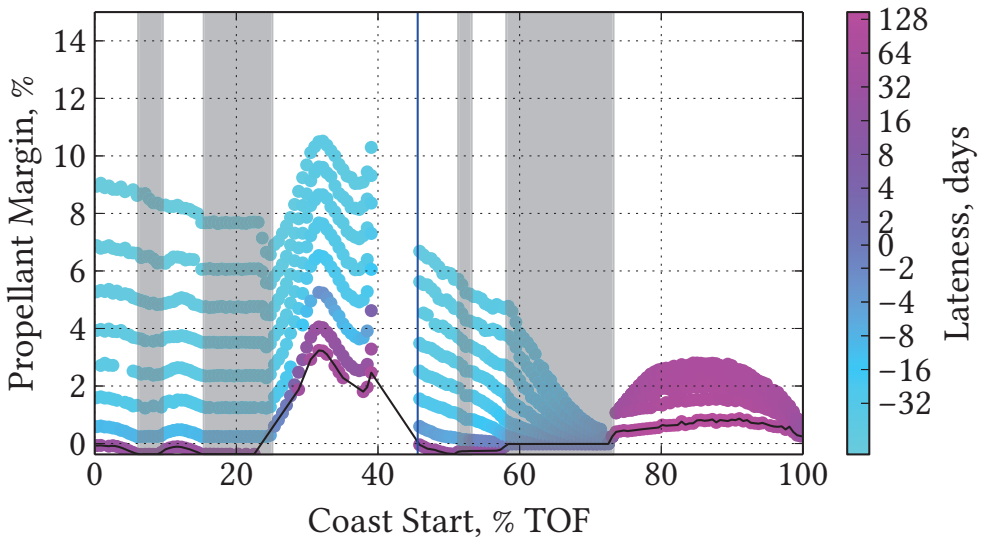

Figure 5.15.. Lateness and propellant margin for a 10-day missed thrust during a gravity-assist trajectory to Psyche.

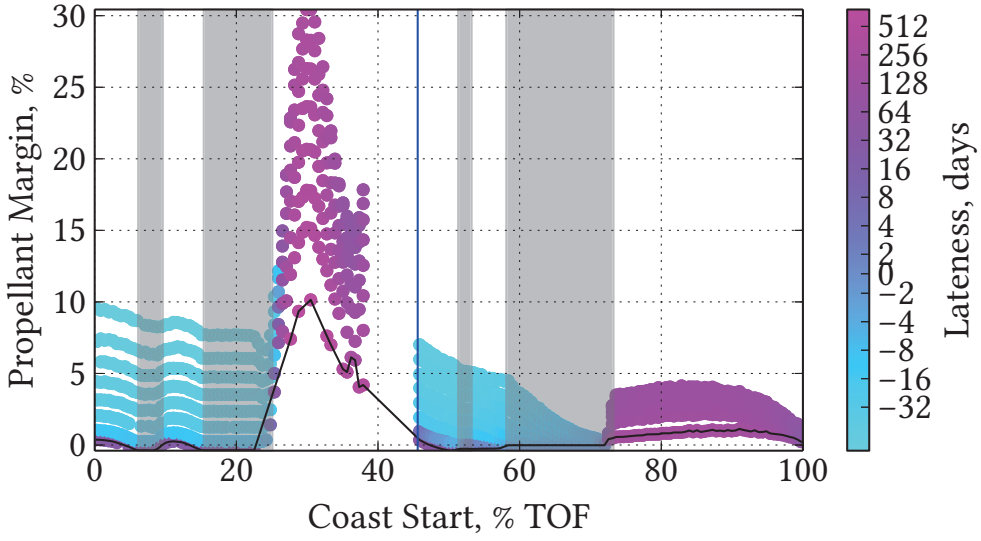

Figure 5.16.. Lateness and propellant margin for a 20-day missed thrust during a gravity-assist trajectory to Psyche.

The results of the missed-thrust analysis on the trajectory with the coast arc before the missed thrust are shown in Figs. 5.17–5.20. The analysis shows that adding a coast arc before the gravity assist does indeed reduce the overall sensitivity to missed thrust. Missed thrusts of 10 days or less do not result in loss of the mission at any time, although a 20-day missed thrust in the period before the gravity assist still may cause a mission failure. While we are able to mitigate the problem of missed thrust by adding a forced coast at the gravity assist, we see that it is important to take missed thrust into account when designing the nominal trajectory. In the prior example of a direct trajectory from Earth to Mars, missed thrust could be overcome by some combination of spending more propellant or delaying arrival, however in the gravity-assist example, the nominal trajectory is unsuitable for a mission without modification. Some gaps exist in the data where the optimizer failed to converge, however because solutions exist for both higher and lower propellant margins these gaps do not indicate a severe issue with missed thrust sensitivity at that location. In Fig. 5.18 we see some gaps in the solution set prior to the gravity assist, however because the gap does not extend through the entire vertical span of propellant margins (like the gap in Fig. 5.16 for example), it does not indicate that the spacecraft cannot recover from a missed thrust at that time.

There are several considerations that may require a coast arc leading up to the gravity assist other than missed thrust. The critical nature of the gravity-assist maneuver calls for increased fidelity in the knowledge of the trajectory. Thrust introduces some level of uncertainty in the spacecraft's orbit, so mission planners may require a coast before the gravity assist to help in navigation. The effect of missed thrust on the trajectory prior to a gravity assist reinforces the requirement to coast before the flyby.

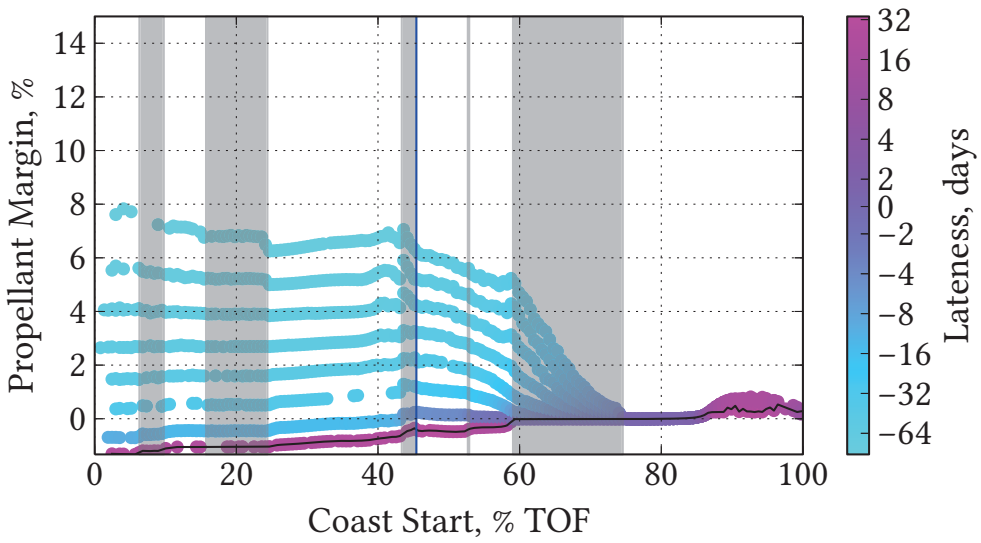

Figure 5.17.. Lateness and propellant margin for a 1-day missed thrust with a coast arc prior to the gravity assist.

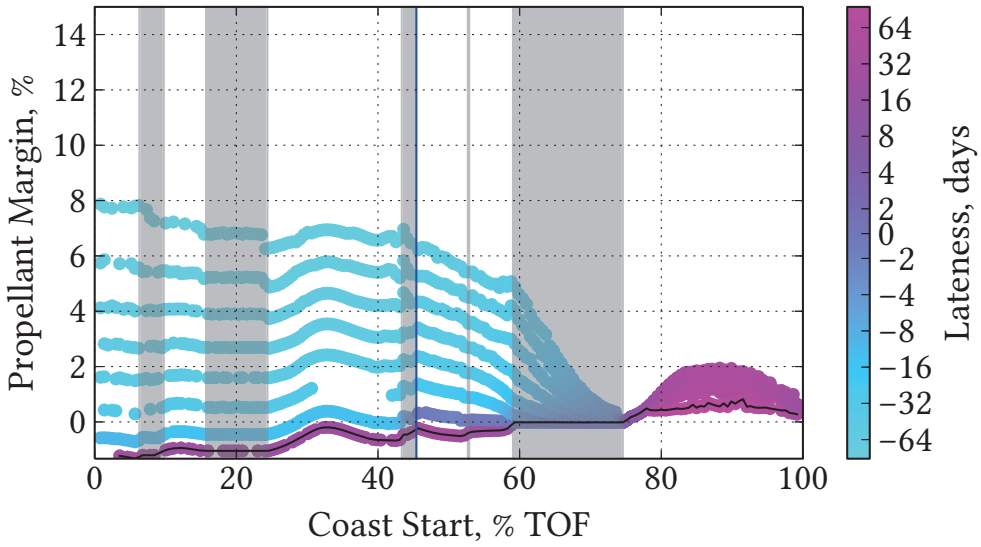

Figure 5.18.. Lateness and propellant margin for a 5-day missed thrust with a coast arc prior to the gravity assist.

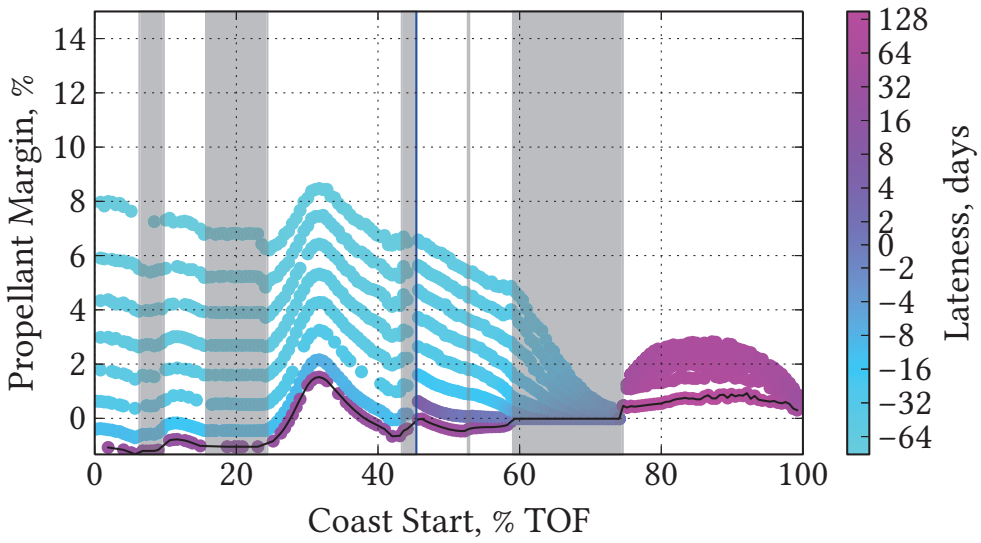

Figure 5.19.. Lateness and propellant margin for a 10-day missed thrust with a coast arc prior to the gravity assist.

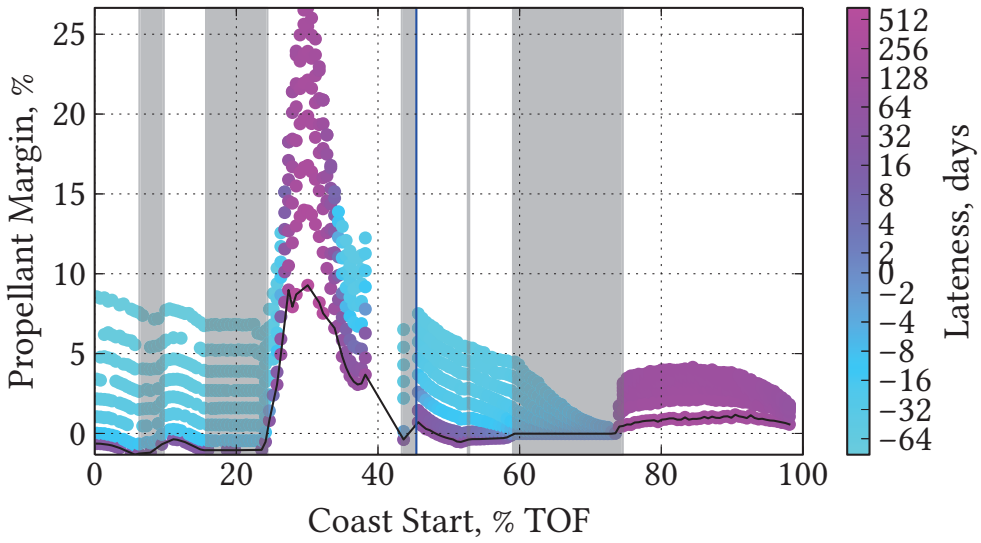

Figure 5.20.. Lateness and propellant margin for a 20-day missed thrust with a coast arc prior to the gravity assist.

Table 5.4.. Orbital information for asteroid 1991 VG

Parameter	Value
a	1.03 AU
e	0.049
i	1.45 deg
Ω	74.0 deg
ω	24.6 deg
Time of Periapsis	JD 2456981.78
Time of Periapsis	Nov. 20, 2014
Period	380 d

5.4.3 Solar Sail Trajectory

The solar sail example has a spacecraft departing Earth on Jan. 25, 2018, and arriving at the near-Earth asteroid 1991 VG on Nov. 8, 2019. The orbital elements of 1991 VG are summarized in Table 5.4 [3]. The spacecraft has a sail area-to-mass ratio of 6.6 m^2/kg. The nominal trajectory to 1991 VG was designed to minimize time of flight.

In Fig. 5.21, instead of missed thrust, we have plotted the effect of an event which forces the spacecraft into safe mode. Furthermore, we assume that while in safe mode, the spacecraft automatically aligns its sail to be normal to the Sun direction, resulting in a radial acceleration from the sail. This safe mode condition is a likely scenario, especially in the case where the solar sail and solar panels are in the same plane [73]. While thrust is not missed in this case, it is not in the direction specified by the nominal trajectory.

Because a solar sail spacecraft does not require propellant for its primary thrust, we can simply plot the delay in arrival as a function of the time in the trajectory

[3]Orbit data available at: http://ssd.jpl.nasa.gov/sbdb.cgi [Retrieved June 2014]

that an uncontrolled thrust occurs for a series of uncontrolled thrust durations. If the solar sail spacecraft encounters an unplanned radial thrust, it will arrive late at its target. In Fig. 5.21, we can see that even a 30-day outage will not delay the mission by more than 50 days for the first year of the mission. However, after the first year sensitivity to an outage begins to increase greatly for the longer outage durations, with delays increasing to over 200 days.

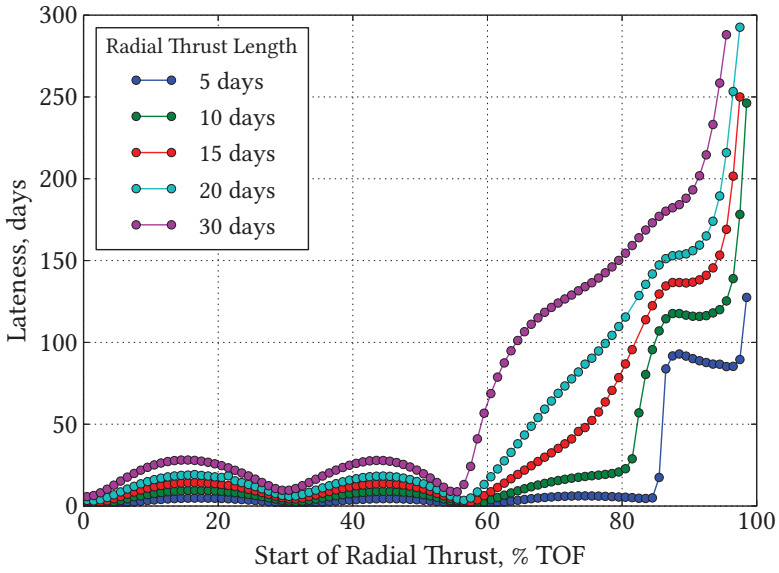

Figure 5.21.. Sensitivity to an unplanned radial thrust event is plotted as a function of time during the trajectory.

For this study, we assumed the solar sail spacecraft would apply radial thrust in the event of an outage. However, other safe-mode pointing strategies are available to mission designers. The analysis method presented here may provide a way of comparing these alternate strategies to select one that minimizes the delay in arrival for a solar sail spacecraft.

5.5 Conclusion

We have presented a systematic method to quantify the effect of missed thrust on a trajectory by measuring the propellant margin required to recover from a missed thrust and the delay in arrival resulting from a missed thrust. This method was tested on three cases: a direct low-thrust transfer to Mars and a solar sail mission to a near-Earth asteroid. The results from these tests are generally positive, indicating that recovering from a significant missed thrust is feasible for both electric and solar sail propulsion. However, missed thrust affects each trajectory differently, and cannot be accounted for with a general-purpose rule. The results presented here are relevant in cases where the nominal trajectory is optimized for maximum payload mass given a time constraint, but the analysis algorithm can also be applied to nominal trajectories where final mass and flight time are optimized from the outset as a weighted sum.

For the electric propulsion mission to Mars, propellant margins between 5–15% are needed to recover from missed thrust. We find (a non-intuitive result) that while higher power levels increase final mass, a higher propellant margin is required to recover from missed thrust at any time in the mission.

Including a gravity-assist maneuver in a low-thrust trajectory introduces very high sensitivity to missed thrust in the period before the gravity assist if the nominal trajectory has a thrust arc during that time. This sensitivity can be mitigated by constraining the spacecraft to coast before the gravity assist when designing the trajectory, but the mission is still vulnerable to longer thrust outages. Importantly, for a low-thrust trajectory with a gravity assist, missed-thrust must be considered in the design of the nominal trajectory.

For the solar sail mission to 1991 VG, the delay on arrival is under 50 days for outages during the first half of the mission, but begins to increase to over 200 days for later outages as the spacecraft approaches the target. Based on the favorable results obtained here, it appears that missed-thrust arcs can be accommodated with

reasonable propellant margins, increases in time of flight, or by modifying the nominal trajectory, thus adding robustness to such low-thrust missions.

6. Conclusions

6.1 Human Mission to Ceres

The dwarf planet Ceres is an interesting target for human exploration. While it is further away than Mars, its small size and lack of atmosphere mean that landing on the surface (a very risky operation at Mars) should be far safer. Likewise, departing the surface and returning to Earth would be far less costly. We have seen that a human mission to Ceres could be accomplished with an IMLEO of similar scales to that of a mission to Mars. In addition, Ceres likely posses large quantities of water (in the form of ice) that could be used by a human mission for both human consumption and as a propellant. The key technology enabling a human mission to Ceres is high-power nuclear electric propulsion, which could drive flight times down to 270 days each way.

6.2 Missions to the Jupiter Trojans

We searched for trajectories to pairs of Jupiter Trojan asteroids comprised of objects from two groups: those with spectral data skewed towards red, and those that are less red. We find that the pair 1986 TS6 and Hektor presents the best opportunity for launch dates between 2020–2040 in that the delivered mass is greatest compared to other Trojan pairs in that time period. The orbital plane change required by a spacecraft traveling between Trojan asteroids is somewhat correlated to the mass cost of the mission, with reduced payload masses for plane changes greater than 15°. Net masses of greater than 1400 kg can be achieved with a commercially available Hall thruster and a 40 kW SEP system. A more reasonable 30 kW SEP system, using the

same thruster, can deliver 1300 kg of net mass. Mission times of 11.3 to 12 years are possible with these propulsion systems.

6.3 Sample Return Trajectories to Kleopatra

Our search for sample-return trajectories to Kleopatra examined a series of different gravity-assist sequences using Venus, Earth, and Mars. We found that Earth and Mars are useful as gravity-assist bodies, while Venus does not appear to offer much benefit. A 20 kW SEP system is capable of delivering a 1000 kg payload mass with flight times of under 10 years from Earth launch to Earth return.

6.4 Missed-Thrust Margin Analysis

Electric propulsion offers the potential for increased performance over chemical propulsion, however there is a new set of practical concerns that should be considered in the mission design process for electric propulsion. Missed-thrust is one such concern. We have seen that for simple trajectories that depart Earth and rendezvous with Mars, a missed-thrust event can be overcome at the cost of extra propellant and a late arrival at Mars. However in that case the nominal trajectory itself did not need to be modified in the design process.

For the more complex example of trajectory to the asteroid Psyche via a Mars gravity assist, the nominal trajectory is too risky to use. Because the gravity assist occurs during a thrust arc, a missed-thrust event (even a short one) in the leg leading up to the gravity assist results in a loss of the mission. In this case, inserting a 30-day coast arc immediately before the gravity assist reduced sensitivity to missed thrust such that the mission could tolerate a 10-day missed-thrust event at the most sensitive point. Inserting this coast arc comes at a cost of reducing the final mass compared to the unmodified nominal trajectory.

The missed-thrust analysis can also be applied to solar sail missions. In a solar sail mission, a safe-mode event may result in the spacecraft pointing its sail directly

towards the Sun while it awaits commands from the ground. In this case, a radial acceleration is applied to the spacecraft instead of the acceleration prescribed for the nominal, time-optimal trajectory. We have seen that in the example of a solar sail mission to the NEA 1991 VG, an unplanned radial thrust delays the arrival at the target, with greater delays seen for off-nominal accelerations later in the trajectory.

7. Future Work

7.1 Missed-Thrust Problem

In Chapter 5 we present a method for analyzing the effect of missed thrust on a nominal trajectory. This analysis allows mission planners to determine how much propellant margin a spacecraft must carry to overcome a missed-thrust event, however, the next step in this research is to feed the information collected from the missed-thrust analysis back into the trajectory design process. We can then design trajectories from the outset which are inherently robust to missed thrust.

One way we might add this analysis to the design process is by adding a constraint to the optimization problem. For example, we may constrain the propellant margin required by

$$\text{Minimize } J = -m_f \tag{7.1}$$

subject to

$$\text{Max}[M(\eta = 0)] \leq M_{max} \tag{7.2}$$

The constraint given in Equation 7.2 means that the maximum propellant margin required in a mass optimal trajectory ($\eta = 0$) must be less than a specified level. If a trajectory has a spike in the propellant margin at a specific time, there may be a way to modify the nominal trajectory to reduce the spike at the expense of a small raise in the average propellant margin required throughout the trajectory.

As of now, the most fundamental obstacle to incorporating the missed-thrust analysis into the trajectory optimization loop is the computational expense of performing the analysis. Each nominal trajectory can take 2–6 hours to analyze. While this time is acceptable for performing the analysis once on a given trajectory, adding it to a larger optimization scheme would mean it would need to be performed at each optimization step (possibly thousands of times). In addition, we would require the

derivatives of the maximum propellant margin with respect to the design variables if we are to use a gradient based method. The direct optimization method employed by MALTO has hundreds of design variables, meaning hundreds of analyses would be required to obtain the derivatives.

There are several possible solutions to this problem:

1. Estimate the missed-thrust propellant margin without performing the full analysis. This estimation could be accomplished with a surrogate function quickly predicts the propellant margin as a function of the design variables at the expense of some accuracy.

2. Perform a reduced version of the missed-thrust analysis. For example, if a trajectory is found to have one location where the propellant margin is very high, it can be redesigned by performing the missed thrust analysis repeatedly at only that one spot. This method reduces the overall computational demands, however a new spike could appear elsewhere in the trajectory during the redesign.

3. Use an indirect, optimal control-based method for solving the optimization problem. The major drawbacks to an indirect method are the need for a very close initial guess and the high sensitivity shown for multi-leg (multiple gravity assist) trajectories. The former drawback can be overcome by designing the nominal trajectory in MALTO, then using that guess to initialize an optimal control-based solver. Switching to an indirect method greatly reduces the total number of design variables in the problem, going from hundreds of ΔV components to seven initial values of the co-state equations.

7.2 A Human Mission to Ceres

One of the key differences between a human mission to Ceres and a human mission to Mars is landing and taking off from the surface. Mars' atmosphere and much greater mass mean that entry, descent, and landing (EDL) would be a much costlier

and riskier prospect than the corresponding operations at Ceres. However, a detailed study of EDL at Ceres has yet to be performed. Such an analysis would be useful for a direct comparison of Ceres and Mars as destinations for astronauts, and could make a strong case for visiting Ceres. The challenge of returning from Mars is so great that no-return mission concepts are gaining popularity. If it can be shown that returning from Ceres is feasible and safe, Ceres may even be a more attractive target for those who do not wish to commit to a one-way mission to Mars.

REFERENCES

REFERENCES

[1] Marc D. Rayman, Philip Varghese, David H. Lehman, and Leslie L. Livesay. Results from the Deep Space 1 technology validation mission. *Acta Astronautica*, 47:475–487, 2000.

[2] Jun'ichiro Kawaguchi, Kuninori Uesugi, and Akira Fujiwara. The MUSES-C mission for the sample and return—its technology development status and readiness. *Acta Astronautica*, 52:117–123, 2003.

[3] C. T. Russell, F. Capaccioni, A. Coradini, M. C. De Sanctis, W. C. Feldman, R. Jaumann, H. U. Keller, T. B. McCord, L. A. McFadden, S. Mottola, C. M. Pieters, T. H. Prettyman, C. A. Raymond, M. V. Sykes, D. E. Smith, and M. T. Zuber. Dawn mission to Vesta and Ceres. *Earth, Moon, and Planets*, 101:65–91, 2007.

[4] John W. Dankanich, Laura M. Burke, and Joseph A. Hemminger. Mars sample return orbiter/Earth return vehicle technology needs and mission risk assessment. In *IEEE Aerospace Conference*, Big Sky, MT, 2010.

[5] Peter Y. Peterson, Hani Kamhawi, David H. Manzella, and David T. Jacobson. Hall thruster technology for NASA science missions: HiVHAC status update. In *43rd AIAA/ASME/SAE/ASEE Joint Propulsion Conference*, Cincinnati, OH, 2007.

[6] John T. Betts. Survey of numerical methods for trajectory optimization. *Journal of Guidance, Control, and Dynamics*, 21:193–207, 1998.

[7] K. Joseph Chen, Kevin W. Kloster, and James M. Longuski. A graphical method for preliminary design of low-thrust gravity-assist trajectories. In *AIAA/AAS Astrodynamics Specialist Conference and Exhibit*, Honolulu, HI, August 2008. AIAA 2008-6952.

[8] Lorenzo Casalino and Guido Colasurdo. Optimization of variable-specific-impulse interplanetary trajectories. *Journal of Guidance, Control, and Dynamics*, 27:678–684, 2004.

[9] Anastassios E. Petropoulos and James M. Longuski. Shape-based algorithm for automated design of low-thrust, gravity-assist trajectories. *Journal of Spacecraft and Rockets*, 41:787–796, 2004.

[10] M. Vasile, Paolo De Pascale, and Stefano Casotto. On the optimality of a shape-based approach based on pseudo-equinoctial elements. *Acta Astronautica*, 61:286–297, 2007.

[11] Sean Tang and Bruce A. Conway. Optimization of low-thrust interplanetary trajectories using collocation and nonlinear programming. *Journal of Guidance, Control, and Dynamics*, 18:599–604, 1995.

[12] Mark G. Benton. Spaceship discovery – NTR vehicle architecture for human exploration of the solar system. In *45th AIAA/ASME/SAE/ASEE Joint Propulsion Conference and Exhibit*, August 2009. AIAA 2009-5309.

[13] Gerald Walberg. How shall we go to Mars? A review of mission scenarios. *Journal of Spacecraft and Rockets*, 30(2):129 – 139, 1993.

[14] Brett G. Drake. Human exploration of Mars Design Reference Architecture 5.0. Technical Report NASA-SP-2009-566, NASA, 2009.

[15] Damon F. Landau and James M. Longuski. Trajectories for human missions to Mars, part 1: Impulsive transfers. *Journal of Spacecraft and Rockets*, 43(5):1035–1042, September–October 2006.

[16] Damon F. Landau and James M. Longuski. Trajectories for human missions to Mars, part 2: Low-thrust transfers. *Journal of Spacecraft and Rockets*, 43(5):1043–1047, September–October 2006.

[17] Damon Landau. *Strategies for the Sustained Human Exploration of Mars*. PhD thesis, Purdue University, 2006.

[18] Damon F. Landau and James M. Longuski. Comparative assessment of human–Mars-mission technologies and architectures. *Acta Astronautica*, 65:893–911, 2009.

[19] Jean Marc Salotti. Simplified scenario for manned Mars missions. *Acta Astronautica*, 69:266–279, 2011.

[20] Brent W. Barbee, Timothy Esposito, Elfego Piñon III, Sun Hur-Diaz, Ronald G. Mink, and Daniel R. Adamo. A comprehensive ongoing survey of the near-Earth asteroid population for human mission accessibility. In *AIAA Guidance, Navigation, and Control Conference*, Toronto, Canada, August 2010. AIAA 2010-8368.

[21] B. Sherwood, M. Adler, L. Alkalai, G. Burdick, D. Coulter, F. Jordan, F. Naderi, L. Graham, R. Landis, B. Drake, S. Hoffman, J. Grunsfeld, and B. D. Seery. Flexible-path human exploration. In *AIAA SPACE 2010 Conference and Exposition*, August 2010. AIAA 2010-8607.

[22] David R. Brooks. Solar electric missions to Ceres. *Journal of Spacecraft*, 8(8):889–890, 1971.

[23] Larry A. Lebofsky, Michael A. Feierberg, Alan T. Tokunaga, Harold P. Larson, and James R. Johnson. The 1.7- to 4.2-μm spectrum of asteroid 1 Ceres: Evidence for structural water in clay minerals. *Icarus*, 48:453–459, July 1981.

[24] Fraser P. Fanale and James R. Salvail. The water regime of asteroid (1) Ceres. *Icarus*, 82:97–110, March 1989.

[25] Myung-Hee Y. Kim, Giovanni De Angelis, and Francis A. Cucinotta. Probabalistic assessment of radiation risk for astronauts in space missions. *Acta Astronautica*, 68:747–759, 2011.

[26] Francis A. Cucinotta and Marco Durante. Cancer risk from exposure to galactic cosmic rays: implications for space exploration by human beings. *Lancet Oncology*, 7(5):431–435, 2006.

[27] Ron J. Litchford, L. J. Bitteker, and J. E. Jones. Prospects for nuclear electric propulsion using closed-cycle magnetohydrodynamic energy conversion. Technical Report TP–2001-211274, NASA, Marshall Space Flight Center, October 2001.

[28] Ron J. Litchford and Nobuhiro Harada. Multi-MW closed cycle MHD nuclear space power via nonequilibrium He/Xe working plasma. In *Proceedings of Nuclear and Emerging Technologies for Space 2011*, February 2011.

[29] Edgar A. Bering III, Benjamin W. Longmier, Maxwell Ballenger, Chris S. Olsen, Jared P. Squire, and Franklin R. Chang Diaz. Performance studies of the VASIMR VX-200. In *AIAA Aerospace Sciences Meeting and Exhibit*, January 2011.

[30] James S. Sovey and Maris A. Mantenieks. Performance and lifetime assessment of magnetoplasmadynamic arc thruster technology. *Journal of Propulsion*, 7(1):71 – 83, 1991.

[31] Jon A. Sims, Paul A. Finlayson, Edward A. Rinderle, Matthew A. Vavrina, and Theresa D. Kowalkowski. Implementation of a low-thrust trajectory optimization algorithm for preliminary design. In *AIAA/AAS Astrodynamics Specialist Conference and Exhibit*, Keystone, CO, August 2006. AIAA Paper 2006-6746.

[32] Theodore H. Sweetser, Michael J. Cherng, Paul A. Penzo, and Paul A. Finlayson. Watch out, it's hot! Earth capture and escape spirals using solar electric propulsion. In *AAS/AIAA Astrodynamics Specialist Conference and Exhibit*, 2001.

[33] M.J.H. Walker, B. Ireland, and Joyce Owens. A set of modified equinoctial orbit elements. *Celestial Mechanics*, 36:409–419, 1985.

[34] Damon Landau, James Chase, Thomas Randolph, Paul Timmerman, and David Oh. Electric propulsion system selection process for interplanetary missions. *Journal of Spacecraft and Rockets*, 48(3):467–476, May–June 2011.

[35] Claude A. Graves and Jon C. Harpold. Apollo experience report – mission planning for Apollo entry. Technical Report TN D-6725, NASA, March 1972.

[36] Space Studies Board. Vision and voyages for planetary science in the decade 2013–2022. Technical report, National Research Council, 2012.

[37] K. Tsiganis, R. Gomes, A. Morbidelli, and H. F. Levison. Origin of the orbital architecture of the giant planets of the Solar System. *Nature*, 435:459–461, 2005.

[38] A. Morbidelli, H. F. Levison, K. Tsiganis, and R. Gomes. Chaotic capture of Jupiter's Trojan asteroids in the early Solar System. *Nature*, 435:462–465, 2005.

[39] David Nesvorny, David Vokrouhlicky, and Alessandro Morbidelli. Capture of Trojans by jumping Jupiter. *Astrophysical Journal*, 768:1–8, 2013.

[40] J. P. Emery, D. M. Burr, and D. P. Cruikshank. Near-infrared spectroscopy of Trojan asteroids: Evidence for two compositional groups. *The Astronomical Journal*, 141(25):1–18, January 2011.

[41] Jeffrey R. Stuart and Kathleen C. Howell. An automated search procedure to generate optimal low-thrust rendezvous tours of the Sun-Jupiter Trojan asteroids. In *23rd International Symposium on Space Flight Dynamics*, Pasadena, CA, October 2012.

[42] Jeffrey Stuart, Kathleen Howell, and Roby Wilson. Automated design of propellant-optimal, end-to-end, low-thrust trajectories for Trojan asteroid tours. In *AAS/AIAA 23rd Space Flight Mechanics Meeting*, Kauai, HI, 2013.

[43] Jeffrey Stuart, Kathleen Howell, and Roby Wilson. Design of end-to-end Trojan asteroid rendezvous tours incorporating potential scientific value. In *AAS/AIAA 24th Space Flight Mechanics Meeting*, Santa Fe, NM, 2014.

[44] Jeffrey R. Stuart and Kathleen C. Howell. Automated design of propellant-optimal, low-thrust trajectories for Trojan asteroid tours. *Journal of Spacecraft and Rockets*, 51:1631–1647, 2014.

[45] Serina Diniega, Kunio M. Sayanagi, Jeffrey Balcerski, Bryce Carande, Ricardo A. Diaz-Silva, Abigail A. Fraeman, Scott D. Guzewich, Jennifer Hudson, Amanda L. Nahm, Sally Potter-McIntyre, Matthew Route, Keven D. Urban, Soumya Vasisht, Bjoern Benneke, Stephanie Gil, Roberto Livi, Brian Williams, Charles J. Budney, and Leslie L. Lowes. Mission to the Trojan asteroids: Lessons learned during the JPL Planetary Science Summer School mission design exercise. *Planetary and Space Science*, 76:68–82, 2013.

[46] Eugene P. Bonfiglio, David Oh, and Chen-Wan Yen. Analysis of chemical, REP, and SEP missions to the Trojan asteroids. In *AAS/AIAA Astrodynamics Specialist Conference*, 2005.

[47] David M. Murphy. MegaFlex - the scaling potential of UltraFlex technology. In *53rd AIAA/ASME/ASCE/AHS/ASC Structures, Structural Dynamics and Meterials Conference*, Honolulu, HI, 2012.

[48] Richard R. Hofer. High-specific impulse operation of the BPT-4000 Hall thruster for NASA science missions. In *46th AIAA/ASME/SAE/ASEE Joint Propulsion Conference*, 2010. AIAA Paper 2010-6623.

[49] S. Fornasier, E. Dotto, O. Hainaut, F. Marzari, H. Boehnhardt, F. De Luise, and M.A. Barucci. Visible spectroscopic and photometric survey of Jupiter Trojans: Final results on dynamical families. *Icarus*, 190:622–642, 2007.

[50] F. Marchis, J. Durech, J. Castillo-Rogez, F. Vachier, M. Cuk, J. Berthier, M. H. Wong, P. Kalas, G. Duchene, M. A. van Dam, H. Hamanowa, and M. Viikinkoski. The puzzling mutual orbit of the binary Trojan asteroid (624) Hektor. *The Astrophysical Journal Letters*, 783:1–6, 2014.

[51] M.E. Ockert-Bell, B.E. Clark, M.K. Shepard, R.A. Isaacs, E.A. Cloutis, S. Fornasier, and S.J. Bus. The composition of M-type asteroids: Synthesis of spectroscopic radar observations. *Icarus*, 210:674–692, 2010.

[52] P. Descamps, F. Marchis, J. Berthier, J.P. Emery, G. Duchene, I. de Pater, M.H. Wong, L. Lim, H.B. Hammel, F. Vachier, P. Wiggins, J.-P. Teng-Chuen-Yu, A. Peyrot, J. Pollock, M. Assafin, R. Vieira-Martins, J.I.B. Camargo, F. Braga-Ribas, and B. Macomber. Triplicity and physical characteristics of Asteroid (216) Kleopatra. *Icarus*, 211:1022–1033, 2011.

[53] J.E.P. Matzel, H.A. Ishii, D. Joswiak, I.D. Hutcheon, J.P. Bradley, D. Brownlee, P.K. Weber, N. Teslich, G. Matrajt, K.D. McKeegan, and G.J. MacPherson. Constraints on the formation age of cometary material from the NASA Stardust mission. *Science*, 328:483–486, 2010.

[54] Hisayoshi Yurimoto, Ken ishi Abe, Masanao Abe, Mitsuru Ebihara, Aski Fujimura, Minako Hashiguchi, Ko Hashizume, Trevor R. Ireland, Shoichi Itoh, Juri Katayama, Chizu Kato, Junichiro Kawaguchi, Noriyuki Kawasaki, Fumio Kitajima, Sachio Kobayashi, Tatsuji Meike, Toshifumi Mukai, Keisuke Nagao, Tomoki Nakamura, Hiroshi Naraoka, Takaaki Noguchi, Ryuji Okazaki, Changkun Park, Naoya Sakamoto, Yusuke Seto, Masashi Takei, Akira Tsuchiyama, Masayuki Uesugi, Shigeyuki Wakaki, Toru Yada, Kosuke Yamamoto, Makoto Yoshikawa, and Michael E. Zolensky. Oxygen isotopic compositions of asteroid materials returned from Itokawa by the Hayabusa mission. *Science*, 333:1116–1119, 2011.

[55] D.S. Lauretta. An overview of the OSIRIS-REx asteroid sample return mission. In *43rd Lunar and Planetary Science Conference*, The Woodlands, TX, 2012.

[56] Maria Antonietta Barucci, A.F. Cheng, P. Michel, L.A.M. Benner, R.P. Binzel, P.A. Bland, H. Böhnhardt, J.R. Brucato, A. Campo Bagatin, P. Cerroni, E. Dotto, A. Fitzsimmons, I.A. Franchi, S.F. Green, L.-M. Lara, J. Licandro, B. Marty, K. Muinonen, A. Nathues, J. Oberst, A.S. Rivkin, F. Robert, R. Saladino, J.M. Trigo-Rodriguez, S. Ulamec, and M. Zolensky. MarcoPolo-R near Earth asteroid sample return mission. *Experimental Astronomy*, 33:645–684, 2012.

[57] Michael J. Patterson and Scott W. Benson. NEXT ion propulsion system development status and performance. Technical report, NASA, 2008. NASA/TM—2008-214986.

[58] Jon A. Sims, James M. Longuski, and Andrew J. Staugler. v_∞ leveraging for interplanetary missions: Multiple-revolution orbit techniques. *Journal of Guidance, Control, and Dynamics*, 20:409–415, 1997.

[59] Ian O'Neill. Safe Mode Slows Dawn Mission's Progress to Ceres. *Discovery News*, September 2014.

[60] Bruce A. Conway, editor. *Spacecraft Trajectory Optimization*. Cambridge University Press, Cambridge, UK, 2010.

[61] John T. Betts. Very low-thrust trajectory optimization using a direct SQP method. *Journal of Computational and Applied Mathematics*, 120:27–40, 2000.

[62] P. De Pascale and M. Vasile. Preliminary design of low-thrust multiple gravity-assist trajectories. *Journal of Spacecraft and Rockets*, 43(5):1065 – 1076, September – October 2006.

[63] Marco La Mantia and Lorenzo Casalino. Indirect optimization of low-thrust capture trajectories. *Journal of Guidance, Control, and Dynamics*, 29(4):1011–1014, 2006.

[64] Craig A. Kluever. Efficient computation of optimal interplanetary trajectories using solar electric propulsion. *Journal of Guidance, Control, and Dynamics*, pages 1–10, April 2014.

[65] T. C. Tsu. Interplanetary travel by solar sail. *ARS Journal*, 29(6):422–427, June 1959.

[66] Marc D. Rayman, Thomas C. Fraschetti, Carol A. Raymond, and Christopher T. Russel. Coupling of system resource margins through the use of electric propulsion: Implications in preparing for the Dawn mission to Ceres and Vesta. *Acta Astronautica*, 60:930–938, 2007.

[67] David Y. Oh, Damon Landau, Thomas Randolph, Paul Timmerman, James Chase, Jon Sims, and Theresa Kowalkowski. Analysis of system margins on deep space missions utilizing solar electric propulsion. In *44th AIAA/ASME/SAE/ASEE Joint Propulsion Conference and Exhibit*, Hartford, CT, 2008. AIAA Paper 2008-5286.

[68] Iman Alizadeh and Benjamin F. Villac. Targeting requirements and stability characterization fro a class of ballistic transfers. *Journal of Guidance, Control, and Dynamics*, 33(5):1473 – 1489, 2010.

[69] Joris T. Olympio and Chit Hong Yam. Deterministic method for space trajectory design with mission margin constraints. In *61st International Astronautical Congress*, Prague, CZ, 2010.

[70] Jacob A. Englander, Bruce A. Conway, and Trevor Williams. Automated mission planning via evolutionary algorithms. *Journal of Guidance, Control, and Dynamics*, 35:1878–1887, 2012.

[71] Steven N. Williams and Victoria Coverstone-Carroll. Mars missions using solar electric propulsion. *Journal of Spacecraft and Rockets*, 37:71–77, 2000.

[72] Prashant Patel, Daniel Scheeres, and Alec Gallimore. Maximizing payload mass fractions of spacecraft for interplanetary electric propulsion missions. *Journal of Spacecraft and Rockets*, 43(4):822–827, July–August 2006.

[73] Leslie McNutt, Les Johnson, Dennon Clardy, Julie Castillo-Rogez, Andreas Frick, and Laura Jones. Near-Earth Asteroid Scout. In *AIAA SPACE 2014 Conference*, San Diego, CA, August 2014. AIAA Paper 2014-4435.

APPENDIX

A. Missed Thrust: Additional Results

In Figures A.1–A.12 we have plots of the missed-thrust propellant margin and lateness for the Mars Sample Return Orbiter at missed-thrust durations which we did not include in the main body of Chapter 5.

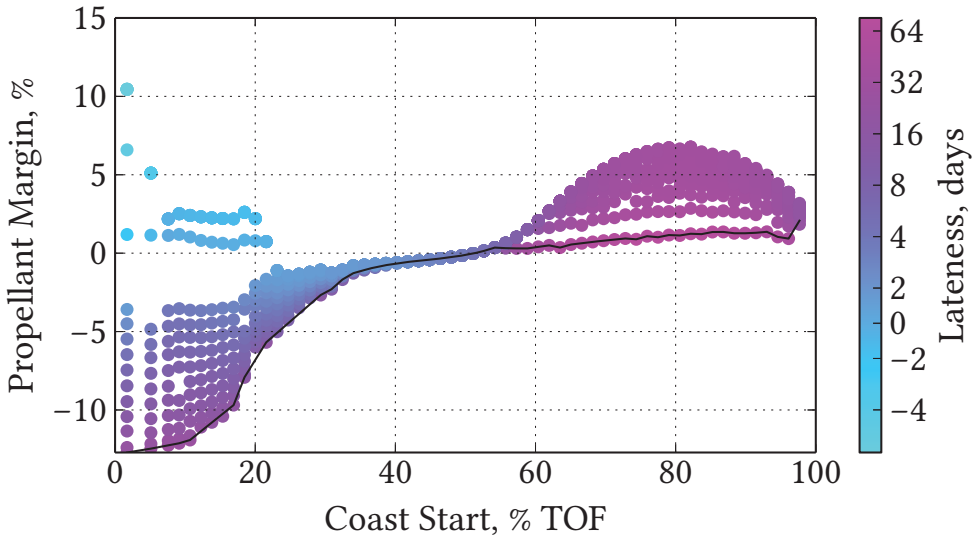

Figure A.1.. Lateness vs Propellant margin for the 10 kW case with a 5-day missed thrust.

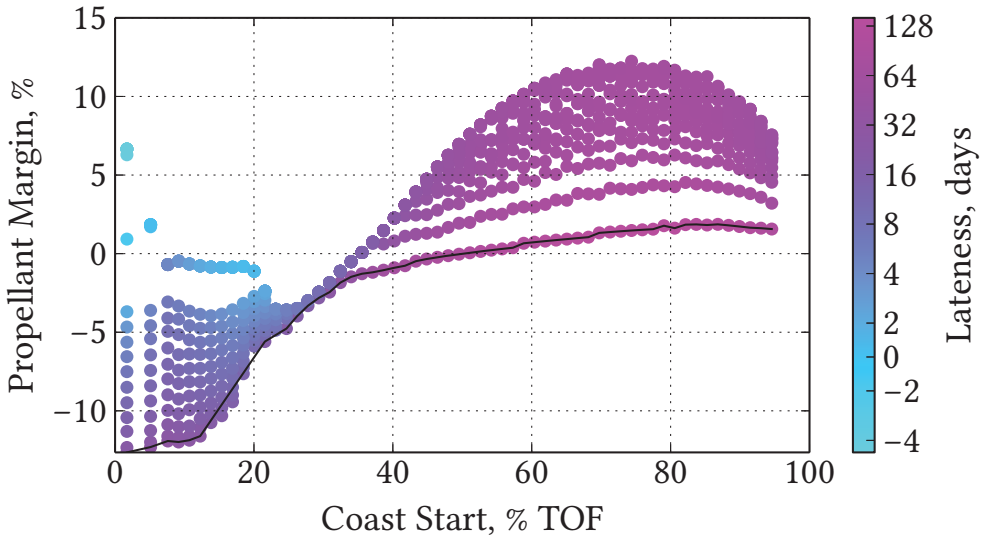

Figure A.2.. Lateness and propellant margin for the 10 kW case with a 15-day missed thrust.

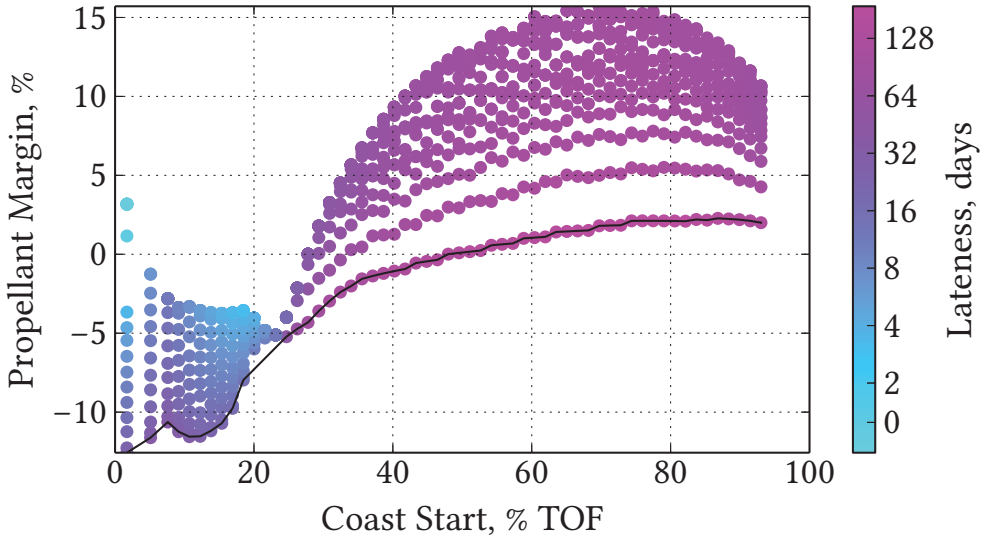

Figure A.3.. Lateness and propellant margin for the 10 kW case with a 25-day missed thrust.

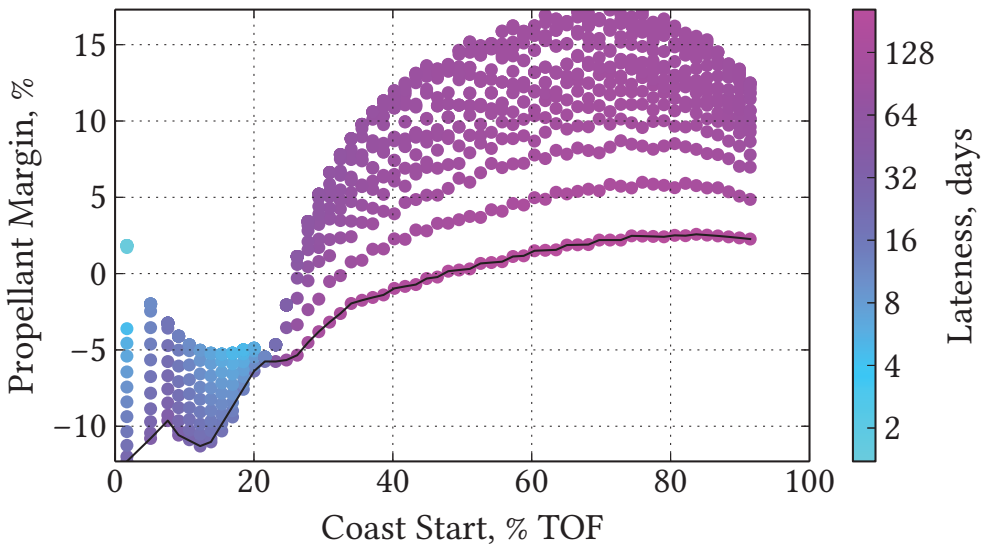

Figure A.4.. Lateness and propellant margin for the 10 kW case with a 30-day missed thrust.

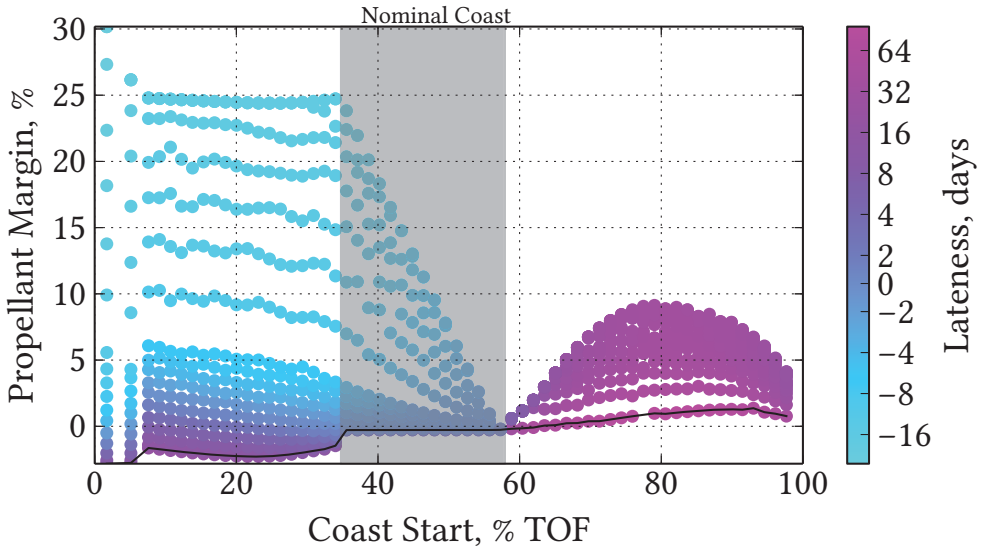

Figure A.5.. Lateness vs Propellant margin for the 15 kW case with a 5-day missed thrust.

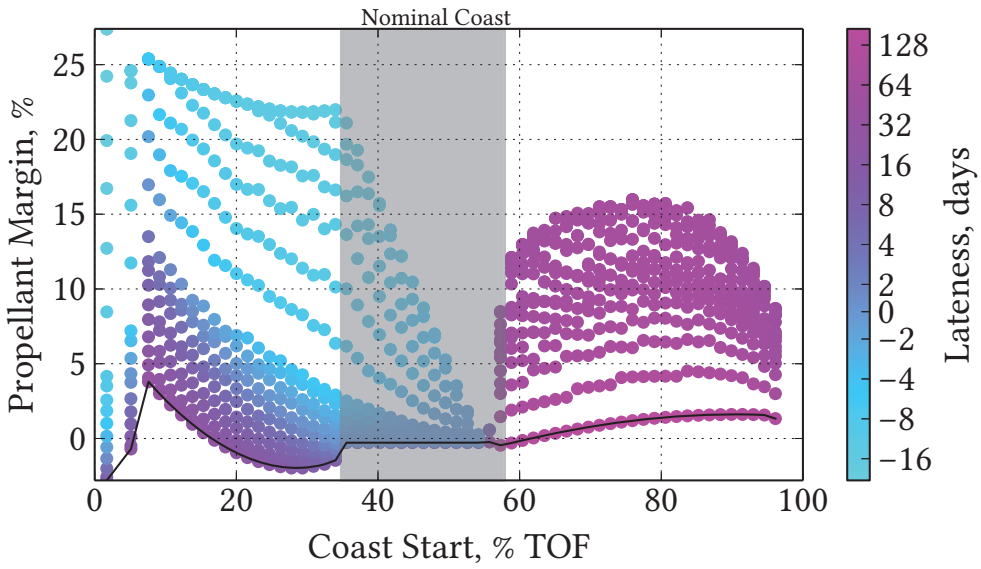

Figure A.6.. Lateness and propellant margin for the 15 kW case with a 15-day missed thrust.

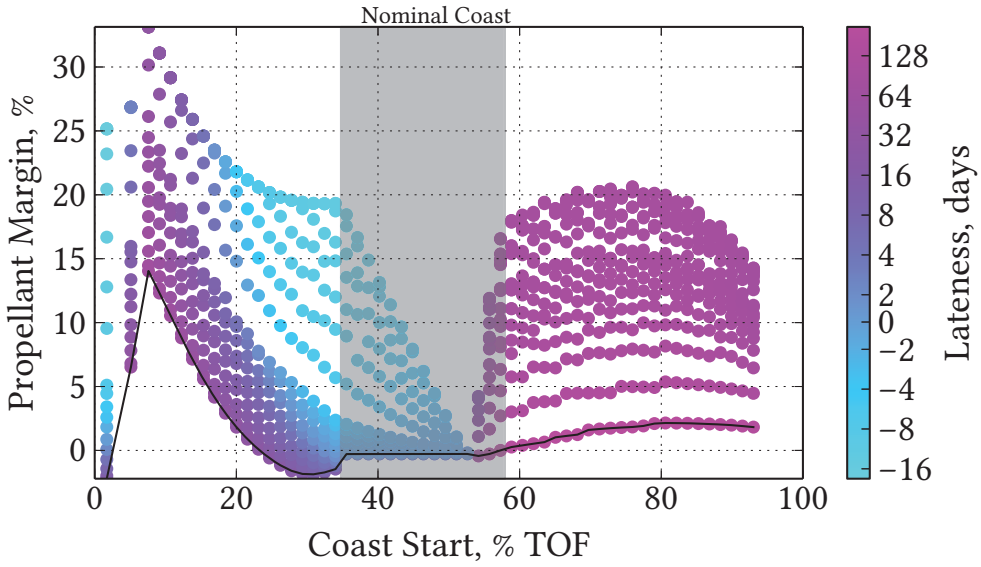

Figure A.7.. Lateness and propellant margin for the 15 kW case with a 25-day missed thrust.

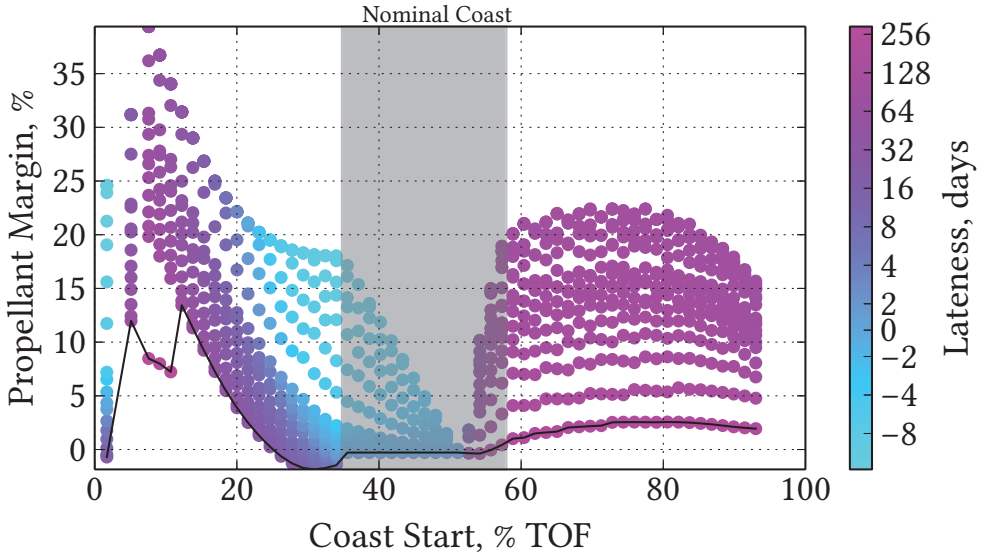

Figure A.8.. Lateness and propellant margin for the 15 kW case with a 30-day missed thrust.

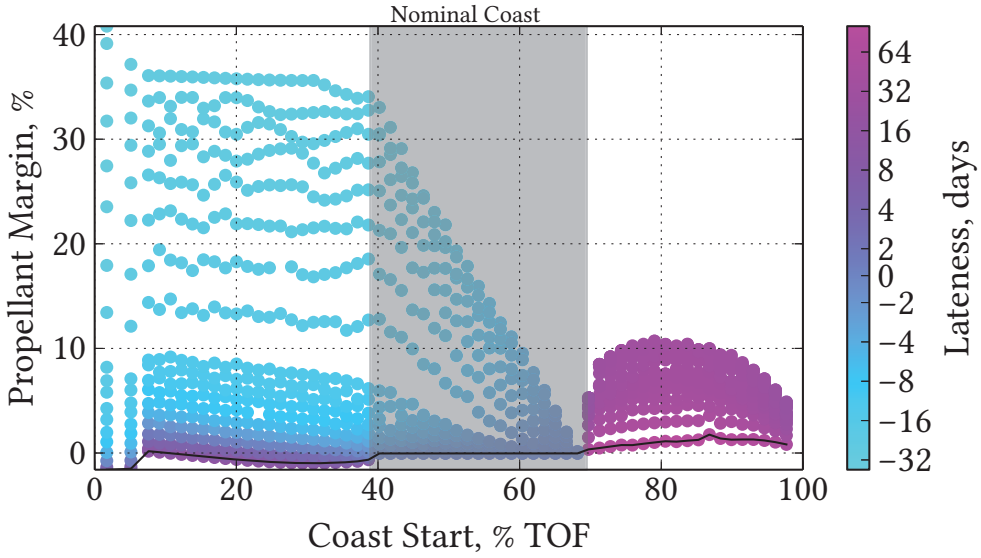

Figure A.9.. Lateness vs Propellant margin for the 20 kW case with a 5-day missed thrust.

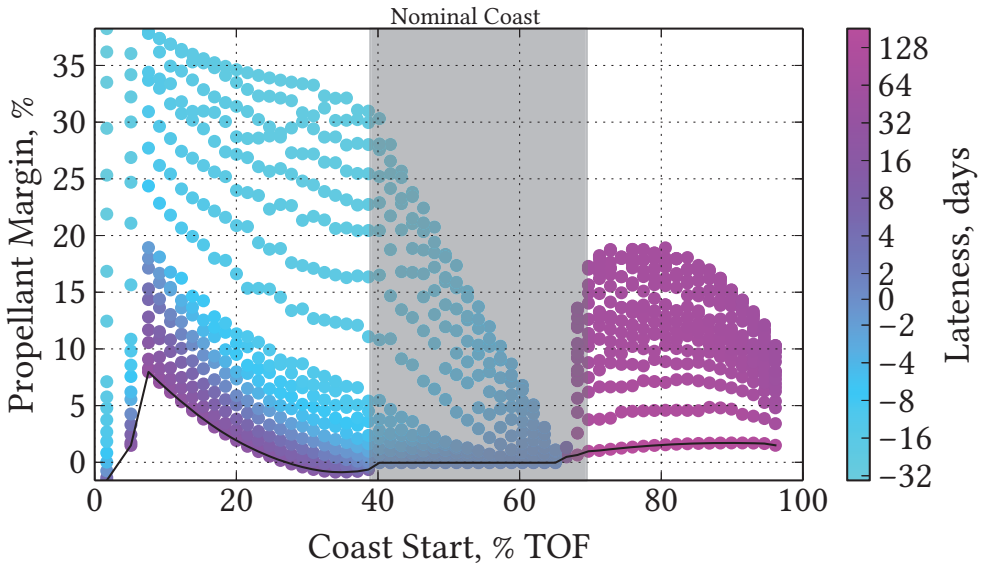

Figure A.10.. Lateness and propellant margin for the 20 kW case with a 15-day missed thrust.

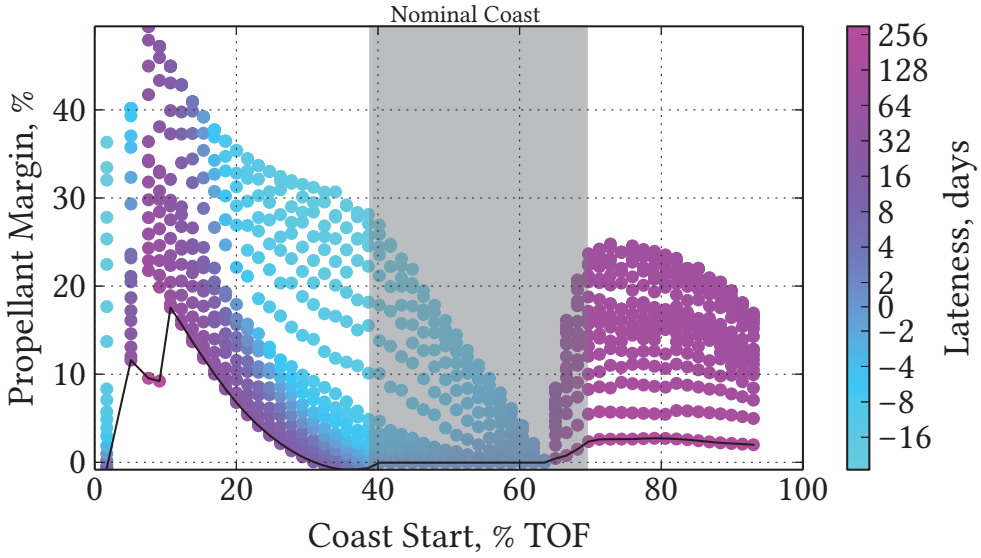

Figure A.11.. Lateness and propellant margin for the 20 kW case with a 25-day missed thrust.

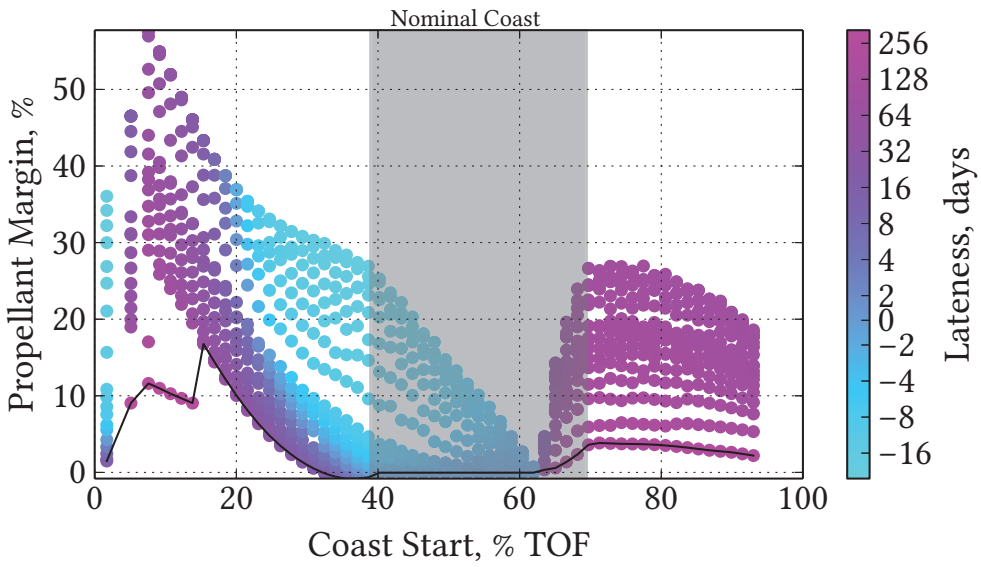

Figure A.12.. Lateness and propellant margin for the 20 kW case with a 30-day missed thrust.

VITA

VITA

Frank Laipert was born in late January, 1987, in the town of Peekskill, New York. Peekskill is a quiet town nestled on the banks of the Hudson river, about 40 miles north of New York City. He lived in the area with his parents, Joseph and Linda, his brother Doug, and his sister Pia, dividing his free time between playing outside, reading Hardy Boys detective novels, and trying to beat *The Legend of Zelda* on Super Nintendo.

In July of 1995, when Frank was eight years old, he and his family moved to Algonquin, Illinois, where he spent the remainder of his childhood. Algonquin is a quiet town nestled on the banks of the Fox River, about 40 miles northwest of Chicago. In 7th grade, Frank won first place in the science fiction category of a district-wide writing contest. In high school he was first chair of the trumpet section, eventually winning the John Phillip Sousa award for excellence in music. When he was 16, Frank finally did beat *The Legend of Zelda* on Super Nintendo.

In 2005, after graduating from Dundee-Crown High School, Frank began his undergraduate studies at Iowa State University, in Ames, Iowa. Ames is a quiet town nestled on the banks of the Skunk River, about 40 miles north of Des Moines. He received his Bachelors Degree in Aerospace Engineering in May, 2009.

In August 2009, Frank started his graduate studies at Purdue University in West Lafayette, Indiana. West Lafayette is a quiet town nestled on the banks of the Wabash River, about 60 miles north of Indianapolis. While at Purdue, Frank researched trajectory design for low-thrust spacecraft under the guidance of Prof. James Longuski. He served as a teaching assistant in the School of Aeronautics and Astronautics and later became an instructor in the Math Department, teaching calculus 1 and 2 to undergraduates. During his time in graduate school, Frank interned at the Aerospace Corporation and the Jet Propulsion Laboratory.